CONTROL OF ACTIVE FILTERS TO ATTENUATE HARMONIC RESONANCE IN POWER DISTRIBUTION NETWORKS

CHONG HWA NG

BEng (Hons) MIEE MIEEE

Thesis presented for the degree of
Doctor of Philosophy at the
University of Northumbria at Newcastle

December 2006

DECLARATION

No portion of the work referred in this thesis has been submitted in support of an application

for another degree qualification in this or any other university or institution of learning.

DEDICATION

To my Father, Mother and Brothers

To my dear wife

ABSTRACT

Harmonic resonance occurs when the network equivalent shunt harmonic capacitive reactance is associated with the network series harmonic inductive reactance. When such resonance occurs, it amplifies harmonic components with frequency close to the resonance point. Solutions used to solve harmonic resonance problems can be divided into two main categories. One is to reduce the content of harmonic components in the network (e.g. by using active or passive harmonic filters, etc.) and the other is to remove the resonance stimulating factor by shifting away the resonance frequency to a non-critical frequency range (e.g. detuning PFC capacitors, redesigning feeder transformers, etc.). Studies show that these techniques are not adequate to solve harmonic resonance problems in power distribution networks which are dynamic by their nature and with complex interconnections. Due to this, solutions in the category one are designed for localised harmonic distortion compensation, while solutions in the category two lack real-time operation feature. Therefore, it was identified that there is a need for real-time harmonic resonance attenuation that is suitable for power distribution networks. In this thesis, a new real-time Harmonic Resonance Attenuation (HRA) technique is proposed. This technique may be used with ordinary shunt harmonic filters to make them behave like a virtual shunt capacitor or inductor. Thus, looking from the harmonic current source side, the filter alters the network harmonic impedance and hence results in harmonic resonance attenuation.

In order to implement the HRA technique, fast measurement of system harmonics in real-time is required. Therefore, in this work, a fast individual harmonic extraction (FIHE) technique is developed to enhance the desired real-time operation of the HRA. The proposed FIHE needs only one sixth of the fundamental cycle to extract any individual harmonic component which is faster than other methods currently available. In addition to the speed, the proposed FIHE provides overshoot free, oscillation free and ripple free extraction characteristics.

The proposed HRA and FIHE techniques are described in this thesis with detailed analysis to illustrate their operating principles. A series of simulations and experiments are conducted to evaluate their functionality and performance. Results of the evaluation are presented and discussed in this thesis together with details of the experimental HRA model developed to verify the theoretical and simulation results.

ACKNOWLEDGEMENT

TABLE OF CONTENTS

ABBREVIATIONS

a.c.	Alternating Current
A/D	Analogue to Digital
ADC	Analogue to Digital Converter
ANN	Artificial Neural Network
ASVC	Advanced Static VAr Compensator
BS	British Standard
CAN	Controller Area Network
CDCC	Current Detect Current Compensation
CH	Channel (oscilloscope)
d.c.	Direct Current
D/A	Digital to Analogue
DFT	Discrete Fourier Transform
DSP	Digital Signal Processor
ESR	Equivalent Series Resistor
FFT	Fast Fourier Transform
FIHE	Fast Individual Harmonic Extraction
FT	Fourier Transform
HRA	Harmonic Resonance Attenuation
I/O	Input/Output Port
IEC	International Electrotechnical Commission
IEEE	Institute of Electrical and Electronics Engineers
IGBT	Isolated Gate Bipolar Transistor

ABBREVIATIONS

IHC	Individual Harmonic Extraction
LPF	Low-pass Filter
LV	Low Voltage
MITI	Ministry of International Trade and Industry (Japan)
OSC	Oscillator
PC	Personal Computer
PCC	Point of Common Coupling
PFC	Power Factor Correction
PI	Proportional-Integral
PWM	Pulse Width Modulation
r.m.s.	Root Mean Square
RTI	Real-time Interface
RTW	Real-time Workshop
SAF	Shunt Active Filter
SHC	Selective Harmonic Compensation
SWIS	South West Interconnection System (Western Australia)
THC	Total Harmonic Compensation
TI	Texas Instruments
UAF	Universal Active Filter
UPFC	Unified Power Flow Controller
UPQC	Universal Power Quality Controller
VDCC	Voltage Detection Current Compensation
VSI	Voltage Source Inverter

LIST OF FIGURES

LIST OF TABLES

CHAPTER 1

INTRODUCTION

1.1 Harmonic Pollution

Since the first a.c. power network was developed around 120 years ago, electricity supply is assumed to have a constant frequency (50 Hz or 60 Hz) sinusoidal voltage. Most of the electrical engineers exercise this assumption when designing and operating electrical equipment. However, in practice, electricity is supplied to both linear and non-linear loads. When a sinusoidal voltage is applied to a non-linear load, the

resulting current would be distorted (non sinusoidal). Due to the presence of system impedance, distorted current causes non-sinusoidal voltage drop across this impedance and causes voltage distortion through out the system. This phenomenon is illustrated in Figure 1.1.
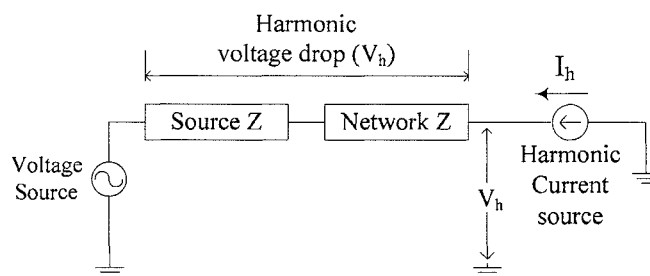
Figure 1.1: Generation of harmonic voltage

Fourier analysis shows that, distorted waveforms can be decomposed into a series of sine waves with different amplitudes, phases, and frequencies. Periodic components with frequencies that are integer multiples of the fundamental (generated) frequency are referred to as 'harmonics'. Components with frequencies that are non-integer multiples of the fundamental frequency are referred to as 'sub-harmonics' and 'inter-harmonics'

In a balanced three-phase system, the generated fundamental voltages are evenly displaced by 120° in phase; consequently, harmonic components in three-phase systems are shifted proportionally in this order. Applying symmetrical component analysis; harmonic components caused by three-phase, non-linear loads in such systems can be grouped into three sequences:

- Positive sequence – for the harmonic order $3n+1$ (i.e. 1st, 4th, 7th etc.)

- Negative sequence – for the harmonic order $3n$-1 (i.e. 2nd, 5th, 8th etc.)

- Zero sequence – for the harmonic order $3n$ (i.e. 3rd, 6th, 9th etc.)

Note: 'n' is an integer from 1 to infinity

As a common practice, power suppliers try to maintain three-phase systems symmetrical, free of d.c. component and even order harmonics. However, odd order harmonic components associated with three-phase, non-linear loads are more difficult to be eliminated and hence their level in power distribution networks is significant.

Due to the 120° phase shift, 'delta/star' transformer configuration is widely used to stop circulation of the triple-n (zero sequence) harmonic components in the supply network. Therefore, it is common to assume that, odd order positive sequence and negative sequence harmonic components are the significant parts when studying system distortion.

1.1.1 Harmonics sources

In the past, non-linear loads were often referred to electric arc furnaces, fluorescent lamps, faulty machines, and overloaded/saturated transformers, as these were the main harmonic sources in power networks. However, in the past two decades, the success in semiconductor technology has sharply increased the use of power electronic devices in the modern electrical equipment [1]. Often, power electronic components are used in power supply units of such equipment for power conversion and regulation purposes

(e.g. adjustable speed drives, frequency converters, switching mode power supplies, etc.).

Harmonic distortion caused by power electronic based equipment has attracted a great concern from both utilities and the end-users [2,3], as these equipment have pushed the level of harmonics pollution to a point that has never been experienced before [4-11].

In the near future, the growth of renewable power generation is expected to introduce more power electronic devices to power networks at both transmission and distribution networks levels [12]. This will require power electronics based interface to ensure the maximum power delivery and good quality of supply (i.e. stability, efficiency, continuity, etc.). However, it is anticipated that the switching nature of these interface devices will introduce a significant amount of harmonics to the network.

1.1.2 Effect of harmonics

Voltage and current distortions are associated with energy and economic losses for both, suppliers and consumers of electricity. Main detrimental effects introduced by harmonics are [13]:

- Mal-function of the control systems, protective devices, etc.

- Interference with metering, instrumentation, communications systems, etc.

- Extra losses causing heating and overloading on devices and equipment.

- Torque pulsation effect on rotating machines

Electrical machines are designed based on the assumption that the voltage supply is sinusoidal. Distorted supply causes extra eddy current and skin effect losses in the stator and rotor, and produces extra heat. Presence of harmonic currents in the machine windings introduces instable motoring action that causes uneven torque generation (torque pulsation). These effects would eventually shorten the useful life of a machine.

When harmonic currents flow in a transmission line, extra loss due to increased r.m.s. value and skin effect would be created. In a 'weak' power network, higher line impedance causes greater harmonic voltage drop resulting in higher electromagnetic interference and voltage disturbance. As a result, adjacent communication networks and power system's protection devices are affected (e.g. missed triggering, lower accuracy, etc.).

Harmonic currents create extra eddy current loss in the windings, and hysteresis loss in the core of transformers. These losses generate extra heat in the transformer, which reduce its efficiency and stresses the insulation consequently shorten its life expectancy. Excessive harmonic currents would eventually saturate the transformer and might create short circuit between the windings.

Harmonic currents shorten the service life of a capacitor. Capacitors exhibit lower impedance to high frequency components. When harmonic currents flow in a capacitor, higher I^2R loss would be generated due to the capacitor's equivalent series resistance. This resistance increases slowly throughout the capacitor life, which leads

to a gradual rise in power loss (heat) and eventually to thermal run away or excessive capacitance drift.

1.2 Harmonic Resonance

Harmonic resonance occurs when the natural frequency of a power system matches the frequency of a harmonic component. At this frequency, system's equivalent inductive reactance (e.g. source, line, transformers, etc.) is equal to the equivalent capacitive reactance; e.g. Power Factor Correction (PFC) capacitors, passive filters, long distance underground cable's capacitance[14,15], etc.

A low impedance path appears to the harmonic current when the equivalent inductance and capacitance are in series (series resonance). When parallel resonance occurs, it exhibits a high impedance path to the harmonic current and results in a proportional rise in the harmonic voltage.

Figure 1.2(a) shows a schematic diagram of a typical power distribution network. The equivalent circuit of this network that is suitable for harmonic current flow analysis is shown in Figure 1.2(b). In this case, non-linear loads are modelled as an ideal harmonic current source, and the generator is represented by its internal impedance. All equivalent series resistances are ignored in this example.

(a) Typical power system   (b) Equivalent circuit of the system
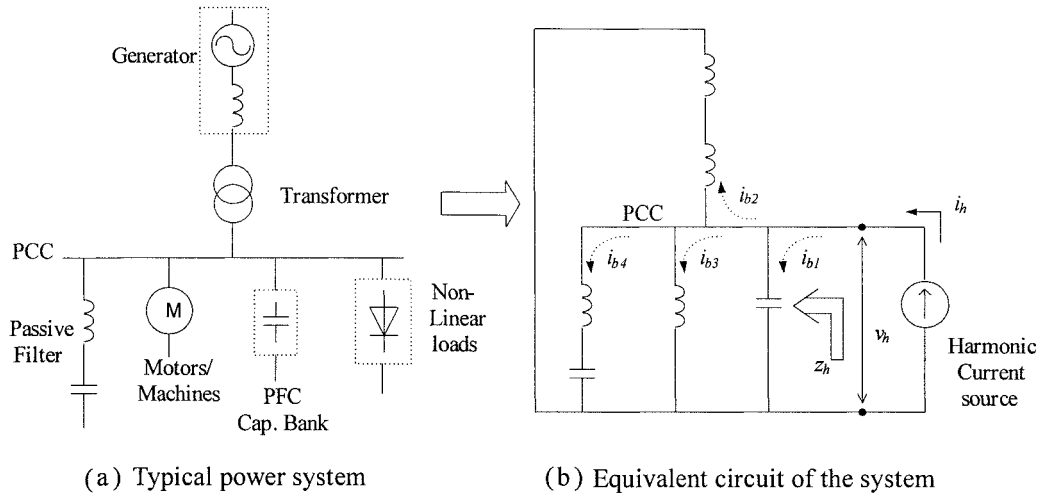
Figure 1.2: A simplified power system network and its equivalent circuit

Looking into the system from the harmonic current source side, it forms a parallel circuit. Therefore, the harmonic impedance (z_h) at the network natural frequency as seen at the Point of Common Coupling (PCC) rises significantly and results in a corresponding rise in the same frequency harmonic voltage of the same frequency at the PCC (v_h). This results in a proportional increase in the harmonic current in every branch $(i_{b1}, i_{b2}, i_{b3}, i_{b4})$.

Amplification of harmonic voltage and current in this manner may create problems to network users, which may have significant economical consequences and in some cases, human life might be endangered.

1.2.1 Previous studies

Several research studies have been carried out to understand and try to solve the problems caused by the harmonic resonances. In order to have a better understanding

about harmonic resonance, causes, symptoms shown when it occurs, consequences and solutions applied, a series of documented harmonic resonance cases were carefully studied and these are summarised in this section.

A case of harmonic resonance that occurred at a paper mill in the British Columbia, Kitimat was reported in the year 1990 [16]. Use of an extra (standby) PFC capacitor bank creates 5th order harmonic resonance. The resonance amplifies 5th order harmonic current (approximately 80 times), and causes a major failure on its standby incoming 13.8 kV circuit breaker. As a result, the protection system was completely destroyed by fire. The procedure adopted to solve this problem was to detune the PFC capacitor bank with a series reactor.

McLean et al. published a case of harmonic resonance at the offshore oil plant in 1993 due to the sub-sea cable[17].The problem was caused by a 22.5 km submarine power cable that was used to supply power from a mother platform to one of the satellite platform. Capacitance of the cable associates with the reactance of a 6.6/20 kV transformer located at the main platform and creates an 11th order harmonic resonance. As a result, 11th order harmonic current generated by a drilling rectifier connected at the satellite platform was amplified and causes voltage harmonic distortion that is over the limit of G5/3. Several solutions were proposed, but a cost effective one was implemented by utilising a passive notch filter to filter out the harmonic current generated. Initially, a notch filter bank, which includes 7th, 11th and 13th order harmonic notch filters, was designed. However, due to the parallel resonance effect of the tuned 7th order harmonic filter an additional 5th order harmonic notch filter was required in

order to prevent parallel resonance caused by the 7th harmonic notch filter which occurs at the 5th harmonic frequency (more details on this effect are given in section 2.1).

A harmonic resonance case that occurred at a plastic extrusion plant in Massachusetts was reported in 1995 by N. K. Medora [18]. A 250-hp thyristor dc-adjustable speed drive used in the plant was supplied through a 13.8 kV to 480 V step down transformer. The transformer was a 300 kVA utility service transformer which was installed by the supplier. In order to improve the power factor and reduce voltage drops during heavy loading, a PFC capacitor bank was installed in the plant. For many years, no problem reported, until one day the utility service transformer was upgraded to a higher power rating (750 kVA) for plant expansion. After this, frequent tripping of the drive's protection devices and noisy operation were noticed. Investigation was conducted, and results show that the 5th order harmonic component was amplified by a harmonic resonance. This was due to the change of the transformer's impedance, which resulted in a resonance mode with the existing PFC capacitance at the 5th order harmonic frequency. Solutions proposed were either to detune the PFC capacitance or change/relocate the supply transformer.

In 1997, another paper mill in British Columbia, Low Mainland experienced similar incident to the one described earlier, where harmonic resonance occurred at the 5th order harmonic frequency [19]. The 22 MW paper mill utilised a 12 kV, 4800 kVAr capacitor bank to improve its power factor. When resonance occurs, the capacitor bank was seriously overloaded and eventually broke down. Investigation carried out found

that the harmonic resonance was caused by the change of network impedance due to a system fault-level improvement at the PCC. Detuning the PFC capacitor bank to avoid the harmonic resonance was enough to solve the problem at the cost of less satisfactory power factor.

A Harmonic resonance in a wind power plant during its trial run was reported in 1998 [20]. Asynchronous generators and PFC capacitor banks were used in this wind power plant. The PFC capacitor banks were designed to handle the full power rating of the plant but designers neglected some of the light load conditions. As a result, at a particular light load condition, the generator's impedance and PFC capacitance created a harmonic resonance circuit at the 11th order harmonic frequency. The amplified 11th order harmonic component caused unstable operation of the generator. Studies carried out concluded that it was necessary to implement a passive filter for shifting away the harmonic resonance. These studies also indicated that, this solution might not be adequate, as it was not able to handle the fluctuations in the system frequency and the dynamic nature of the system.

Another resonance problem occurred in the urban area of Japan where it was first reported by K. Oku in 1994 and the results of further investigation were published later in 1999 by H. Akagi et al. [21]. It was reported that some of the harmonic components in the 6.6 kV distribution network in the downtown area of Japan were frequently amplified during light load conditions (off-peak hour). Reports indicated that the 5th order harmonic voltage at the end of the 6.6 kV feeder was amplified by 3.5 times as compared to the value at the beginning of the feeder. Investigation showed that the

system impedance and load condition during off-peak hours associated with the connected PFC capacitor bank (245 kVAr) had created harmonic resonance. Active harmonic filter solution was proposed to attenuate harmonic components in the network.

In 1999, a harmonic resonance problem in an offshore oil-drilling platform in the UK was reported [22]. Analysis of the 21 kV offshore network showed that the 5th order harmonic current would be amplified under certain load conditions when the system impedance matched with the equivalent capacitance of the sub-sea cables. Due to the large frequency fluctuation in such systems, passive filter compensation method is not practical, and the solution suggested was to use an active filter to prevent the harmonic resonance.

Another harmonic resonance case that happened in Western Australia was reported in 2000 by D. Tong [23]. The South West Interconnection System (SWIS) in Western Australia was experiencing a rapid development due to the continuous growth in electrical power demand. At the same time, PFC capacitors were progressively installed into the system to improve the voltage profile and compensate the excessive reactive power required by the loads. The consequences of the increased capacitance or multiple installations of capacitors were the growing number of reported PFC capacitor bank tripping and system failures. A series of measurement tests and computer simulations were carried out. The results of the investigation revealed that the 5th and 7th order harmonic components in some areas were amplified due to the parallel harmonic resonance between PFC capacitors and system impedance. Based on the

simulation results, it was suggested that the size of the series reactors in the LV zone had to increase in order to detune the resonance point. This suggestion proved to be an effective solution for the problem.

Solution involved utility is reported in one of the publication of K. S. Murthy [24]. In that incident, harmonic resonance caused by the PFC capacitor and system impedance due to the expansion of industry estate power capacity was occurred. Circuit breakers were tripped by the resonance and cause power interruptions to the end users (both industrial and residential consumers). This problem was solved by restructuring the network into two separate lines. This is to separate the supply line to differentiate the industry customers and domestic customers.

These well documented harmonic resonance cases show that many power system networks are exposed to the risk of harmonic resonance. Due to the dynamic nature of power system networks and the presence of harmonic pollution, harmonic resonance can occur at anytime when the system's natural frequency is excited by the harmonic current source.

1.2.2 Solutions for harmonic resonance

Existing solutions for harmonic resonance are mainly based on two principles; one is to eliminate (or minimise) the excitation source of the resonance – the harmonic current; the other solution is to amend the stimulation factor – the systems natural frequency. Due to the nature of power networks, the first type (harmonic elimination) is more suitable for localised harmonic source compensation and hence is better suited for

individual end users. The second method (shifting the system natural frequency) is more suitable for network applications (distribution network operators).

1.2.2.1 Reducing the source of excitation – harmonic source

Reducing the harmonic source means that the effects of harmonic resonance will also be reduced. There are several ways to reduce the harmonics current flow into a network:

- **Compliance with regulation**

The risk of harmonic resonance may be reduced if the harmonic currents generated from the non-linear loads are kept well within the limits specified by harmonic regulations. There are different harmonic regulations being implemented in different countries, for example, Engineering recommendation G5/4 in the UK [25], IEEE 519-1992 in the USA, IEC 611000-3-2 in Europe and MITI in Japan. Ideally, this is the best way of reducing large scale harmonic currents flow in power networks. However, the effect of this method is often limited as the combined effect of many harmonic sources can become significant. In addition, compliance with regulations can only reduce the growing speed/rate of harmonic source to be connected to the network instead of actually reducing the harmonics. As new version of regulations are usually only applicable to the loads installed after the date which the new regulations are implemented. Therefore, if a high percentage of harmonic sources are connected into the system before new rules are introduced, harmonic distortion on that network will not be improved very much. Therefore, regulations are a good means to limit but not reduce the growth of harmonic distortion.

- **Passive filters**

This is the most fundamental and cost effective harmonic filtering method that has been used in power networks. However, it has several disadvantages; e.g. it is bulky and inflexible. Its performance greatly depends on system's impedance and in some cases it might produce extra harmonic resonance modes [26,27]. Further details of passive filter are presented in section 2.1.

- **Active filters**

The use of active filters to deal with harmonic distortion overcomes most of the disadvantages of passive filters. Active filters are much smaller in size, flexible and rarely produce extra harmonic resonance as compared with passive filters. However, they are more costly and more complicated in term of design. Further details of active filters are given in section 2.2.

1.2.2.2 Shifting the stimulation factor – system natural frequency

Solving harmonic resonance by shifting the stimulation factor is always an alternative solution to those mentioned earlier. Existing techniques in this category have better effect when the network condition is less dynamic/complex. As these types of solutions do not have real-time monitoring/adjusting capability and some required offline installation.

- **Relocating network's reactive components**

Changing network resonance frequency by relocating/relaying inductive or capacitive components in the network (e.g. feeder transformer, PFC capacitor bank, reroute the network, etc.) that causes harmonic resonance. In certain circumstances this method

may be unrealistic as it may involve an unacceptable relocation cost, environmental limitation or political constrains.

- **Detuning PFC capacitor banks**

PFC capacitors are used to improve the power factor, but this increases the chance to cause harmonic resonance [28,29]. To prevent resonance, additional reactors are connected in series with the PFC capacitors to detune the network's resonance frequency. Currently, this is a widely used method to solve harmonic resonance problem caused by the PFC capacitors. It is suitable for both utilities and individual end users, as it involves only PFC devices, which themselves the cause of the problem. This method involves minimum system changes, but it does not support real-time monitoring and on-line adjustment. In practice, the kVAr rating of the PFC devices usually depends on the required compensation level [10,30]. This means that, each individual PFC device requires a separate series reactor to maintain the network resonance frequency at a non-critical range. However, due to the dynamic behaviour of the power systems, solutions without real-time monitoring and on-line self-adjusting capabilities could fail to perform in some unforeseen network impedance combinations or unexpected excitations.

- **Switching PFC capacitors**

Switching PFC capacitors are better in handling dynamic network conditions as compared to static capacitors bank. In this method, PFC capacitors are designed such that they can be switched in and out to form the optimum combination in order to gain the best power factor without causing harmonic resonance. This method is particularly suitable for highly dynamic power networks, where loads are constantly switching. The

15

number of discrete capacitance combinations is a function of the number of capacitors used. Therefore, in some cases, resultant combinations are either not sufficient to handle the changes of the network's condition or require an expensive capacitor switching arrangement. In some cases, it may not even be possible to avoid the resonance frequency without sacrificing power factor compensation.

1.3 Project Overview

Harmonic currents and/or voltages in a power network are usually amplified when harmonic resonance occurs. Such amplification often results in problems caused by nuisance fuse blowing, circuit breaker tripping and equipment overheating [31]. In some cases, it may endanger human life in addition to the direct economical losses [16,18-20,22,24,32]. Engineering standards require electrical power suppliers to be responsible for the quality of the supplied voltage [32]. The literature review conducted showed that, most of the studies focused on solving the problem of localised harmonic distortion from the end user side. Conventionally, techniques like redesigning/relaying power networks or detuning PFC capacitors are used by utilities to avoid resonance at any dominant harmonic frequency. Passive or active harmonic filters are usually employed by end users to attenuate the source of harmonics and hence to reduce the resonance effect. However, due to the dynamic nature of power systems, conventional non real-time solutions (mentioned earlier) are usually not capable of handling harmonic resonance effectively. On the other hand, using active filters (with real-time current detection) at the load side, would significantly increases the overall system cost and might not be able to fully prevent harmonic resonance.

In this research programme, a voltage controlled active filter with real-time control is employed at the distribution network side to solve the harmonic resonance problem. This research concentrates on using a Shunt Active Filter (SAF) as a controllable reactance to attenuate harmonic resonance at the PCC in a distribution network. A real-time harmonic voltage detection technique is used to achieve the requirements of the PCC compensation [22,32]. Also, a fast individual harmonic extraction technique is proposed to enhance the real-time operation by increasing the harmonic extraction speed. In general, 'Real-time harmonic voltage detection technique' is the technique that continuously sensing harmonic voltage. It is a general technique, which does not constrain by response time and it can be operate either individual or total harmonic detection. However, the proposed fast individual harmonic extraction technique is a more application specified harmonic extraction technique that provides "high speed" "individual" harmonic voltage or current extraction. Investigation carried out in this project is based on both simulation and experimental work.

1.4 Research Objectives

The primary objective in this project is to develop a controller, which can provide real-time harmonic resonance attenuation in power distribution networks. In addition to the mathematical analysis, computer simulations and experimental tests are carried out to justify the proposed techniques. A laboratory prototype of the proposed harmonic resonance attenuator which includes the FIHE has been developed in order to

demonstrate the performance of the proposed techniques and verify the analytical and simulation results obtained.

A summary of the main specifications of the developed controller are:

- Attenuate harmonic resonance by shifting away the system natural frequency. This type of harmonic resonance control is more suitable for the utilities (distribution network operators).

- To achieve large scale compensation, a technique based on the principles of Voltage-detection voltage-compensation technique is adopted. This is because voltage is a common element in a multi-branched distribution network. In such networks, a single voltage depended compensator is better than multiple current depended compensators. Common point compensation is a better option for networks with many branches and also for future 'active distribution networks'[33,34].

- A fast and accurate individual harmonic extraction is essential to obtain the desired real-time operation of the proposed controller.

Figure 1.3 presents a chart-based diagram that clarifies the concept presented in this thesis.
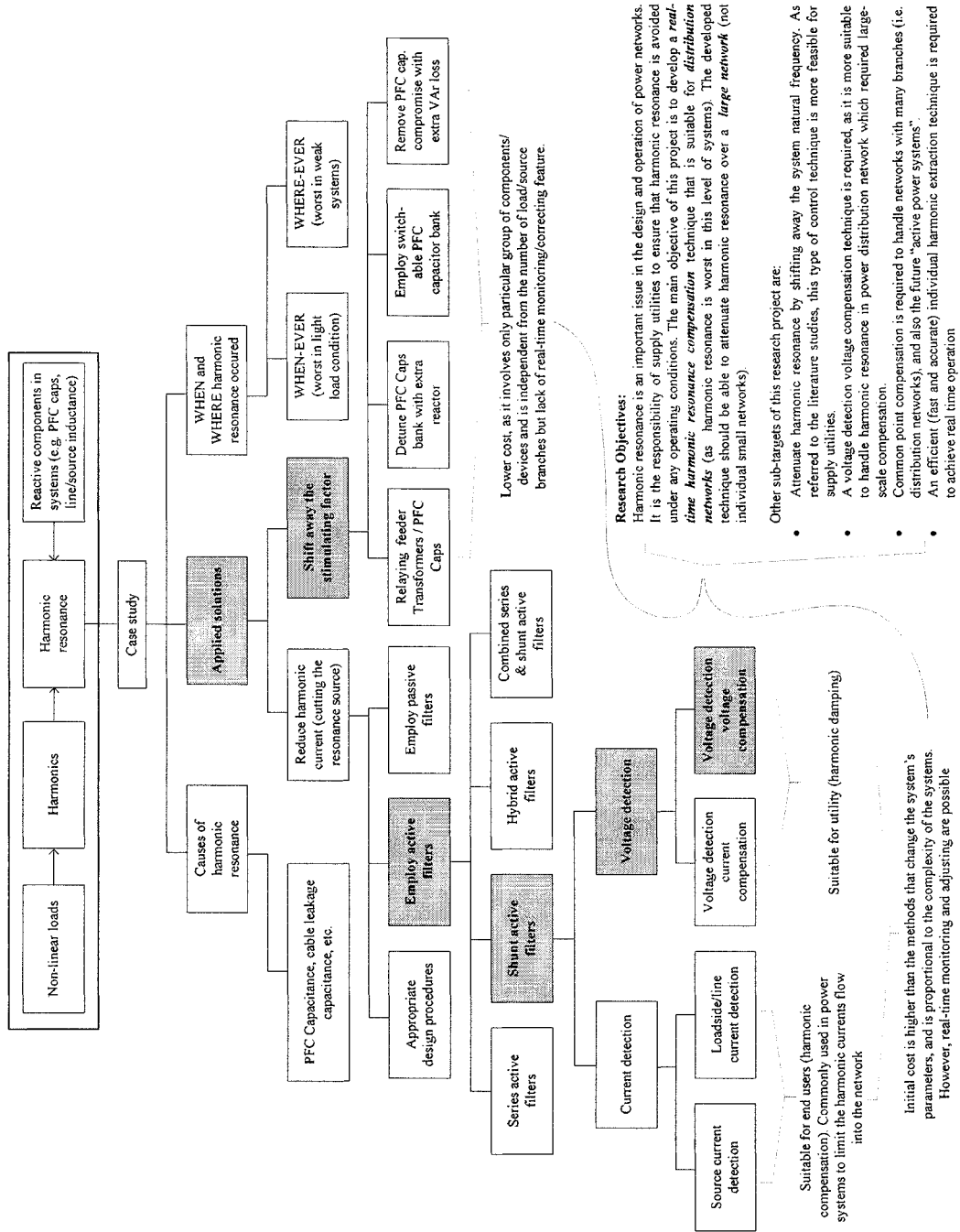
Figure 1.3: Mapping diagram of the project's concept (shaded blocks are the selected solutions)

1.5 Thesis Outline

Chapter 2 gives detailed background information about filters, including the principles and main features of different types of passive and active filters. In addition, advantages and disadvantages of existing harmonic sensing and compensating techniques are discussed.

Chapter 3 reviews the available harmonic extraction techniques (e.g. frequency domain, time domains, etc.). Detailed investigations and analyses were carried out and the need of a high speed individual harmonic extraction technique is addressed as a result of the studies.

Chapter 4 presents the proposed Fast Individual Harmonic Extraction (FIHE) technique. Characteristics of the proposed FIHE in balanced and unbalanced conditions are analysed and discussed in detail.

Chapter 5 presents the simulation results of the performance evaluation of the proposed FIHE technique under balanced, unbalanced and system frequency drift conditions are considered in the simulation.

Chapter 6 introduces the principles of the proposed harmonic resonance attenuation (HRA) technique. The characteristics and effects of the proposed HRA on the distribution network are analysed in detail.

Chapter 7 presents the computer simulation results for the theoretical performance analysis of the proposed HRA technique. Principles of the technique discussed in chapter 6 are evaluated in this chapter.

Chapter 8 gives details of the experimental verification of the proposed controller and techniques implemented (FIHE and HRA). Details of the experimental model design e.g. system resonance condition, DS1103 PPC real-time controller set-up, PWM inverter, etc. are discussed.

Chapter 9 summarises the conclusions drawn from the theoretical analysis, simulations and the laboratory work of the entire project. Suggestions are given for further research.

1.6 Original Contributions of the Thesis

The research carried out has resulted in the following contributions:

1. The occurrence of harmonic resonance in the power systems has been systematically investigated and summarised. This gives a better understanding upon the problem of harmonic resonance in the power systems (e.g. the causes, the consequences, the symptoms, etc.)

2. Operation and performance of the existing harmonic extraction techniques were carefully studied, analysed and presented in Chapter 3. These studies have given a better understanding upon existing harmonic extraction

algorithms and as a result, the need of high speed individual harmonic extraction is identified.

3. A fast individual harmonic extraction (FIHE) technique is developed. This technique gives high speed individual harmonic extraction without compromising the side effects such as overshoot, oscillation, or lowering the attenuation capability. In the proposed FIHE technique, principle of the Park's transformation is used in a modified way to extract harmonic components. This is done by mapping process where the d-q rotating frame rotated at the selected harmonic frequency. After the mapping process, the unwanted harmonic components will then be eliminated based on the principle of the orthogonal function. As one of the requirement of the proposed harmonic resonance attenuator, a reverse transformation process is used to reconstruct the harmonic component back to the three phase quantity.

4. Detailed analyses and evaluations (e.g. simulations and experimentally) were carried out to evaluate and demonstrate the operation and performance of the proposed FIHE technique under balanced, unbalanced and frequency drifted conditions.

5. A harmonic resonance attenuation technique that is suitable to be used in the distribution networks is developed. Without the use of current sensor enables the proposed technique to be installed at the point of common coupling (PCC). This feature makes it independent from the number of up stream and down stream branches in the network where it is installed, in

which it would significantly reduces the cost of attenuate harmonic resonance (e.g. unit cost, installation cost, maintenance cost, etc.).

6.   Simulation model and a prototype (include both the proposed HRA and FIHE) have been constructed/built to evaluate the functionality and performance of the proposed techniques.

1.7 Author's Publication List

i.   Wijayakulasooriya, J.V., Putrus, G.P., and Ng, C.H., "Fast Non-Recursive Extraction of Individual Harmonics Using Artificial Neural Networks," *IEE Proc. Generation, Transmission & Distribution*, Vol. 152, No. 4, July 2005, pp. 539 - 543.

ii.   Ng, C.H., Busawon, K., Putrus, G.A., and Ran, L., "Fast Individual Harmonic Extraction Technique," *IEE Proc. Generation, Transmission & Distribution*, Vol. 152, No. 4, July 2005, pp. 556 - 562.

iii.   Putrus, G.A., Wijayakulasooriya, J.V., Ng, C.H., Minns, P.D., "Disturbance Extraction for Power Quality Monitoring and Mitigation," *The IEE Seminar on Power-It's a Quality Thing*, pp. 2/1 – 2/10, 16 Feb, 2005, London, UK.

iv.   Ng, C.H., Ran L., Putrus, G.A., and Busawan, K., "A new approach to real time individual harmonic extraction," *The Fifth International Conference on Power Electronics and Drive Systems*, vol. 1, pp. 825 - 829, 2003, Singapore.

v.   Ng, C.H., Ran, L., Putrus, G.A., and Busawon, K., "Analysis of Aliasing in Active Power Filters", *37th International Universities Power Engineering Conference (UPEC 2002)*, vol. 1, pp. 142-146, 2002, Staffordshire, UK.

vi.   Ng, C.H., Putrus, G.A., Ran, L., Busawon, K., "Non-localised harmonic attenuation technique", *Prepared for publication in IEE Proc. Generation, Transmission & Distribution.*

vii.   Ng, C.H., Putrus, G.A., Busawon, K., Ran, L., "Time Domain Harmonic Extraction", *Prepared for publication in IEE Proc. Generation, Transmission & Distribution*

viii.   Ng, C.H., Putrus, G.A., Ran, L., Busawon, K., "Use of FIHE in symmetrical components filtering," *Prepared for publication in IEE Proc. Generation, Transmission & Distribution.*

CHAPTER 2

POWER SYSTEM HARMONIC COMPENSATION

2.1 Passive Harmonic Filters

Passive harmonic filters are widely used in the power networks to prevent harmonic currents generated by non-linear loads from flowing into the supply network. Usually, they are built by combining inductors, capacitors and sometimes resistors either in series or series-parallel, as shown in Figure 2.1. These filters are usually connected in shunt to the load as shown in Figure 2.1c, and behave as a sink to absorb the unwanted

harmonic currents. A tuned notch filter (Figure 2.1a) is usually applied to filter out

elected low frequency (dominant) harmonic component. In some applications, a high

pass filter (Figure 2.1b) is used in conjunction with the tuned filters to deal with higher

order (non-dominant) harmonic components. The high pass filter works as a sink for

harmonic components with frequencies higher than the filter's cut-off frequency.

| a) Series configured tuned filter | b) Series-parallel configured tuned filter | c) A passive filter in a power network |
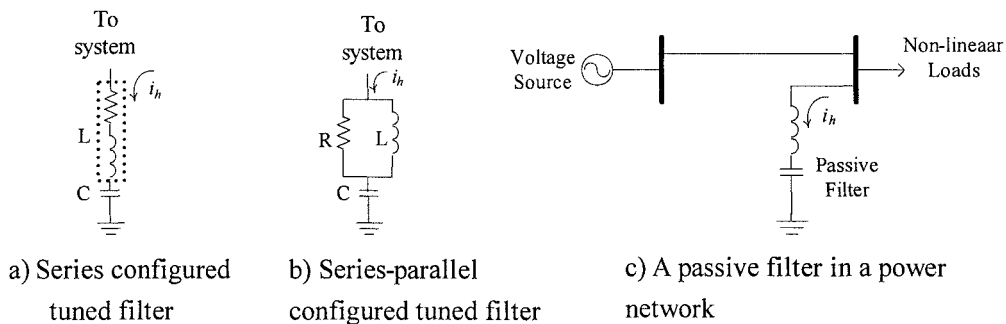
Figure 2.1: Types of passive filters

Due to their simplicity and low cost, passive filters are still the cheapest and easiest

solutions to reduce/compensate harmonics distortion when compared to other methods

of reducing such distortion, e.g. active filters, as long as size is not an issue [35].

As aforementioned, the basic operating principle of passive filters is to exhibit a lower

impedance path with respect to the system (source) impedance at the tuned frequency,

to prevent harmonic currents flow to the downstream networks. This means that, the

filtering quality would be very much determined by the ratio of the source impedance

to the impedance of the filter itself at the tuned frequency. Therefore, in order to

determine the variations in the network source impedance, passive filter designs are

always include a huge amount of network topology studies. However, modern power

networks are becoming more dynamic, hence variation of the source impedance might be difficult to determine without a real-time measurement. As a result, filter's performance is affected by the variations in the system impedance. Furthermore, even if real-time network impedance information are in hand, passive filters are still not easy to retune.

2.1.1 Single tuned filters

Single tuned notch filter is a filter that is sharply tuned to a selected harmonic frequency (high quality ('Q') filter). Generally, these filters are used to eliminate lower characteristic harmonic components (dominant harmonic components e.g. 5th, 7th and 11th). They can be designed and implemented into a power system with a relatively low cost. The biggest disadvantage of using notch filter is that, it creates a sharp parallel resonance when the filter impedance matches the network impedance at the resonance frequency [10,36-39]. A simplified example of a notch filter connected in a simple power network is shown in Figure 2.2.
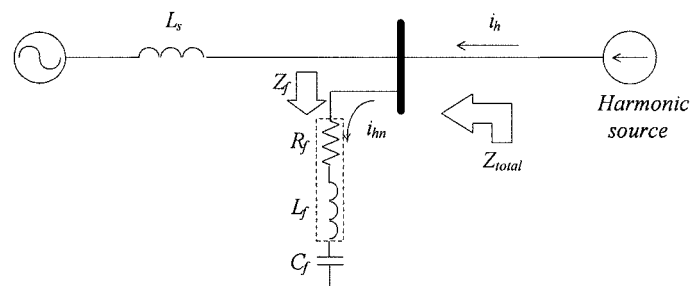
Figure 2.2: Simplified power network with a notch harmonic filter

The impedance function for the filter (Z_f) is given as:

$$Z_f = R_f + j(\omega L - \frac{1}{\omega C})$$
(2.1)

The resonance frequency (f_{sr}) of the filter is:

$$f_{sr} = \frac{1}{2\pi\sqrt{L_f C_f}}$$
(2.2)

As seen from the direction of harmonic source, the filter impedance and network impedance form a parallel resonance circuit, with the resonance frequency (f_{pr}) equal to:

$$f_{pr} = \frac{1}{2\pi\sqrt{(L_f + L_s)C_f}}$$
(2.3)

Equation(2.2) and (2.3) show that, due to the system inductance (L_s), parallel resonance will always happen at a frequency lower than the filter's tuned frequency. Using harmonic flow analysis, this phenomenon is graphically shown in the Figure 2.3.
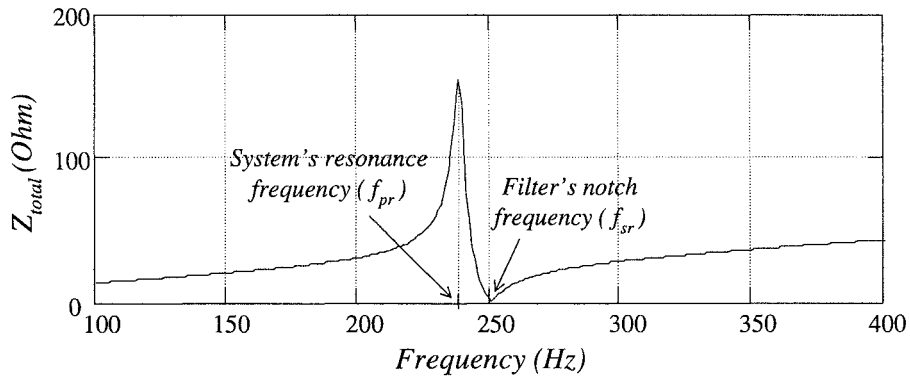
Figure 2.3: The effect of a fifth harmonic filter on the network impedance

Therefore, it is very important to know the system's source impedance and the harmonics generated in the network in order to shift the system resonance frequency to a harmonic free zone (e.g. non-integer multiple of fundamental frequency). As a common practice, passive filters added into a network are always started from the lowest problem harmonic order. For example, when network user requires to use a 7th order harmonic filter to keep the level of 7th order harmonic component within a limit. A 5th order harmonic filter will always be included to avoid the possibility of 5th order harmonic component being amplified by the parallel resonance caused by the 7th order harmonic filter [40].

2.1.2 Double tuned filters

Double tuned filters are designed to eliminate two harmonic frequencies components in a single filter setup. Generally, they are used to attenuate two dominant harmonic components (most commonly 5th and 7th order harmonic components). Figure 2.4(a) shows the schematic of a typical single tuned notch filter bank for 5th, 7th and 11th order harmonic components. Figure 2.4(b) shows an equivalent double tuned notch filter (for 5th and 7th as the one in Figure 2.4(a) and the same single tuned notch filter for 11th order harmonic component.
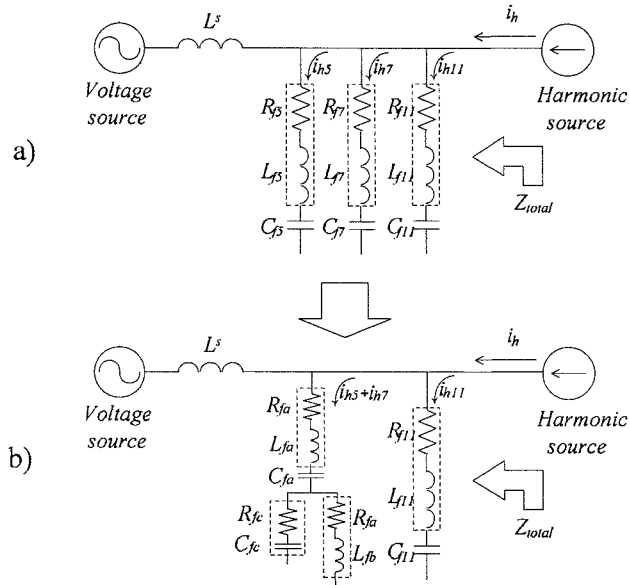
Figure 2.4: Simplified power network with (a) 3 single tuned n-notch filters, and (b) An equivalent double tuned notch filter and a single tuned notch filter.

Figure 2.5 presents the frequency response of the double tuned notch filter shown in Figure 2.4(b).
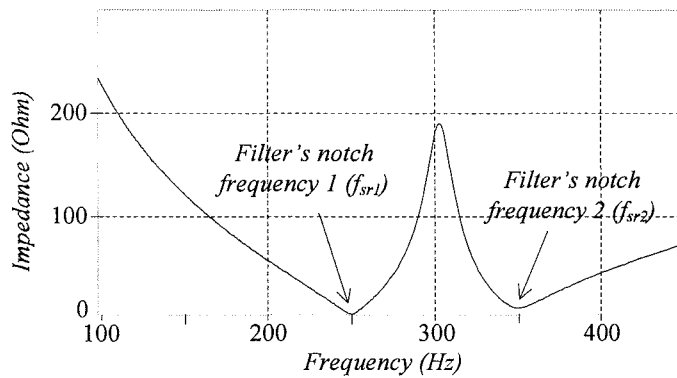
Figure 2.5: Frequency response of the double tuned notch filter shown in Figure 2.4(b)

Generally, double tuned filters are used in high voltage applications. As compared to single tuned filter, double tuned filter reduces the voltage stress of components.

2.2 Active Filters

Performance of a passive filter is dependent on the power network's impedance. The lack of real-time tracking and adjusting features cause them to be less popular in modern power system harmonic filtering applications. To solve this problem, active harmonic filters are suggested.

Since 1970s, active filters are developed to replace/enhance the performance of conventional passive filters [36,41]. They have several advantages in terms of size, multi-harmonic compensation capability, real-time operating capability, and reduced risk of causing harmonic resonance. The advances in semiconductor technology during the past two decades have stimulated the development and utilisation of active filters.

Active filters usually consist of three main parts; an inverter, a d.c. storage device, and a controller. Insulated Gate Bipolar Transistor (IGBT) is one of the most frequently used power devices at low and medium voltage levels [42]. Active filters can be grouped into four main topologies:

- Shunt active filters

- Series active filters

- Combined series-shunt active filters

- Hybrid active filters

2.2.1 Shunt active filters

As the name implies, a shunt active filter is applied in parallel to the load. Figure 2.6 shows the basic structure of a stand-alone shunt active filter.
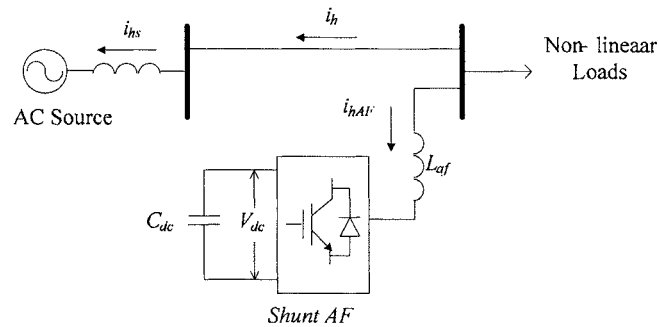
Figure 2.6: Shunt active filter

The main operating concept of shunt active filters is to compensate/cancel the load current harmonics by injecting an anti-phase harmonic current into the system. For example, active filter senses the harmonic current flowing in a network and uses this as the reference signal to control the PWM inverter in order to produce the same amplitude but opposite phase harmonic current. Since the generated harmonic currents are out of phase with respect to the original harmonic currents in the network, their super-positioning effect will result in full harmonic currents compensation.

For many years, shunt active filters have been the most widely used configuration [37] due to their high efficiency and low cost as compared to other topologies. Moreover, they have the potential of expanding their applicability to some other power quality areas such as; flicker and voltage regulation and reactive power compensation [43].

Unlike series active filters, which will be described next, shunt active filters are designed to carry only the compensating currents (plus a small amount of active fundamental current to supply switches and DC-link losses) [44]. Therefore, a shunt filter does not need to have a full current rating of the system. In addition, it is also easier to protect shunt active filters during network faults, as they can be easily disconnected from the faulty network.

2.2.2 Series active filters

Series active filters are placed in series between non-linear loads and a.c. sources. The basic structure of a series active filter shown in Figure 2.7 is similar to that of a shunt filter.
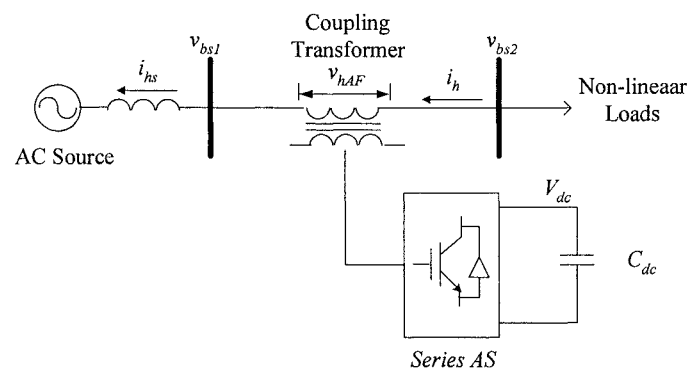
Figure 2.7: Series active filter

Instead of operating like a sink for harmonic currents (e.g. shunt active filter), the series active filter works by isolating the harmonic currents flow from one side of the network to another [45]. Its operating principles are based on controlling output voltages at the required harmonic frequencies, to present a high impedance (harmonics impedance) path to the selected harmonic components. With this, harmonic currents

are blocked from flowing into the networks beyond the point where the filter is installed.

The greater the harmonic voltage being generated at the series coupling transformer (V_{hAF}), the higher the harmonic impedance is presented to the harmonic current flows from the non-linear load. Ideally, series active filter should present a zero volt ($V_{1AF} = 0$ V) across the coupling inductor at fundamental frequency.

Series active filters may also be used to eliminate supply voltage flickering or balance the unbalanced load conditions. However, the series placement of such active filter has made it less attractive due to the inherent I^2R loss and the high inverter current during fault conditions.

2.2.3 Combined series-shunt active filters

Combined series-shunt active filter is not purely a power harmonic filter, it may also operate as a power quality conditioner. Therefore, it is sometime called as Unified Power Quality Conditioner (UPQC) or Universal Active Filter (UAF) [32,46,47]. This is because the function of UPQC is not only to compensate harmonics but also dealing with problems like reactive power compensation, voltage flicker, and system unbalance. A basic structure of the UPQC is shown in Figure 2.8.
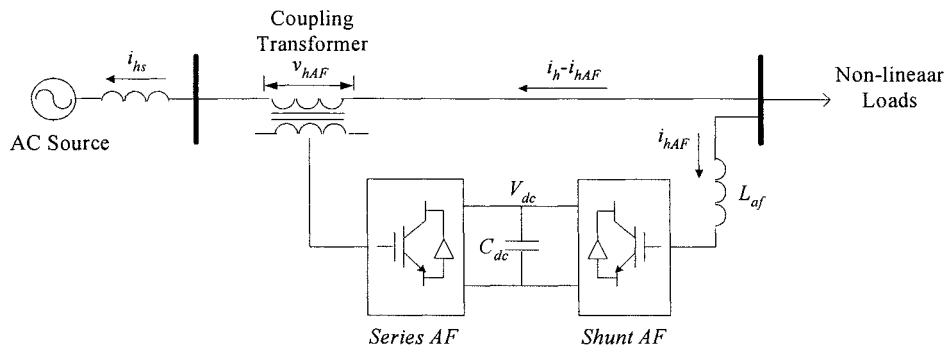
Figure 2.8: Combined series-shunt active filter

The series part (series active filter) is programmed to handle problems like voltage flickers, system's voltage unbalance, and to isolate voltage harmonics (as described earlier). The main function of the shunt part (shunt active filter) is to compensate harmonic currents in the network, compensate reactive power, and regulate the DC-link voltage of the UPQC.

The main disadvantages of the combined series-shunt configuration are high cost and complex in control as it involves a large number of switching devices and require a number of compensation functions (multi-tasking) [44].

2.2.4 Hybrid filters

The development of power semiconductor device technology has brought the concept of active power filter out from laboratories into the commercial world. However, the cost of implementing active filters in high power applications is still relatively high compared to the conventional passive filters. Therefore, 'Hybrid Filter' is developed to

combine the advantages of both the active and passive filters [8,32,36,41,47-51].

Figure 2.9 to Figure 2.11 show a few common hybrid filters configurations.
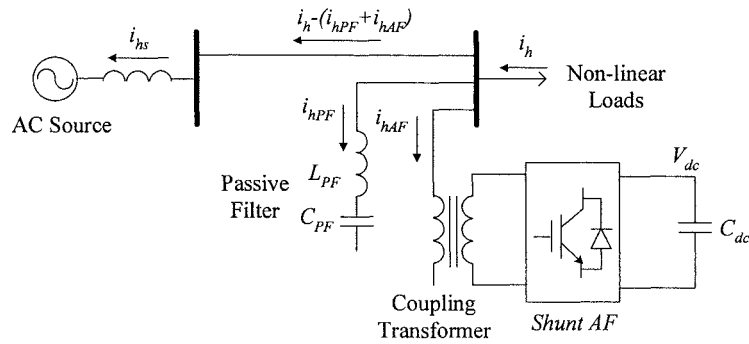
Figure 2.9: Parallel active and parallel passive combined hybrid filter
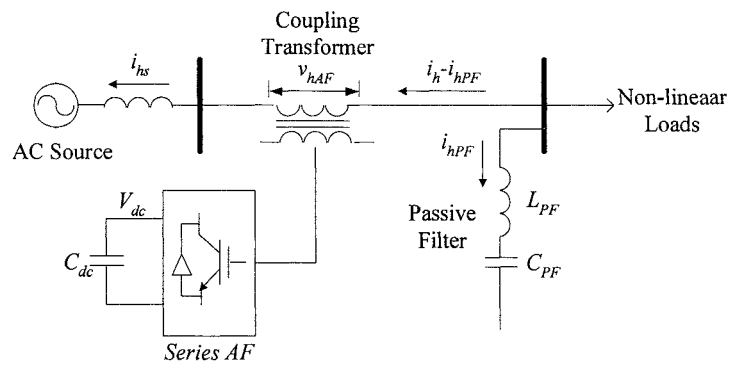
Figure 2.10: Series active and parallel passive combined hybrid filter
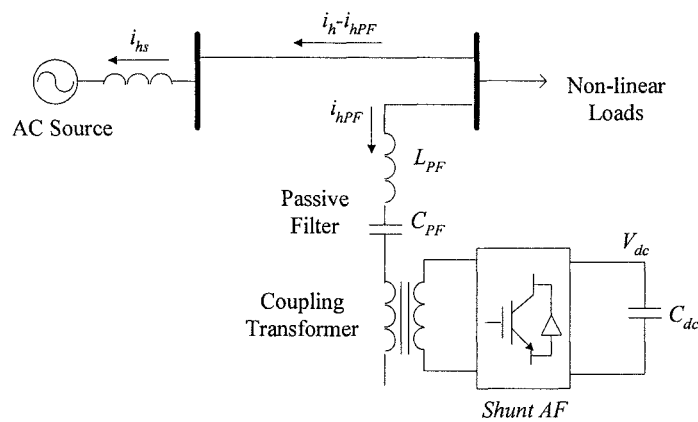
Figure 2.11: Parallel active in series with passive combination hybrid filter

Generally, a hybrid filter combines an active filter with one or more LC tuned passive

filters working as notch filters for selected harmonics compensation or with a high pass

filter for total/overall harmonics compensation. Figure 2.9 shows a hybrid filter

configuration that has been commercially applied to compensate harmonic distortion

for high power rated loads [32,41]. For this type of hybrid filters, the integrated shunt

active filter is designed to only compensate a few low order/dominant harmonic

components. The passive filter in the unit is designed to handle the rest of the higher

order harmonic components. As the active filter needs only compensate low order

harmonic components, its switching frequency can be minimised and so as the watts

per pound rating of the switching devices. Therefore, with this combination, a

compensator can be designed to handle higher power without the need for high power

semiconductor devices. The main drawback is that the passive filter has no real-time

adjustable feature. Thus, this approach is only suitable for predefined harmonic

producing loads (less dynamic power networks) [44] which do not require online

tuning.

Figure 2.10 shows a hybrid filter topology that combines a series active filter and a

parallel passive filter. In this combination, in addition to the features mentioned in

section 2.2.2, series active filter may also be used to improve the filtering capability of

the shunt passive filter by exhibiting a high impedance for harmonic frequencies at

which the passive filter is tuned. With this, the impedance problem (described in

section 2.1), which affects the passive tuned filter performance can be overcome.

However, due to the problems associated with series active filter (described in section 2.2.2), such hybrid topology appears to be less popular than the previous one [44].

Hybrid filter topology consists of a shunt active filter and a passive filter connected in series as shown in Figure 2.11. The passive filter is tuned as a high pass filter that passes all harmonics other than the fundamental frequency component. With this, the shunt active filter connected in series with the passive filter is only required to handle the non-fundamental harmonic components. Hence, the voltage rating of the switching devices can be significantly reduced. This type of combination can also be used for individual harmonic compensation (e.g. as a single or multiple tuned notch filter to eliminate dominant harmonic components). In such application, filtering quality of the passive notch filter is complemented by a small rating active filter (e.g. in case of frequency drift, system impedance changed, component value changed, etc.).

2.3 Existing Harmonic Sensing and Compensating Techniques

Two main sensing and compensating methods are found in the literatures. The first one is to sense the line distorted current and compensate this by injecting harmonic current. This method is called as Current-Detection Current-Compensation (CDCC) [52,53]. The other one is to sense the system's distorted voltage and compensate it by injecting harmonic current. This one is named as Voltage-Detection Current-Compensation (VDCC) [21,32].

2.3.1 Current-Detection Current-Compensation (CDCC)

Vast majority of the practically implemented active harmonic filters are based on the current detection method [53]. CDCC is the most basic control strategy used in the active filter design. As described by the name, this type of control strategy detects and process the load-side distorted current, and uses it as a feed-forward signal to compensate harmonic current distortion. The term "feed-forward" rather than "feedback" is used here because harmonic current is fed in by the non-linear load, hence from a harmonic current point of view, active filter's current detection point is located before the compensation point. This type of detection and control method is suitable for localized harmonic current compensation. It is less cost effective when more than one load branches require harmonic compensation. This is because more than one active filter (or remote sensing point) is required in such multi branches network. Therefore, source side current detection method is suggested in order to overcome the shortage of the load side current detection method. Detecting source side current for compensation require fewer compensators or sensors as the number of the source side branches is usually less than that of the load side branches.

This type of harmonic detection method has the risk of creating harmonic resonance if passive harmonic filters are installed in parallel with the active filter [53,54]. In this case, certain harmonic component will be amplified rather than eliminated. Figure 2.12 shows a system with both source current detection active filter and passive filter connected in parallel.
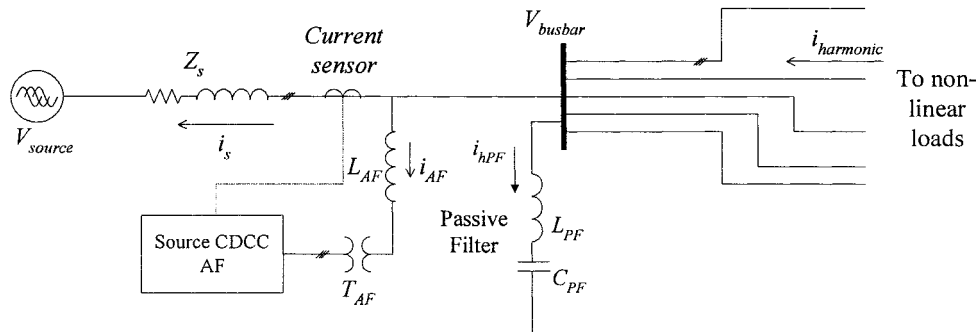
Figure 2.12: A typical power system consisting of a source of harmonics current detection circuit, active filter and passive harmonic filter

The active filter changes the natural frequency of the network (passive filter impedance associates with the system's source impedance). Recall the Equation 2.3 and Figure 2.3; where, a parallel resonance phenomenon will always appear lower than the passive filter tuned frequency. When an active filter is installed into the system, it causes system's resonance frequency to change from the one shown in Equation (2.3) to:

$$f_r = \frac{1}{2\pi} \sqrt{\frac{1-k}{\left[(1-k)L_{PF} + L_{sys}\right]C_{PF}}} \qquad (2.4)$$

Equation (2.4) shows that, the parallel frequency caused by the passive filter (associated with the system's source impedance) is shifted (affected) by the proportional gain (controller) of the active filter (k) [53,54], and the graphical representation of this phenomenon is shown in Figure 2.13. The figure shows that, without proper control, at a particular gain (k) the resonance point, parallel resonance can happen at one of the dominant harmonic frequency.
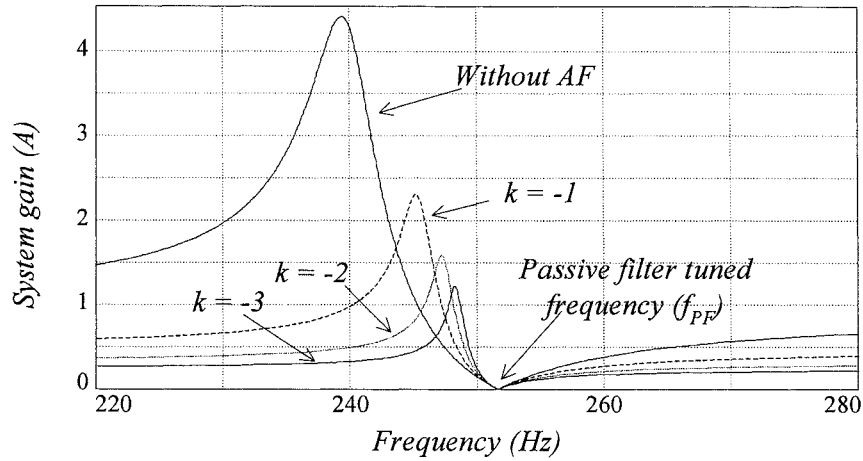
Figure 2.13: System resonance point affected by the active filter gain (*k*)

In fact, there is another concern to be taken into account when installing source side current detection active filter together with passive component, like PFC capacitor. If the PFC capacitor is connected between the sensing and the compensation points of the active filter as shown in Figure 2.14, it has the risk of elevating system's resonance probability. The reason is that, when harmonic resonance occurs, the voltage across the source/system impedance and the capacitor (V_{busbar}) will be amplified (and in phase with the harmonic current generated by the non-linear load (i_h)). The voltage amplification at that point will cause the current flow into the junction to increase (both i_s and i_c). If the sensing point of the active filter is located at the source branch (detecting i_s), then the current detected by the active filter will be the current produced by the resonated busbar voltage and the branch inductive impedance (which is in 90 degree phase lagging and much higher when compared to the i_h). Therefore, the compensation current (i_{AF}) injected by the active filter into the system is different from the desired compensation current. This current is no longer 180 degree out of phase and is much higher in amplitude. When this happens, the active filter is acting as a

positive feedback gain as the difference between i_h and the compensation current (i_{AF}) will produce a higher excitation current to the resonance.
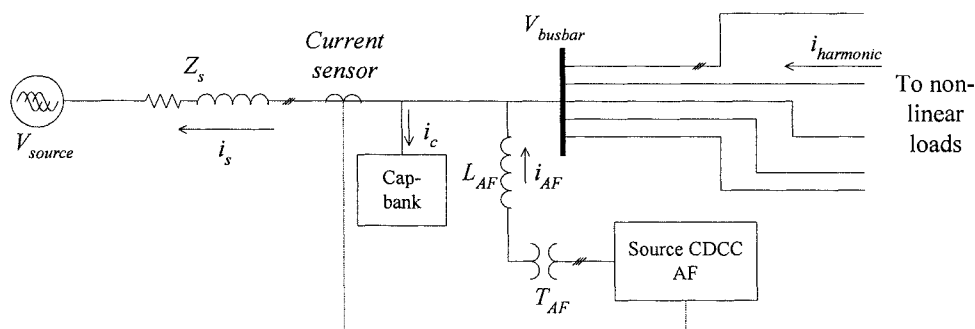
Figure 2.14: A simplified power system diagram

2.3.2 Voltage-Detection Current-Compensation (VDCC)

Most active filters used in power systems are based on the CDCC method, and they are utilised by individual end users/power consumers. CDCC base active filter is not cost effective for use in distribution networks. In general, distribution networks consist of more than one source and load branches [55]. In addition, utilities are required to deal with the overall power quality of a power network instead of localized harmonic problem. From this point of view, a voltage detection control strategy that can be used by utilities was proposed in the mid 90s by H. Akagi, et al. [21,32,56-58]. The voltage detection method is the most suitable solution for the system with many load and source branches. With the voltage detection, location of the active filter is no longer a critical issue as it was in the CDCC controlled active filters.

An active filter implementing this type of control strategy behaves like a resistor to the selected harmonic component. In such control method, detected harmonic voltage (V_h) is processed and used as a reference to regenerate the compensation current (I_{af}) that is going to be injected into the system by the active filter. The amount of compensation current (opposite in polarity to the system harmonic current) injected into the system will depend on a controllable gain (K_v). As a result, active filters utilising this control strategy behave as a pure resistor (refer to Equation (2.5)) and provide a low resistance path to the selected harmonic components. This results in a resonance damping effect.

$$I_{af} = V_h \cdot K_v \tag{2.5}$$

The voltage detection strategy mentioned above is a better solution to avoid the problem of multiple sensing points and active filters installation point in the power networks with more than one load and source branches. However, there is a problem when converting the detected harmonic voltage into a compensation current. In VDCC method, harmonic voltage at the resonance point (during resonance) is always assumed to be in phase with the harmonic current generated by non-linear load (the excitation source). Thus, compensation current is controlled to be 180 degree out of phase with respect to the detected voltage in order to cancel off the harmonic current that causes resonance. However, in practice, harmonic voltage and current at the resonance point will only be in phase when the resonance is happens exactly at that harmonic frequency. Otherwise, harmonic impedance at the resonance point can still be inductive or capacitive (depends on the system's condition). This creates problem for producing the desire compensation current as the detected harmonic voltage is no longer in phase with the harmonic current that is due to be compensated.

2.4 Dynamic Response in Real-time Harmonic Resonance

Attenuation Applications

Active filters may be used to provide better harmonic resonance attenuation in modern power networks. The use of power electronics devices in active filters gives highly flexible and dynamic characteristics. Active filters monitor harmonics components in the network and use these as reference signals to perform real-time adjustments in order to track and compensate the selected harmonic components. In such applications, the speed of obtaining the reference signal is very important as it determines the response of the active filter and hence the resultant harmonic attenuation [59]. Harmonics extraction is a major delay component in obtaining the PWM reference signal and implementing the harmonic compensation algorithm.

CHAPTER 3

HARMONIC EXTRACTION

3.1 Introduction

An active filter works as a harmonic source. It reproduces the selected harmonic component that is synchronised but opposite to the harmonic current in the network to achieve the desired compensation. Generally, the desired harmonic components are reproduced by a PWM inverter. It is necessary to extract the interested harmonic component from the distorted current or voltage waveforms at the compensation point to obtain the reference signal for the PWM inverter. In some compensation schemes,

fundamental component is removed from the distorted signal and use the remaining non-fundamental components (harmonics) to performance Total Harmonic Compensation (THC) [21,36].

Typically, harmonic orders higher than 13th are considered as non-dominant harmonic components. They are relatively small (negligible) compared to the dominant harmonic components. Therefore, in some approaches e.g. hybrid filter, active harmonic filter is only required to handle one or several selected dominant harmonic components. This type of compensation method is referred to as Individual Harmonic Compensation (IHC) or Selective Harmonic Compensation (SHC).

Regardless of the use of THC or IHC (or SHC), active filter always needs the selected harmonic information to perform harmonic compensation. Existing harmonic extraction techniques can be largely categorised into two major categories. They are either based on spectra techniques (e.g. Fourier Transform) in frequency domain or filtering techniques in time domain (e.g. synchronous fundamental).

3.2 Frequency Domain Harmonic Extraction

Harmonic extraction in frequency domain is also known as 'Frequency Domain Filtering'. During the extraction operation, harmonic contents of a distorted signal are transformed from time domain into frequency domain and the results are always presented in the form of spectra. Extraction is performed directly in the frequency

spectrum by selecting only the interested harmonic components and excluding the unwanted harmonic components and noises. Extracted harmonic component is represented by its frequency, amplitude and phase. Active filter will then use these information to reconstruct the selected harmonic components and present in the time-domain. Due to the process of inter-domains transformation, this type of harmonic analysis is more complicated and more computationally intensive compared to time-domain extraction techniques.

Many frequency domain extractions are developed based on the orthogonal principle to transform harmonic component from time domain to frequency domain (e.g Fourier transform, Walsh transform, Hartley transform, etc.). Among all, Fourier transform (FT) is the most widely used time to frequency transformation method. The basic mathematical representation of the FT is shown by Equation (3.1).

$$F(n,\omega) = \frac{1}{T_0} \int_t^{T_0+t} f(t)e^{-jn\omega_0 t} \tag{3.1}$$

where,

n -   harmonic order

ω -   frequency of the fundamental harmonic component (rad/sec)

T_0 -   period of the fundamental harmonic component

Due to the increasing use of digital data processing, principle of FT is further developed to accommodate the requirement of digitisation. As a result, Discrete Fourier Transform (DFT) is developed. DFT sampled both time and frequency

information in to an equal number of samples (N). Thus, a total of N^2 times of complex multiplication are required for every periodic signal transformation. The intensive computational process has made it impractical to implement DFT in real life applications. Fast Fourier Transform (FFT) is known as the simplified version of DFT. It reduces the calculation process required by DFT and hence the burden of digital processor. These techniques are developed based on the Fourier transform.

The advantages of using Fourier transform for individual harmonic extraction are that; it has a very good attenuation factor, no overshoot and no oscillation/stability problems. With these three advantages, Fourier transform provides an almost perfect extraction profile as can be seen in Figure 3.1. The figure shows that, a Fourier transform base harmonic extractor extracts a 7th order harmonic component out from a distorted signal that consists of 1st, 5th, 7th and 11th harmonic components. A step response is introduced to 7th order harmonic at t = 50 ms to test the response of the Fourier transform. The result showed that, Fourier transform needs a minimum of 20 ms to react to the change.
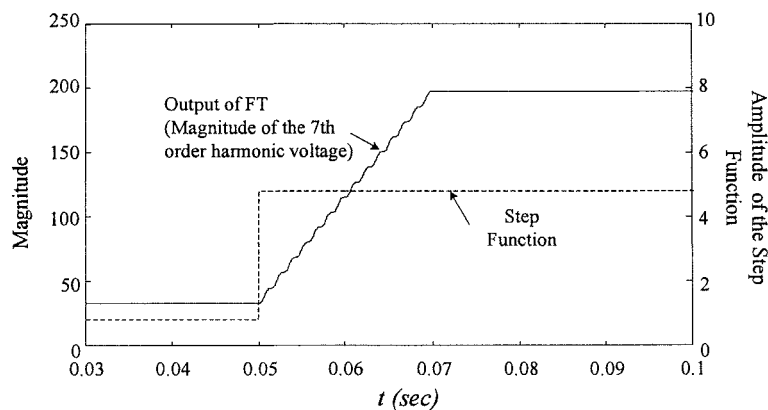
Figure 3.1: Response time of the Fourier Transform

However, few disadvantages appeared when using Fourier transform base techniques in real-time harmonic related applications. In [60] the authors discussed how the accuracy of Fourier transform may be affected by effects such as aliasing, leakage and picket fence.

- **Aliasing effect**

Aliasing effect is also known as "Fold over" effect, which is caused by insufficient sampling rate. This happens when the sampling rate is less than the Nyquist's Sampling Theorem ($f_{sw} \geq 2f_{max}$), and causes the image of the high frequency components being folded over from sampling frequency. When this happens, the original spectrum is affected by the folded over harmonic components. This phenomenon is graphically presented in Figure 3.2. The folded over effect is indicated by the dotted line, and it shows that the spectrum of original signal is distorted (at its edge). A detailed analysis of aliasing effect is presented in author's publication [61].
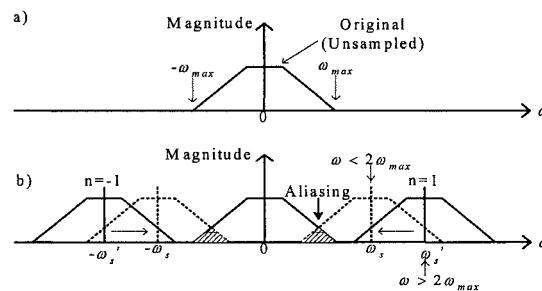
Figure 3.2: Aliasing phenomenon

- **Leakage effect**

Leakage effect mentioned in [60] is a phenomenon caused by interharmonics components. Interharmonics are classified as the non-characteristic harmonic components. It appears in between two characteristic harmonic frequencies, with a frequency that is a non-integer multiple of the fundamental harmonic frequency.

Therefore, when they exist, the integration process of the Fourier transform on these components causes non-zero result that affects the transformation. This phenomenon is sometime called as "pseudo-aliasing".

- **Waste of resources**

Waste of resources is another problem associated with Fourier transform in real time harmonic monitoring or extraction applications. As a general approach to the harmonic analysis, all the harmonic components within the selected window are calculated, which is not necessary in some applications e.g. individual harmonic extraction. Many harmonic related applications may require only the information of a few dominant harmonic components (i.e.: 5th, 7th, 11th, etc.) to perform Individual Harmonic Compensation. The total harmonic calculation carried out by Fourier transform results a waste of resources. High computational requirement increases the total cost.

- **Time delay**

The biggest drawback when using Fourier transform base harmonic extractor to extract power system's harmonic component is its inherent time delay introduced by the periodic integral function in Fourier transform. With this, sample over one cycle of the lowest frequency signal is required in order for the Fourier transform to compute the harmonic content in the distorted signal. In the case of power system's harmonic problem, fundamental harmonic component is always treated as the lowest frequency component. Therefore, a minimum of one fundamental cycle is always required for Fourier transform to complete the process of transformation. This means, a minimum

transaction period of 20 *ms* (in 50 *Hz* power systems) is always needed. This phenomenon is clearly shown in the Figure 3.1, where, when a step function is introduced to the 7th order harmonic component, time taken for Fourier transform to change from one state to another is 20 *ms* (one fundamental cycle).

Apart from Fourier analysis, techniques such as nim-nom and prony were proposed in the more recent research discussion. These techniques were discussed by Leonowicz, et al. in [62]. It has been shown that, these techniques are generally capable of providing better accuracy than Fourier's. However, the computational complexity of nim-nom and prony techniques is far beyond Fourier transformation. In addition, similar to Fourier transform, the basic time required for these techniques to process is at least one fundamental cycle.

3.3 Time Domain Harmonic Extraction

In this section, time domain harmonic extraction techniques that are based on the filtering principle are discussed.

3.3.1 Conventional filtering

This is the simplest time-domain harmonic extraction technique that is used since late sixties to extract harmonic components from the distorted signal [2]. It uses a conventional analogue filter (e.g. high-pass, low-pass, notch filter, etc) to extract the

interested harmonic components from a distorted signal. This technique is used mainly

due to the simplicity and its highly competitive cost (it is cheap to use analogue

component in time-domain). However, it suffers from a few drawbacks, such as phase

delay, magnitude errors, time delay, etc. For the application like active harmonic filter,

the effect of magnitude error and slow response are unacceptable as the active filter's

output needs to synchronise to the system's harmonic component.

There are several ways of implementing filters to obtain the required harmonic

voltage/current reference for the PWM inverter. One is via the use of high-pass filter to

remove the low frequency harmonic components (i.e.: fundamental harmonic

component) and uses the remaining higher frequency (non-fundamental) harmonic

components as the reference signal for the regeneration process. This type of filtering

technique is very simple and low cost, but the use of high-pass filter makes it very

vulnerable to noise. As all components higher than the filter cut-off frequency

(including white noise) are bypassed.

An alternative to this is implementing a low-pass filter to obtain the fundamental

harmonic component, then inverts it and uses it in the later stage to subtract (cancel

off) the fundamental component in the distorted signal. As a result, only non-

fundamental harmonic components remain in the signal. This process is graphically

shown in the Figure 3.3.
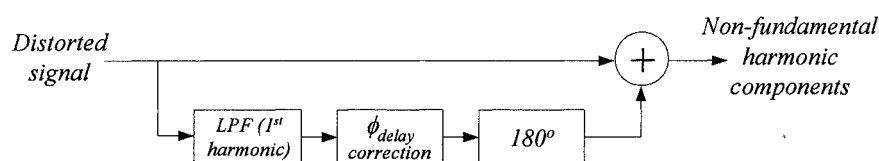
Figure 3.3: Fundamental component extraction process

With the use of low-pass filter, the noise issue found in the previous method (use high-pass filter) can be resolved. However, it still has drawbacks, such as time delay (slow response) and the magnitude error due to the attenuation factor of the filter. As a nature of time domain filter, higher attenuation causes slower response.

Both techniques mentioned above are mainly for total harmonic extraction (THD), in which the fundamental harmonic component is removed and other remained non-fundamental harmonic components are processed as reference signals for the PWM inverter. For individual harmonic extraction, band-pass or notch filters are usually applied. They are tuned to a selected harmonic frequency in order to extract one or several harmonic components. These methods are rather straightforward and less explore to the noise. Again, they suffer on compromising both response and attenuation.

3.3.2 Frequency modulation method

This is one of the classic methods of harmonic extraction. This technique is based on the frequency modulation method; a very common technique used in the communication field [63] to demodulate the carrier at the receiving end. Figure 3.4 shows the block diagram of the technique [64].
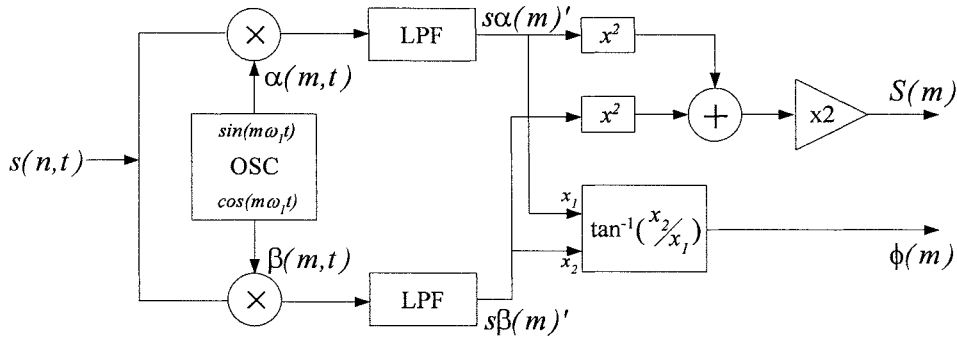
Figure 3.4: A block diagram of the frequency modulation method

As shown in the figure, detected signal ($s(n,t)$) is multiplied with a sinusoidal signal ($\alpha(m,t)$) and a cosine signal ($\beta(m,t)$) that are generated by a local oscillator. Frequency of the oscillator can be tuned to any of the integer multiple (m) of the system fundamental frequency ($m\omega_1$), where,

$$s(n,t) = \sum_{n=1}^{\infty} S(n)\sin(n\omega t \pm \phi) \tag{3.2}$$

and,

$$\alpha(m,t) = \sin(m\omega_1 t) \tag{3.3}$$

$$\beta(m,t) = \cos(m\omega_1 t) \tag{3.4}$$

Therefore, the multiplication yield,

$$s\alpha(m,n,t) = \frac{1}{2}\left\{ S(m)\cos(\phi(m)) - \sum_{n=1}^{\infty} S(n)\cos\left[(n+m)\omega_1 t + \phi(m)\right] \right\} \tag{3.5}$$

$$s\beta(m,n,t) = \frac{1}{2}\left\{ S(m)\sin(\phi(m)) + \sum_{n=1}^{\infty} S(n)\sin\left[(n+m)\omega_1 t + \phi(m)\right] \right\} \tag{3.6}$$

It can be seen that, both results shown in Equation (3.5) and (3.6) are consist of a constant and an a.c. term. The a.c. term is then filter out via a low pass filter and left

only the d.c. value that has the information of the selected harmonic component. Equation (3.7) and (3.8) showed that the resulted signal after low pass filtering.

$$s\alpha(m)' = \frac{1}{2}S(m)\cos(\phi(m)) \tag{3.7}$$

and

$$s\beta(m)' = \frac{1}{2}S(m)\sin(\phi(m)) \tag{3.8}$$

The magnitude and phase information of the signal can be obtained via:

$$S(m) = 2\left[s\alpha(m)^2 + s\beta(m)^2\right]^{\frac{1}{2}} \tag{3.9}$$

and

$$\phi(m) = \tan^{-1}\left[\frac{s\beta(m)}{s\alpha(m)}\right] \tag{3.10}$$

Amplitude and phase information shown in (3.9) and (3.10) can be used in the reconstruction process to convert the extracted harmonic signal back to the time varying signal, and use it as a reference signal for active filter's controller.

This method is simple and applicable to both single phase and three-phase systems. However, both low pass filters have to be very selective in order to eliminate the ripple signal. Therefore, to obtain a 5% accuracy, it usually require a minimum response time of 60 ms [64].

3.3.3 Instantaneous reactive power harmonic extraction technique (p-q method)

This is a very famous time-domain harmonic extraction technique based on p-q transformation [65,66]. This technique has now been practically implemented in commercial applications. With the use of the generalised Clark's transformation, instantaneous three-phase voltage and current signals are transformed into 2-axis $\alpha\beta$ components by,

$$\begin{bmatrix} v_\alpha(t) \\ v_\beta(t) \end{bmatrix} = \sqrt{\frac{2}{3}} \begin{bmatrix} 1 & -\dfrac{1}{2} & -\dfrac{1}{2} \\ 0 & \dfrac{\sqrt{3}}{2} & -\dfrac{\sqrt{3}}{2} \end{bmatrix} \begin{bmatrix} v_a(t) \\ v_b(t) \\ v_c(t) \end{bmatrix} \qquad (3.11)$$

and,

$$\begin{bmatrix} i_\alpha(n,t) \\ i_\beta(n,t) \end{bmatrix} = \sqrt{\frac{2}{3}} \begin{bmatrix} 1 & -\dfrac{1}{2} & -\dfrac{1}{2} \\ 0 & \dfrac{\sqrt{3}}{2} & -\dfrac{\sqrt{3}}{2} \end{bmatrix} \begin{bmatrix} i_a(n,t) \\ i_b(n,t) \\ i_c(n,t) \end{bmatrix} \qquad (3.12)$$

Where the three-phase instantaneous voltage signal are:

$$\begin{aligned} v_a(t) &= V_{pk}\, sin(\omega_0 t) \\ v_b(t) &= V_{pk}\, sin(\omega_0 t - \frac{2\pi}{3}) \\ v_c(t) &= V_{pk}\, sin(\omega_0 t + \frac{2\pi}{3}) \end{aligned} \qquad (3.13)$$

and the three-phase instantaneous current signal are:

$$i_a(n,t) = \sum_{n=1}^{\infty} I_{pk}(n)\, sin(n\omega_0 t)$$

$$i_b(n,t) = \sum_{n=1}^{\infty} I_{pk}(n)\, sin(n\omega_0 t - \frac{2n\pi}{3})$$ (3.14)

$$i_c(n,t) = \sum_{n=1}^{\infty} I_{pk}(n)\, sin(n\omega_0 t + \frac{2n\pi}{3})$$

Equations (3.11) to (3.14) reveal that, the technique assumes only current distortion exist, no voltage distortion (or it is negligible) and that all three phases are balanced

With the voltage and current component in $\alpha\beta$-domain, the instantaneous active $(p(n,t))$ and reactive $(q(n,t))$ power of the detected (distorted) signal can be obtained via:

$$\begin{bmatrix} p(n,t) \\ q(n,t) \end{bmatrix} = \begin{bmatrix} v_\alpha(t) & v_\beta(t) \\ -v_\beta(t) & v_\alpha(t) \end{bmatrix} \begin{bmatrix} i_\alpha(n,t) \\ i_\beta(n,t) \end{bmatrix}$$ (3.15)

Both active and reactive power shown in Equation (3.15) contain a d.c. term and an a.c. term, which can be represented as,

$$p(n,t) = p_{dc} + p_{ac}(n,t)$$
$$q(n,t) = q_{dc} + q_{ac}(n,t)$$ (3.16)

For the purpose of harmonic extraction, all the a.c. terms in both active and reactive power are eliminated by applying low-pass filters as shown in Figure 3.5. Cut-off frequencies of the low-pass filters are set to only pass the d.c. component of p and q. After the filtering process, all a.c. terms ($p_{ac}(n,t)$ and $q_{ac}(n,t)$) are no longer exist.

Magnitude and phase of the fundamental voltage and current are contained in the p_{dc} and q_{dc}. As only current information is interested, a reverse transformation is then

required in order to obtain the current information from the active and reactive power components. This involved inversed voltage matrix that was shown in Equation (3.15) to this,

$$\begin{bmatrix} i_\alpha(t) \\ i_\beta(t) \end{bmatrix} = \begin{bmatrix} v_\alpha(t) & v_\beta(t) \\ -v_\beta(t) & v_\alpha(t) \end{bmatrix}^{-1} \begin{bmatrix} p_{dc} \\ q_{dc} \end{bmatrix} \qquad (3.17)$$

As shown in Figure 3.5, in order to convert the current from i_α and i_β back to three-phase fundamental current (i^*_a, i^*_b and i^*_c), a transposed matrix that is shown in Equation (3.12) is used,

$$\begin{bmatrix} i^*_a(t) \\ i^*_b(t) \\ i^*_c(t) \end{bmatrix} = \sqrt{\frac{2}{3}} \begin{bmatrix} 1 & 0 \\ -\dfrac{1}{2} & \dfrac{\sqrt{3}}{2} \\ -\dfrac{1}{2} & -\dfrac{\sqrt{3}}{2} \end{bmatrix} \begin{bmatrix} i_\alpha(t) \\ i_\beta(t) \end{bmatrix} \qquad (3.18)$$

The harmonic free three-phase fundamental currents will be used to subtract the fundamental harmonic component in the original current signals (shown in Equation (3.14)). After the subtraction, the remaining non-fundamental harmonic components will later be used as a reference signal for the active filter to performance total harmonic compensation. Algorithm of this technique is graphically shown in Figure 3.5.
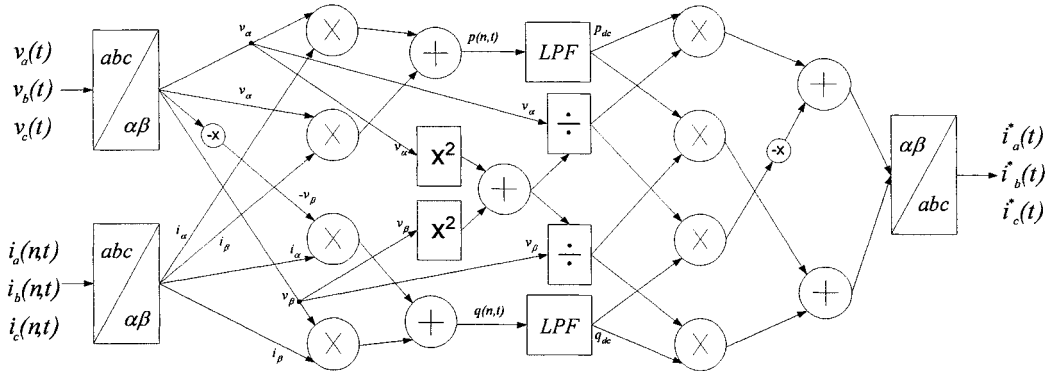
Figure 3.5: A block diagram of the instantaneous active and reactive harmonic extraction technique

3.3.4 Synchronous-detection harmonic extraction

This is a simplified version of the above mentioned harmonic extraction technique. This technique is cleverly making use of the relationship of those available power elements (i.e.: voltage, current and active power) [67]. Apart from not calculating the reactive power, this technique is very similar to the one discussed in section 3.3.3, which relies on non-distorted system voltage and balanced three-phase quantities. Average power of the system is calculated and divided equally among the three phases and use it to obtain the required compensation current.

The very first step of this extraction technique is to work out the total power consumed by the loads/systems:

$$p_{total}(n,t) = \begin{bmatrix} v_a(t) & v_b(t) & v_c(t) \end{bmatrix} \begin{bmatrix} i_a(n,t) \\ i_b(n,t) \\ i_c(n,t) \end{bmatrix} \tag{3.19}$$

Instantaneous voltage and current used in above equation are same as the one predefined in the section 3.3.3 (Equation (3.13) and (3.14)). Whiles, $P_{total}(n,t)$ is the

total instantaneous power in the system, which consists of instantaneous active power (d.c. term) and instantaneous fictitious power (a.c. term), as described in the previous section (first half of Equation (3.16)).

The real power (d.c. term) is the product of the fundamental component of THE detected voltage and current. Thus, it is consists only fundamental harmonic information. Similarly, a low-pass filter is used to eliminate the unwanted a.c. term, and obtain the total active power (the d.c. term). However, for this algorithm, per phase active power is of interest instead of the total power. Therefore, the following procedures are used to figure out the phase power for all three-phases (p_a, p_b and p_c). Due to the balanced condition assumption, per phase power is able to obtain by splitting the total active power equally into three equal quantities as shown in the following equations:

$$p_a = p_{dc} \frac{V_{apk}}{V_{apk} + V_{bpk} + V_{cpk}} \tag{3.20}$$

and,

$$p_a = p_b = p_c \tag{3.21}$$

By knowing that (use phase-a as an example), the phase impedance (z_a) can be derived from the r.m.s. phase voltage (V_{aRMS}) and the phase power (p_a):

$$p_a = \frac{V_{aRMS}^2}{z_a} = \frac{V_{apk}^2}{2z_a} \tag{3.22}$$

And the phase impedance (z_a) is the ratio of the instantaneous phase voltage ($v_a(t)$) and the instantaneous phase current ($i_a^*(t)$):

$$z_a = \frac{v_a(t)}{i_a^*(t)} \qquad (3.23)$$

Equation (3.22) can be further expanded, and the phase current $(i_a^*(t))$ can be obtained via:

$$i_a^*(t) = \frac{2v_a(t)p_a}{V_{apk}^2} \qquad (3.24)$$

The phase current $(i_a^*(t))$ shown in Equation (3.24) is the fundamental component of the distorted current that is shown in Equation(3.19). With this, the active filter reference (compensation) current $(i_{aREF}(n,t))$ can be calculated via:

$$i_{aREF}(n,t) = i_a(n,t) - i_a^*(t) \qquad (3.25)$$
$$\scriptstyle n<1\to\infty \qquad\quad n=0\to\infty$$

Similar steps (from Equation (3.22) to (3.25)) are applied to another two phases (phase-b, and phase-c) to obtain the relevant compensation (reference) currents. Figure 3.6 shows the block diagram of the extraction algorithm. This algorithm is only applicable to total harmonic compensation applications.
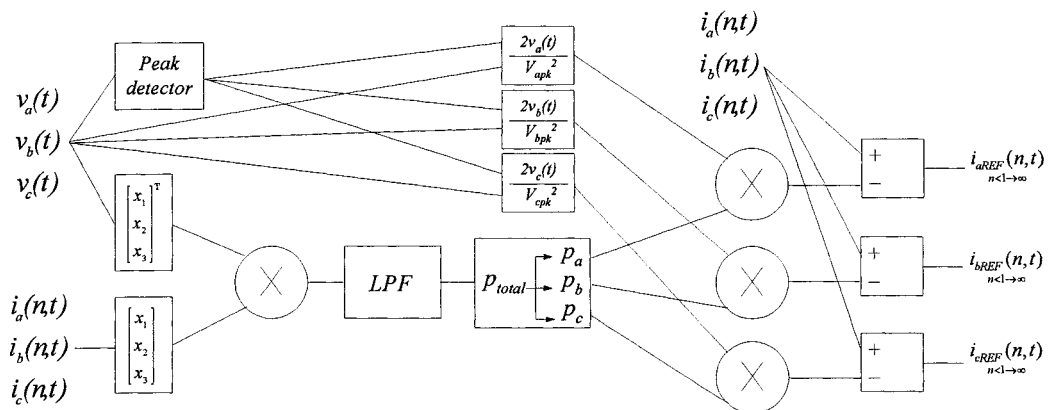
Figure 3.6: A block diagram of the synchronise-detection harmonic extraction method

3.3.5 Synchronous frame base harmonic extraction

Instantaneous reactive power harmonic extraction technique and synchronous-detection harmonic extraction technique are used in applications requiring total harmonic compensation. They are designed for harmonic current compensation and no voltage distortion is allowed. The use of system's voltage in the calculation has made them sensitive to the voltage harmonics. In order to get rid of all these constrains (only applicable to THC and voltage harmonics dependency), a different approach based on d-q technique is developed. This technique makes use of the generalised Park Transformation to convert the selected harmonic component from a 3-phase stationary reference frame to a synchronous reference frame and then perform harmonic extraction by three simple constructed low-pass filters [64,68,69]. It sounds similar to the aforementioned techniques, but because of not utilising the systems voltage during the extraction, this technique is in fact independent from the voltage harmonic distortion. In addition, it is capable to performance both total and individual harmonic extractions. Figure 3.7 shows the block diagram for this harmonic extraction technique.
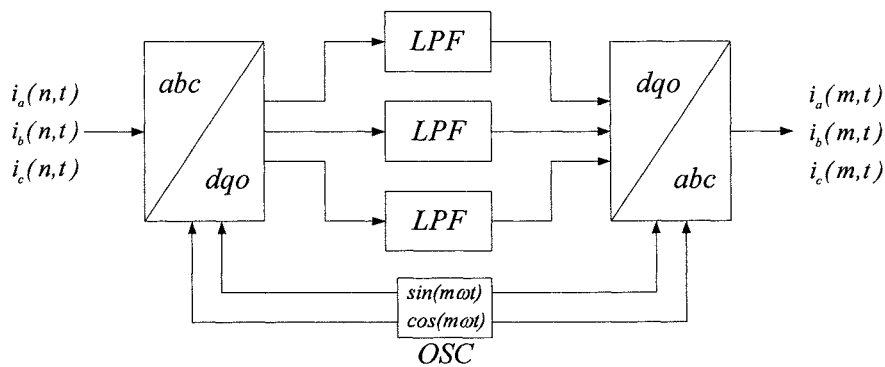
Figure 3.7: Harmonic extraction using d-q technique

The reason it can be independent from voltage distortion is due to the use of frequency adjustable local oscillator (OSC). This local OSC is used to substitute the function of system voltage stage in the previous mentioned techniques. With this, it gained the consistency and stability from using the oscillation signal for the conversion. In addition, unlike the fixed 50 *Hz* (or 60 *Hz*) voltage signal used in the aforementioned sections, frequency of the oscillator is fully controllable in this technique. This is important, as it enables the technique to perform individual harmonic extraction.

The technique is begun by converting the three-phase signals (a, b, c) into direct (d), quadrature (q), and an extra zero-sequence component (o). Mathematical expression of the conversion is shown in the following equation:

$$
\begin{bmatrix} i_d(m,n,t) \\ i_q(m,n,t) \\ i_o(m,n,t) \end{bmatrix} = \frac{2}{3} \begin{bmatrix} sin(m\omega t) & sin(m\omega t - \frac{2m\pi}{3}) & sin(m\omega t + \frac{2m\pi}{3}) \\ cos(m\omega t) & cos(m\omega t - \frac{2m\pi}{3}) & cos(m\omega t + \frac{2m\pi}{3}) \\ \frac{1}{2} & \frac{1}{2} & \frac{1}{2} \end{bmatrix} \begin{bmatrix} i_a(n,t) \\ i_b(n,t) \\ i_c(n,t) \end{bmatrix} \quad (3.26)
$$

The d and q elements are formed up by a d.c. quantity and the a.c. quantities. In which, d.c. term representing the magnitude of the selected (m^{th} order) harmonic component. The a.c. terms are the rest of the harmonic components. Low-pass filter is used to filter out the a.c. components and bypassed only the d.c. component. The following stage is the back conversion, which used to convert the d.c. only d-q current back to the three-phase quantities. The back conversion is mathematically shown in Equation(3.27):

$$
\begin{bmatrix} i_a(m,t) \\ i_b(m,t) \\ i_c(m,t) \end{bmatrix} = \frac{2}{3} \begin{bmatrix} sin(m\omega t) & sin(m\omega t - \dfrac{2m\pi}{3}) & sin(m\omega t + \dfrac{2m\pi}{3}) \\ cos(m\omega t) & cos(m\omega t - \dfrac{2m\pi}{3}) & cos(m\omega t + \dfrac{2m\pi}{3}) \\ \dfrac{1}{2} & \dfrac{1}{2} & \dfrac{1}{2} \end{bmatrix}^{-1} \begin{bmatrix} I_d(m) \\ I_q(m) \\ I_o(m) \end{bmatrix} \quad (3.27)
$$

The three-phase signal ($i_a(m,t)$, $i_b(m,t)$, $i_c(m,t)$) are now only contents the selected harmonic component (m^{th}).

Other than IHE described above, synchronous frame harmonic detection method is also has the flexibility of performing THE operation. To extract all non-fundamental harmonic components, the local oscillator frequency has to be set to the fundamental frequency ($m = 1$). By doing this, the fundamental harmonic component will be tracked and converted to d.c. quantity. All other non-fundamental harmonic components are turned into a.c. components in the d-q domain. With the help of low-pass filters, all non-fundamental harmonic components (the a.c. term) are filtered off. Only fundamental harmonic component is remained. When applying reverse conversion, only fundamental component is appearing to as the three-phase signal. In order to obtain those non-fundamental harmonic components, the subtraction method mentioned in the section 3.3.1 to 3.3.4 is used. Where, the cleaned/processed fundamental three-phase signal is used to subtract the fundamental component in the original (distorted) three-phase signal. With this, the fundamental harmonic component in the distorted signal is cancelled off by the superimpose effect and results only non-fundamental harmonic components.

CHAPTER 3

3.3.6 Common problems in time domain harmonic extraction

As shown on the previous sections (3.3.1 to 3.3.5), filters are widely occupied in the time-domain harmonic extractions. This creates problem when the extractor is used in a dynamic environment e.g. harmonic extraction application in power systems. Extraction results are often affected by the problems such as time delay (propagation delay) and magnitude distortion due to insufficient attenuation factor.

The most common filter designs are Butterworth, Chebyshev I/II, and Bessel types. However, in this thesis, attention is focused on the Butterworth type lowpass filter; as it has been generally acknowledged as a good "all rounder" filter type that gives flat response in the pass band and an adequate rate of rolloff.

Advantages of the time domain harmonic extraction methods are, straightforward/fewer arithmetic process required and lower computer memory is needed. However, the drawbacks like time delay, phase distortion, and magnitude distortion are also introduced at the same time due to the use of filters.

In order to ensure the synchronisation between reproduced harmonic compensation components and the system harmonic components, active filter has to be highly dynamic. As a result, any delay in the process of regenerating harmonic components use for compensation is principally unacceptable. However, the inherent contradiction between the frequency response and time response of a filter creates problem whether to have a good rolloff (better attenuation) or faster response. The higher the filter order (*n*) the steeper the rolloff in the frequency response and results a better attenuation

CHAPTER 3

effect, but at the same time, it creates a further delay in the time response of the filter. This phenomenon is clearly shown in following figures. Figure 3.8 shows the frequency response curve for different order Butterworth filters and Figure 3.9 shows the step response (time response)
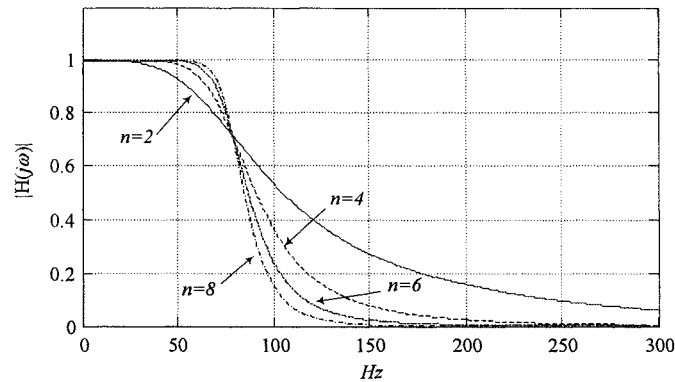
Figure 3.8: Frequency response of nth order Butterworth lowpass filter
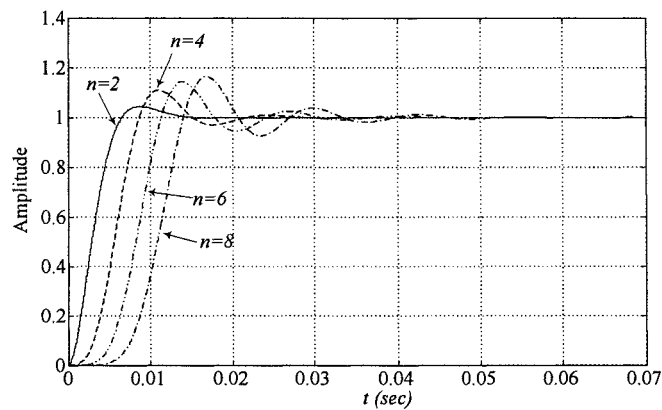
Figure 3.9: Step response of nth order Butterworth filter

Generally, in order to obtain only the interested harmonic component for use in the harmonic compensation, attenuation factor of the filter must be sufficient to be able to filter out the unwanted harmonic components. This is not a problem if only

fundamental harmonic component is of interest in the application. As the ratio of other

harmonic quantities with respect to the fundamental harmonic component is high, a

low attenuation (order) filter is enough to filter out the unwanted (non-fundamental)

harmonic components. However, in the case, when one of the non-fundamental

harmonic components is interested (i.e.: 5th, 7th or, 11th). Its amplitude is often lower

when compared to the fundamental harmonic component. Thus, a high attenuation

filter is required to get rid of other higher magnitude harmonic components (i.e.: 1st &

5th if 7th is of interest). As a result, higher order filter is required and longer delay is

expected.

For example, to extract a 7th order harmonic voltage in a typical 415 V system, which

fundamental voltage is 230 V and 7th harmonic voltage is about 14% (33 V) of the

fundamental voltage. Use technique with generalised Park Transformation and

integrated low-pass filters (synchronous frame based harmonic extraction technique

mentioned in section 3.3.5) as an example to extract the 7th order harmonic voltage. In

order to demonstrate the effect of insufficient attenuation and participation of the time

delay when higher order filter is used; a step function is applied to amplify the 7th

harmonic voltage at $t = 5$ ms. Figure 3.10 shows the result when 2nd order low-pass

filter is used. The result showed that, unwanted harmonic components still appear in

the filtered signal (as a ripple). The same figure also showed the result when higher

order filter ($n = 6$) is used. It produces a smoother/ripple-less output signal with

compare to the previous one. However, the time response of the 6th order filter is

significantly slowed down.
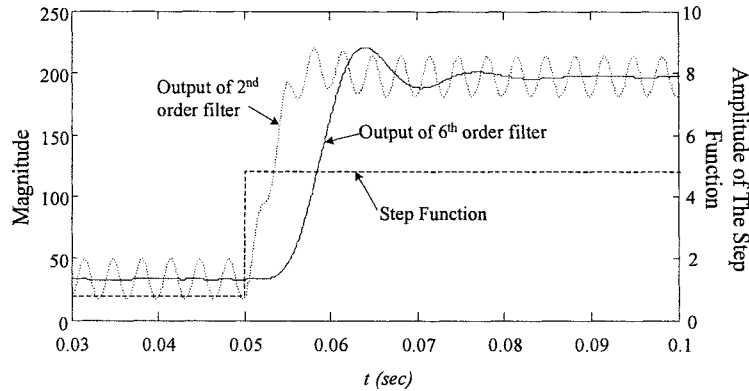
Figure 3.10: Effect of filter order

In practice, despite the longer time delay, high order filter will never be the best approach as every order (stage) brings in offset and noise error to the pass-band region. In addition, high order filters often facing stability issues. It is familiar to most of the filter design engineers that, onboard tweaking (e.g. capacitors, variable resistors, etc) to avoid oscillation is always required when using high order filter in the design.

3.4 Other Approaches of Harmonic Extraction

Apart from the techniques mentioned in sections (3.2 and 3.3), there are numerous other harmonics estimation techniques, which have then proposed for use in the harmonic extraction applications. Techniques based on Least Mean Square algorithm such as Kalman Filter and Artificial Neural Network (ANN) are claimed to have better performance than the conventional harmonic extraction methods. For example, Kalmen filter technique proposed by Girgis, et al [70] requires only half a cycle to extract a harmonic component with high degree of accuracy. Later, an improved Kalmen filter

technique that has a delay of a quarter of a fundamental cycle is proposed by Moreno et. al. [71]. However, the computational complexity involved in Kalman Filter has make it less appealing for real-time hardware implementation [72].

Generally, ANN base harmonic estimators are performed well in steady-state. However, due to the neural learning process, adaptive (recursive) ANNs usually require longer time/delay to perform harmonic extraction in a dynamic condition (required minimum 30 ms as mentioned in [73]). Janaka. W et al [72] have proposed a non-recursive ANN base harmonic estimator to extract selected harmonic component. Without the learning period, response of the non-recursive ANN base harmonic extractor is improved as it requires only quarter of a fundamental cycle.

CHAPTER 4

FAST INDIVIDUAL HARMONIC EXTRACTION (FIHE)

4.1   Introduction

4.2   Principle

4.3   Applying the FIHE in *50* Hz Systems

4.4   Reconstruction of the Extracted Harmonic Component

4.5   Applying the FIHE in Unbalanced

4.1 Introduction

Time delay is the major drawback of using existing harmonic extraction techniques in power systems. A new harmonic extraction technique having better dynamic performance is developed to overcome this problem. This technique is based on the principle of orthogonal and Park's transformation to extract individual harmonic component in time domain. It is named as 'Fast Individual Harmonic Extraction (FIHE)' technique. FIHE provides a faster harmonic extraction than any other previously mentioned techniques without sacrificing (compromising) the accuracy.

4.2 Principles of the FIHE

Consider the following balanced three-phase signal contents of harmonic order $n \in 2\mathcal{N} + 1$:

$$S_{ABC}(n,t) = \begin{pmatrix} S_A(n,t) \\ S_B(n,t) \\ S_C(n,t) \end{pmatrix} = \begin{pmatrix} M_n \sin(n\omega_0 t) \\ M_n \sin\left(n\omega_0 t - \dfrac{2n\pi}{3}\right) \\ M_n \sin\left(n\omega_0 t + \dfrac{2n\pi}{3}\right) \end{pmatrix} \tag{4.1}$$

where $\mathcal{N}$ is the set of natural numbers; consequently $2\mathcal{N} + 1$ is the set of positive odd numbers, and M_n is the magnitude of the nth order harmonic signal.

The signal $S_{ABC}(n,t)$ can be converted to a single-phase signal with a conversion function

$$\Gamma_d(m,t) = \left[\sin(m\omega_0 t) \quad \sin\left(m\omega_0 t - \frac{2m\pi}{3}\right) \quad \sin\left(m\omega_0 t + \frac{2m\pi}{3}\right) \right] \tag{4.2}$$

where $m \in 2\mathcal{N} + 1$. The resulting converted single-phase signal is given by

$$\begin{aligned} \beta(m,n,t) &= \frac{2}{3} \Gamma_d(m,t) S_{ABC}(n,t) \\ &= \frac{2}{3} M_n \sin(m\omega_0 t) \sin(n\omega_0 t) \\ &\quad + \frac{2}{3} M_n \sin\left(m\omega_0 t - \frac{2\pi m}{3}\right) \sin\left(n\omega_0 t - \frac{2\pi n}{3}\right) \\ &\quad + \frac{2}{3} M_n \sin\left(m\omega_0 t + \frac{2\pi m}{3}\right) \sin\left(n\omega_0 t + \frac{2\pi n}{3}\right) \end{aligned} \tag{4.3}$$

Refer to the trigonometry identities, $sin(a)sin(b) = \frac{1}{2}[cos(a-b) - cos(a+b)]$, hence,

Equation (4.3) becomes,

$$\beta(m,n,t) = \frac{1}{3}M_n\left[cos\left((m-n)\omega_0 t\right) - cos\left((m+n)\omega_0 t\right)\right]$$

$$+ \frac{1}{3}M_n\left[cos\left((m-n)\omega_0 t - \frac{2}{3}\pi(m-n)\right) - cos\left((m+n)\omega_0 t - \frac{2}{3}\pi(m+n)\right)\right]$$

$$+ \frac{1}{3}M_n\left[cos\left((m-n)\omega_0 t + \frac{2}{3}\pi(m-n)\right) - cos\left((m+n)\omega_0 t + \frac{2}{3}\pi(m+n)\right)\right]$$

(4.4)

Now, depending on the values of n and m, the value of $\beta(m,n,t)$ can either be zero or non-zero. To have a better and clearer insight of the values of $\beta(m,n,t)$, lets consider the following three sequences $\{u_k\}$, $\{v_k\}$, $\{w_k\}$; $(k = 0,1,2,...)$ defined as

$$\begin{aligned}
u_k &= 3k &&= 0,3,6,... \\
v_k &= 3k+1 &&= 1,4,7,... \\
w_k &= 3k+2 &&= 2,5,8,...
\end{aligned}$$

(4.5)

and let

$$\begin{aligned}
U &= \cup\{u_k\}\big|_{k=0,1,2...} &&= \{0,3,6,...\} \\
V &= \cup\{v_k\}\big|_{k=0,1,2...} &&= \{1,4,7,...\} \\
W &= \cup\{w_k\}\big|_{k=0,1,2...} &&= \{2,5,8,...\}
\end{aligned}$$

(4.6)

It can readily be seen that the sets, U, V and W forms a partition of the set of natural numbers $\mathcal{N}$ with no exceptional. That is,

$$\mathcal{N} = U \cup V \cup W \qquad = \{0,1,2,3,4,5,6,7,...\}$$

(4.7)

As mentioned earlier, both m and n are positive odd numbers. Consequently, the result of $|m-n|$ or $|m+n|$ stated in Equation (4.4) must be an even value. Therefore, it is more sensible to explain and is easier to understand the algorithm of the proposed technique in even number domain. From the sequences described in Equation (4.5), the set of positive even numbers $\mathcal{E}$ can be partitioned into three disjoint sets, X, Y, and Z, defined by:

$$
\begin{aligned}
X &= \cup\{x_k\}\big|_{k=0,1,2,\ldots} \\
Y &= \cup\{y_k\}\big|_{k=0,1,2,\ldots} \\
Z &= \cup\{z_k\}\big|_{k=0,1,2,\ldots}
\end{aligned}
\tag{4.8}
$$

Where the sequences $\{x_k\}$, $\{y_k\}$, and $\{z_k\}$; $(k=0,1,2,\ldots)$ are defined by:

$$
\begin{aligned}
x_k &= 2u_k = 6k && = \{0,6,12,18,\ldots\} \\
y_k &= 2v_k = 6k+2 && = \{2,8,14,20,\ldots\} \\
z_k &= 2w_k = 6k+4 && = \{4,10,16,22,\ldots\}
\end{aligned}
\tag{4.9}
$$

Note that for every number $u_k \in U$, $v_k \in V$ and $w_k \in W$, hence when refer to Equation (4.1), three sequences can be defined:

Zero sequence:

$$
\begin{aligned}
M_n \sin[u_k(\omega_0 t)] &= M_n \sin(\omega_0 t) \\
M_n \sin\left[u_k\left(\omega_0 t - \frac{2\pi}{3}\right)\right] &= M_n \sin(\omega_0 t) \\
M_n \sin\left[u_k\left(\omega_0 t + \frac{2\pi}{3}\right)\right] &= M_n \sin(\omega_0 t)
\end{aligned}
\tag{4.10}
$$

Positive sequence:

$$M_n \sin\left[v_k\left(\omega_0 t\right)\right] = M_n \sin\left(\omega_0 t\right)$$

$$M_n \sin\left[v_k\left(\omega_0 t - \frac{2\pi}{3}\right)\right] = M_n \sin\left(\omega_0 t - \frac{2\pi}{3}\right) \qquad (4.11)$$

$$M_n \sin\left[v_k\left(\omega_0 t + \frac{2\pi}{3}\right)\right] = M_n \sin\left(\omega_0 t + \frac{2\pi}{3}\right)$$

Negative sequence:

$$M_n \sin\left[w_k\left(\omega_0 t\right)\right] = M_n \sin\left(\omega_0 t\right)$$

$$M_n \sin\left[w_k\left(\omega_0 t - \frac{2\pi}{3}\right)\right] = M_n \sin\left(\omega_0 t + \frac{2\pi}{3}\right) \qquad (4.12)$$

$$M_n \sin\left[w_k\left(\omega_0 t + \frac{2\pi}{3}\right)\right] = M_n \sin\left(\omega_0 t - \frac{2\pi}{3}\right)$$

All these sequences can be shortly presented as:

$$\frac{2\pi}{3}\left(u_k\right) = \frac{2\pi}{3}\left(3k\right) = 2\pi = 0° \text{ (zero sequence)}$$

$$\frac{2\pi}{3}\left(v_k\right) = \frac{2\pi}{3}\left(3k+1\right) = 2\pi + \frac{2\pi}{3} = 120° \text{ (positive sequence)} \qquad (4.13)$$

$$\frac{2\pi}{3}\left(w_k\right) = \frac{2\pi}{3}\left(3k+2\right) = 2\pi + \frac{4\pi}{3} = -120° \text{ (negative sequence)}$$

Equations (4.10) to (4.13) show that, as long as the order is within the set of U sequence (3rd, 9th, 15th, etc.), it will always produce a zero sequence component. Similarly, whichever harmonic order found in V sequence (1st, 7th, 13th, etc.) will generate positive sequence component, and harmonic order included in W sequence (2nd, 5th, 11th, etc.) will resulted in a negative sequence component generation. This also happen in the even number domain, for every number $x_k \in X$, $y_k \in Y$ and $z_k \in Z$:

$$\frac{2\pi}{3}(x_k) = \frac{2\pi}{3}(6k) = 4\pi = 0° \text{ (zero sequence)}$$

$$\frac{2\pi}{3}(y_k) = \frac{4\pi}{3}(3k+1) = 4\pi + \frac{4\pi}{3} = -120° \text{ (negative sequence)} \qquad (4.14)$$

$$\frac{2\pi}{3}(z_k) = \frac{4\pi}{3}(3k+2) = 4\pi + \frac{8\pi}{3} = 120° \text{ (positive sequence)}$$

Applying the sequence condition shown in Equation (4.14) into Equation (4.4) revealed that, there are nine cases to study in order to determine the value of $\beta(m,n,t)$:

Case 1: $|m-n| \in X$ **and** $|m+n| \in X$

$$\begin{aligned}
\beta(m,n,t) &= \frac{1}{3}M_n\left[\cos\left((m-n)\omega_0 t\right) - \cos\left((m+n)\omega_0 t\right)\right] \\
&+ \frac{1}{3}M_n\left[\cos\left((m-n)\omega_0 t\right) - \cos\left((m+n)\omega_0 t\right)\right] \\
&+ \frac{1}{3}M_n\left[\cos\left((m-n)\omega_0 t\right) - \cos\left((m+n)\omega_0 t\right)\right] \\
&= M_n\cos\left((m-n)\omega_0 t\right) - M_n\cos\left((m+n)\omega_0 t\right)
\end{aligned} \qquad (4.15)$$

Case 2: $|m-n| \in X$ **and** $|m+n| \in Y$

$$\begin{aligned}
\beta(m,n,t) &= \frac{1}{3}M_n\left[\cos\left((m-n)\omega_0 t\right) - \cos\left((m+n)\omega_0 t\right)\right] \\
&+ \frac{1}{3}M_n\left[\cos\left((m-n)\omega_0 t\right) - \cos\left((m+n)\omega_0 t + \frac{2}{3}\pi\right)\right] \\
&+ \frac{1}{3}M_n\left[\cos\left((m-n)\omega_0 t\right) - \cos\left((m+n)\omega_0 t - \frac{2}{3}\pi\right)\right] \\
&= M_n\cos\left((m-n)\omega_0 t\right)
\end{aligned} \qquad (4.16)$$

Similarly, the values of $\beta(m,n,t)$ in the following cases can be verified:

Case 3: $|m-n| \in X$ **and** $|m+n| \in Z$

$$\beta(m,n,t) = M_n\cos\left((m-n)\omega_0 t\right) \qquad (4.17)$$

Case 4: $|m-n| \in Y$ **and** $|m+n| \in X$

$$\beta(m,n,t) = -M_n \cos\left((m+n)\omega_0 t\right) \tag{4.18}$$

Case 5: $|m-n| \in Y$ **and** $|m+n| \in Y$

$$\beta(m,n,t) = 0 \tag{4.19}$$

Case 6: $|m-n| \in Y$ **and** $|m+n| \in Z$

$$\beta(m,n,t) = 0 \tag{4.20}$$

Case 7: $|m-n| \in Z$ **and** $|m+n| \in X$

$$\beta(m,n,t) = -M_n \cos\left((m+n)\omega_0 t\right) \tag{4.21}$$

Case 8: $|m-n| \in Z$ **and** $|m+n| \in Y$

$$\beta(m,n,t) = 0 \tag{4.22}$$

Case 9: $|m-n| \in Z$ **and** $|m+n| \in Z$

$$\beta(m,n,t) = 0 \tag{4.23}$$

4.3 Applying the FIHE in 50 *Hz* Systems

For three-phase balanced 50 *Hz* systems only five of the above cases (1,2,3,4, and 7) are relevant, as the other cases give zero as the end results (β), hence they are not

excluded from consideration. The relevant nonzero cases are summarised in the following table:

case	$\|m-n\|$	$\|m+n\|$	β
1	X	X	$M_n \cos\big((m-n)\omega_0 t\big) - M_n \cos\big((m+n)\omega_0 t\big)$
2	X	Y	$M_n \cos\big((m-n)\omega_0 t\big)$
3	X	Z	$M_n \cos\big((m-n)\omega_0 t\big)$
4	Y	X	$-M_n \cos\big((m+n)\omega_0 t\big)$
7	Z	X	$-M_n \cos\big((m+n)\omega_0 t\big)$

Table 4-1: Nonzero cases of FIHE in 50 Hz systems

Since when $|m-n| \in X$ (for case 2 and 3), $\beta(m,n,t) = M_n \cos(6k\omega_0 t)$. Similarly, when $|m+n| \in X$ (for case 4 and 7), $\beta(m,n,t) = -M_n \cos(6k\omega_0 t)$.

Finally, for case 1, where both $|m-n| \in X$ and $|m+n| \in X$, result $\beta(m,n,t) = M_n \cos(6k\omega_0 t) - M_n \cos(6k\omega_0 t)$. In this case, $\beta(m,n,t) = 0$ will only happen when $n = m$. $\beta(m,n,t)$ will never be zero if $n \neq m$. This means that a d.c. component with magnitude of M_n will only appear when $n = m$. Otherwise, the smallest frequency a.c. component that appears in $\beta(m,n,t)$ is always $6\omega_0 = 6 \times 2\pi \times 50$ rad/s or 300 Hz (as X set content all the value of x_k). This phenomenon is graphically shown in Figure 4.1.
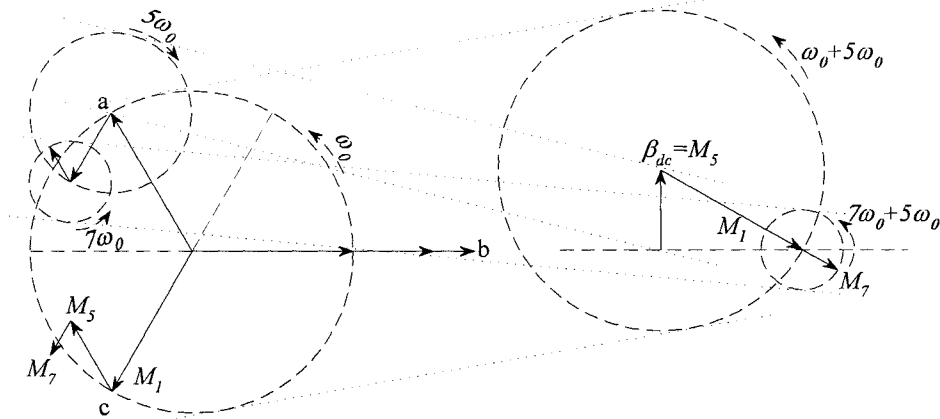
Figure 4.1: Graphical representation of the FIHE algorithm ($m=5$)

Now, let

$$\tau_6 = \frac{T_0}{6} = \frac{1}{6 \times 50} = \frac{1}{300} sec \qquad (4.24)$$

Also, since n is odd and positive, let $n = 2p + 1$ with $p \in \mathcal{N}$. It is clear from the above remark that

$$I_d(m) = \frac{1}{T_0} \int_{T_0} \sum_{p=0}^{+\infty} \beta(m, 2p+1, t) dt$$

$$= \frac{1}{\tau_6} \int_{\tau_6} \sum_{p=0}^{+\infty} \beta(m, 2p+1, t) dt \qquad (4.25)$$

$$= \begin{cases} 0 & \text{if } n = 2p+1 \neq m \\ M_m & \text{if } n = 2p+1 = m \end{cases}$$

where $I_d(m)$ in (4.25) is the purified $\beta(m,n,t)$ and the closed interval of length T_0 is denoted by $T_0 = [t_0, \ t_0 + T_0]$ and t_0 is a real number, consequently $\int_{T_0} f(t) dt = \int_{t_0}^{t_0+T_0} f(t) dt$

This means that there is no need to integrate $\beta(m,n,t)$ over the full period T_0 to obtain

$I(m)$; an integration over a period of one-sixth of T_0 is sufficient. This last observation

forms the basis of the FIHE method. In this method, it is clear that, the time taken to

extract the m harmonic component is 6 times faster that the conventional methods.

Furthermore, as it will be shown, FIHE has the advantages of being overshoot-free,

oscillation free and high attenuation characteristics, which still cannot be found in

existing filtering techniques.

4.4 Reconstruction of the Extracted Harmonic Component

In this section, the reconstruction of the extracted harmonic signal is discussed. As

explained in the previous section, the three-phase harmonic components can be

extracted and expressed in a d.c. form as $I(m)$. However, in some applications, the

time-domain wave-shape of the harmonic is important and need to be available after

extraction (i.e. reference signal for the PWM invertor); hence a bidirectional

transformation is required. To reconstruct the extracted harmonic signal, an equal

weight matrix is required which means that two extra sets of variables are

needed: $\gamma(m,n,t)$ and $\delta(m,n,t)$. For simplicity and to provide all phase

information, $\gamma(m,n,t)$ has to be set in quadrature of the first set of variables $\beta(m,n,t)$;

that is:

$$\gamma(m,n,t) = \frac{2}{3}\Gamma_q(m,t)S_{ABC}(n,t) \qquad (4.26)$$

where

$$\Gamma_q(m,t) = \left[\cos\left(m\omega_0 t\right) \quad \cos\left(m\omega_0 t - \frac{2\pi m}{3}\right) \quad \cos\left(m\omega_0 t + \frac{2\pi m}{3}\right) \right] \qquad (4.27)$$

By using the previous analysis, it can also be checked that the smallest frequency component that appears in $\gamma(m,n,t)$ is also $6\omega_0$. On the other hand, since $\int_{T_0} sin(m\omega_0 t)\cos\left(n\omega_0 t\right)dt = 0$, for all n and m, this results in

$$\begin{aligned} I_q(m) &= \frac{1}{T_0} \int_{T_0} \sum_{p=0}^{+\infty} \gamma(m,2p+1,t)dt \\ &= \frac{1}{\tau_6} \int_{\tau_6} \sum_{p=0}^{+\infty} \gamma(m,2p+1,t)dt = 0 \end{aligned} \qquad (4.28)$$

Finally, $\delta(m,n,t)$ is defined by

$$\delta(m,n,t) = \frac{2}{3}\Gamma_0(t,m)S_{ABC}(t,n) \qquad (4.29)$$

where

$$\Gamma_0 = \left(\frac{1}{2} \quad \frac{1}{2} \quad \frac{1}{2} \right) \qquad (4.30)$$

It is clear that $\delta(m,n,t) = 0$, since $S_{ABC}(n,t)$ is a balanced three-phase signal. Consequently,

$$I_0(m) = \frac{1}{\tau_6} \int_{\tau_6} \sum_{p=0}^{+\infty} \delta(m,2p+1,t)dt = 0 \qquad (4.31)$$

Equations (4.3), (4.26) and (4.29) can be written in compact form as:

$$\Psi(m,n,t) = \frac{2}{3}\Gamma(m,t)S_{ABC}(n,t) \qquad (4.32)$$

where

$$\Psi(m,n,t) = \begin{pmatrix} \beta(m,n,t) \\ \gamma(m,n,t) \\ \delta(m,n,t) \end{pmatrix} \qquad (4.33)$$

and

$$\Gamma(m,t) = \begin{bmatrix} sin(m\omega_0 t) & sin\left(m\omega_0 t - \dfrac{2\pi m}{3}\right) & sin\left(m\omega_0 t + \dfrac{2\pi m}{3}\right) \\ cos(m\omega_0 t) & cos\left(m\omega_0 t - \dfrac{2\pi m}{3}\right) & cos\left(m\omega_0 t + \dfrac{2\pi m}{3}\right) \\ \dfrac{1}{2} & \dfrac{1}{2} & \dfrac{1}{2} \end{bmatrix} \qquad (4.34)$$

Finally, $I(m)$ can be obtained by

$$I(m) = \frac{1}{\tau_6} \int_{\tau_6} \sum_{p=0}^{+\infty} \Psi(m, 2p+1, t) dt \qquad (4.35)$$

To reconstruct the signal $S_{abc}(t,m)$ the following equation is applied:

$$S_{abc}(m,t) = \Gamma^{-1}(m,t) I(m) \qquad (4.36)$$

where $\Gamma^{-1}(t,m)$ is the reverse of $\Gamma(t,m)$ and

$$I(m) = \begin{pmatrix} I_d(m) \\ I_q(m) \\ I_0(m) \end{pmatrix} \qquad (4.37)$$

Performance of the proposed harmonic extraction technique (FIHE) is verified base on the accuracy and functionality in various application environments.

In addition to the fast extraction speed, due to the fact that the separate conversion functions ($\Gamma(m,t)$) are used in different harmonic extractions, the FIHE at the same

time gives a phase independency among different harmonic frequencies. However, in the extraction process of single/same harmonic frequency component, $\Gamma(m,t)$ and its inversed ($\Gamma^{-1}(m,t)$) (but with the same rotating frequency) would be used seperatelly in the decoupling and reconstruction states. Therefore, FIHE can easily shifting the phase of the extracted harmonic component by adding in the desire phase shift angle to the reverse conversion function ($\Gamma^{-1}(m,t)$) used in the reconstruction process

4.5 Applying the FIHE in Unbalanced Systems

Generally, unbalance in power systems is controlled within a very tight margin ($\pm 2\%$ in UK), but it is still a problem that may go worst. In most cases, unbalance studies are assuming systems are freed from harmonic distortion, but in most systems this is not the case [74]. When system unbalanced, both positive and negative sequence harmonic components would appear (on the same frequency).

In this section, use of FIHE in unbalanced condition is analysed. Numerical analysis is presented to evaluate performance of the FIHE in such condition with the presence of harmonic distortion.

In unbalanced situation, positive and negative sequence components (with same frequency) are both appeared. To extract positive sequence harmonic components (for $n = 1, 7, 13$) and negative sequence harmonic components (for $n = 5, 11, 17$) in

balanced condition is presented in earlier sections. During system unbalanced, the

symmetrical components for n^{th} order harmonic are presented as:

$$S'_{ABC}(n,t) = \begin{pmatrix} S_A^+(n,t) + S_A^-(n,t) \\ S_B^+(n,t) + S_B^-(n,t) \\ S_C^+(n,t) + S_C^-(n,t) \end{pmatrix} = \begin{pmatrix} M_n^+ sin(n\omega_0 t) + M_n^- sin(n\omega_0 t) \\ M_n^+ sin\left(n\omega_0 t - \dfrac{2n\pi}{3}\right) + M_n^- sin\left(n\omega_0 t + \dfrac{2n\pi}{3}\right) \\ M_n^+ sin\left(n\omega_0 t + \dfrac{2n\pi}{3}\right) + M_n^- sin\left(n\omega_0 t - \dfrac{2n\pi}{3}\right) \end{pmatrix} \quad (4.38)$$

In equation, superscripts are representing the phase sequences and the rest of the

notations are defined in the earlier sections. With the conversion function shown earlier

$(\Gamma_d(m,t))$, three-phase quantity in Equation (4.38) can be converted to a single phase

quantity, as shown in the following equation.

$$\beta'(m,n,t) = \frac{2}{3}\Gamma_d(m,t)S'_{ABC}(n,t)$$

$$= \frac{2}{3}sin(m\omega_0 t)\left[M_n^+ sin(n\omega_0 t) + M_n^- sin(n\omega_0 t)\right]$$

$$+ \frac{2}{3}sin\left(m\omega_0 t - \frac{2\pi m}{3}\right)\left[M_n^+ sin\left(n\omega_0 t - \frac{2\pi n}{3}\right) + M_n^- sin\left(n\omega_0 t + \frac{2\pi n}{3}\right)\right] \quad (4.39)$$

$$+ \frac{2}{3}sin\left(m\omega_0 t + \frac{2\pi m}{3}\right)\left[M_n^+ sin\left(n\omega_0 t + \frac{2\pi n}{3}\right) + M_n^- sin\left(n\omega_0 t - \frac{2\pi n}{3}\right)\right]$$

This can be expended as:

$$\beta'(m,n,t) = \frac{1}{3}M_n^+\left[\cos\big((m-n)\omega_0 t\big) - \cos\big((m+n)\omega_0 t\big)\right]$$

$$+\frac{1}{3}M_n^+\left[\cos\left((m-n)\omega_0 t - \frac{2}{3}\pi(m-n)\right) - \cos\left((m+n)\omega_0 t - \frac{2}{3}\pi(m+n)\right)\right]$$

$$+\frac{1}{3}M_n^+\left[\cos\left((m-n)\omega_0 t + \frac{2}{3}\pi(m-n)\right) - \cos\left((m+n)\omega_0 t + \frac{2}{3}\pi(m+n)\right)\right]$$

$$+\frac{1}{3}M_n^-\left[\cos\big((m-n)\omega_0 t\big) - \cos\big((m+n)\omega_0 t\big)\right]$$

$$+\frac{1}{3}M_n^-\left[\cos\left((m-n)\omega_0 t - \frac{2}{3}\pi(m+n)\right) - \cos\left((m+n)\omega_0 t - \frac{2}{3}\pi(m-n)\right)\right]$$

$$+\frac{1}{3}M_n^-\left[\cos\left((m-n)\omega_0 t + \frac{2}{3}\pi(m+n)\right) - \cos\left((m+n)\omega_0 t + \frac{2}{3}\pi(m-n)\right)\right]$$

$$(4.40)$$

As mentioned earlier, both m and n are positive odd numbers. Consequently, the result of $|m-n|$ and $|m+n|$ must be even values. Therefore, it is more sensible to analyse the algorithm in even domain with the disjoint sets defined in equation (4.8) (X, Y, and Z). These three sets formed up nine possibilities (cases) for $\beta'(m,n,t)$, they are:

Case 1: $|m-n| \in X$ **and** $|m+n| \in X$

$$\beta(m,n,t) = 0 \qquad (4.41)$$

Case 2: $|m-n| \in X$ **and** $|m+n| \in Y$

$$\beta(m,n,t) = M_n^+ \cos\big((m-n)\omega_0 t\big) - M_n^- \cos\big((m+n)\omega_0 t\big)$$
$$= M_n^+ \cos(6k\,\omega_0 t) - M_n^- \cos\big((6k+2)\omega_0 t\big) \qquad (4.42)$$

Case 3: $|m-n| \in X$ **and** $|m+n| \in Z$

$$\beta(m,n,t) = M_n^+ \cos\left((m-n)\omega_0 t\right) - M_n^- \cos\left((m+n)\omega_0 t\right)$$
$$= M_n^+ \cos\left(6k\omega_0 t\right) - M_n^- \cos\left((6k+4)\omega_0 t\right)$$

$$(4.43)$$

Case 4: $|m-n| \in Y$ **and** $|m+n| \in X$

$$\beta(m,n,t) = -M_n^+ \cos\left((m+n)\omega_0 t\right) + M_n^- \cos\left((m-n)\omega_0 t\right)$$
$$= -M_n^+ \cos\left(6k\omega_0 t\right) + M_n^- \cos\left((6k+2)\omega_0 t\right)$$

$$(4.44)$$

Case 5: $|m-n| \in Y$ **and** $|m+n| \in Y$

$$\beta(m,n,t) = 0 \qquad (4.45)$$

Case 6: $|m-n| \in Y$ **and** $|m+n| \in Z$

$$\beta(m,n,t) = 0 \qquad (4.46)$$

Case 7: $|m-n| \in Z$ **and** $|m+n| \in X$

$$\beta(m,n,t) = -M_n^+ \cos\left((m+n)\omega_0 t\right) + M_n^- \cos\left((m-n)\omega_0 t\right)$$
$$= -M_n^+ \cos\left(6k\omega_0 t\right) + M_n^- \cos\left((6k+4)\omega_0 t\right)$$

$$(4.47)$$

Case 8: $|m-n| \in Z$ **and** $|m+n| \in Y$

$$\beta(m,n,t) = 0 \qquad (4.48)$$

Case 9: $|m-n| \in Z$ **and** $|m+n| \in Z$

$$\beta(m,n,t) = 0 \qquad (4.49)$$

In four cases (1, 5, 6, 8, 9), $\beta'(m,n,t)$ produces nothing (zero) at the end, hence they can be ignored. While $\beta'(m,n,t)$ for the relevant four non-zero cases (2, 3, 4, 7) showed that, d.c. component appeared when $m = n$ and the minimum frequency a.c. components in

$\beta'(m,n,t)$ is always $2\omega_0$ for $|m+n| \in Y$ (for case 2) and $|m-n| \in Y$ (for case 4). Therefore, it is clear that:

$$S_\beta(m) = \frac{\omega_0}{\pi} \int_t^{t+\frac{\pi}{\omega_0}} \sum_{n=0}^{+\infty} \beta(m,n,t)dt$$
$$= \begin{cases} 0 & \text{if } n \neq m \\ M_m^+ & \text{if } n = m \end{cases} \qquad (4.50)$$

Above analysis showed that, FIHE needs half a fundamental cycle to extract harmonic component in unbalanced situation.

Apart from performance deterioration (speed) under unbalanced condition mentioned above, accuracy of the proposed FIHE will also be affected when line frequency changed/drifted. Performance of the FIHE under these conditions was evaluated and the results are presented in Chapter 5 section 5.3.3 and 5.3.4. Related discussions can also be found in Chapter 9 section 9.1.3 and 9.2.

CHAPTER 5

FIHE'S PERFORMANCE EVALUATIONS (SIMULATION WORK)

5.1   Introduction

5.2   Computer Simulation Model

5.3   Simulation Results and Discussion

     5.3.1   Steady-state characteristic

     5.3.2   Dynamic response characteristic

     5.3.3   FIHE characteristics under unbalanced condition

     5.3.4   Performance of FIHE for system frequency

5.1 Introduction

The principle, functionality and accuracy of the FIHE are analysed and verified mathematically, via computer simulations and laboratory experiments. In this chapter, steady state evaluation (to evaluate the accuracy, harmonic immunity, etc.) and dynamic response test (to test the extraction speed, level of overshoot, post extraction stability, etc) were used to evaluate the proposed FIHE and the results of simulation are presented to illustrate its performance.

5.2 Computer Simulation Model

Computer simulation is used to evaluate algorithm of the proposed harmonic extraction technique. The simulation is based on a typical 400 V 3-phase supply system with a 31 kW d.c. RL load. The d.c. load voltage is obtained by a 3-phase diode bridge rectifier, which behaved as a harmonic current source. The system configuration is shown in Figure 5.1.
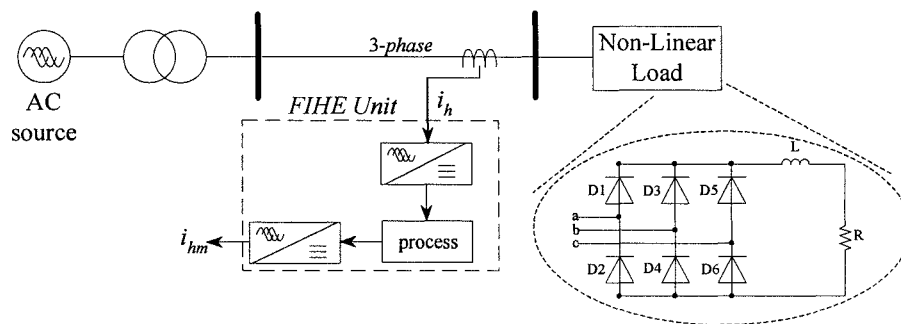
Figure 5.1: System used in the test

Simulation is carried out in Ansoft-Simplorer environment [75]. The simulation package was used due to its complete power electronics model database. Harmonic current (i_h) produced by the non-linear load is detected at the main feeder as indicated in the diagram. The current (i_h) is fed to the FIHE to extract the selected harmonic current (i_{hm}). Extracted harmonic current (i_{hm}) is reshaped as sinusoidal wave-shape as described in Chapter 4.

5.3 Simulation Results and Discussion

5.3.1 Steady-state characteristics

Figure 5.2 shows the waveform of the sensed current (i_h). Fourier analysis is used to analyse the harmonic content of the sensed current and its spectrum is shown in Figure 5.3.
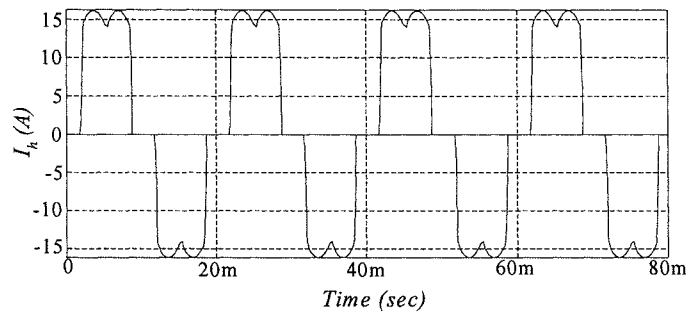
Figure 5.2: Per-phase detected current (i_h)
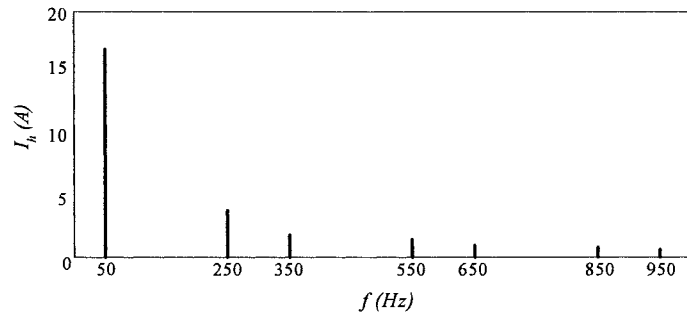
Figure 5.3: Frequency spectrum of the detected current (i_h)

In this simulation, FIHE is tuned to extract 1st, 5th, and 7th order harmonic current. Figure 5.4 shows the waveform of the extracted fundamental harmonic component and is superimposed with the distorted current. Next figure shows the spectrum of the

extracted signal. The spectrum indicated that, only fundamental harmonic component is remained.
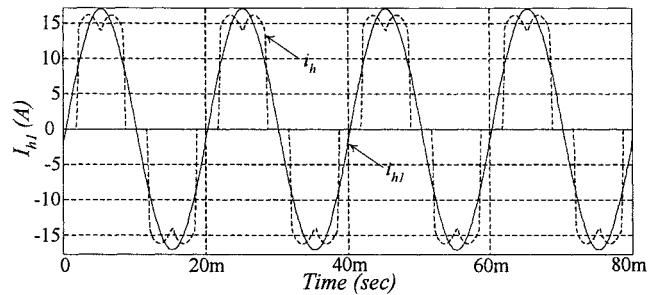
Figure 5.4: Extracted fundamental component (i_{h1}) and the distorted current (i_h)
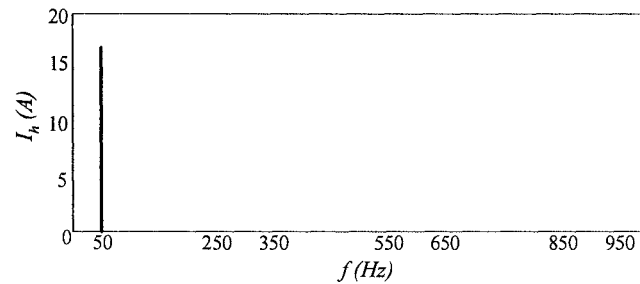
Figure 5.5: Frequency spectrum of i_{h1}

Waveforms shown in Figure 5.6 are the extracted 5th order harmonic current and the distorted line current. Spectrum of the extractor's output signal shown in Figure 5.7 contents only the selected harmonic component (5th order harmonic).
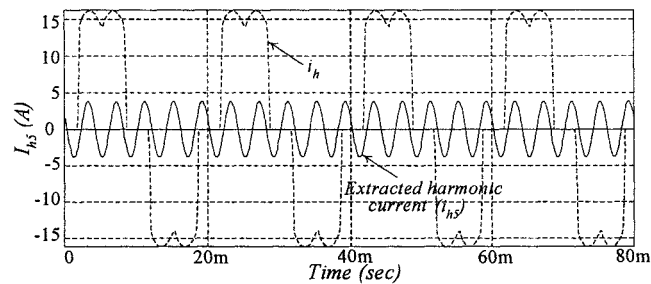
Figure 5.6: Extracted 5th harmonic component (i_{h5}) and the distorted current i_h
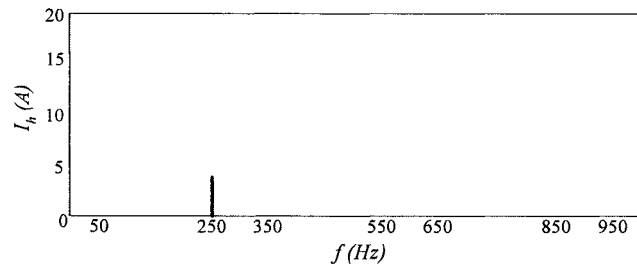
Figure 5.7: Frequency spectrum of i_{h5}

Figure 5.8 shows the result of the 7th order harmonic current extraction and the detected current (as background). Frequency spectrum in Figure 5.9 shows that, only 7th order harmonic component exists after extraction.
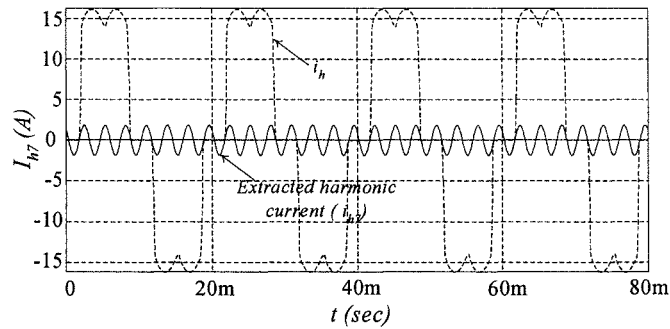
Figure 5.8: Extracted 7th harmonic component (i_{h7}) and the i_h
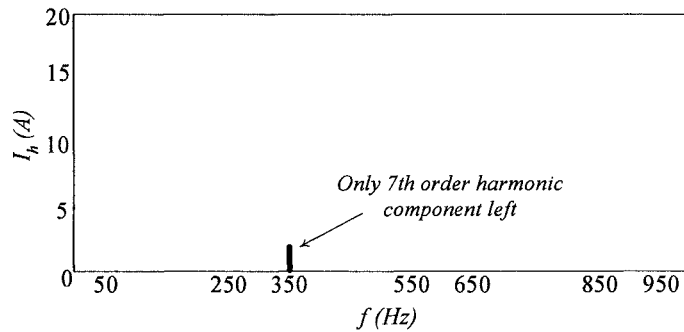
Figure 5.9: Frequency spectrum of i_{h7}

An evaluation has been carried out to verify the accuracy of the used harmonic analysers (the widely used FFT and the FIHE). A set of harmonic components (1st, 5th, 7th and 1% noise) were artificially generated using separate signal generators. All the harmonic components were synthesised to form a distorted signal/waveform, which would be used to evaluate the harmonic analysers. In this test, the original (generated) harmonic components would be used to compare to the extraction results (extracted harmonic components). Summary of this test is shown in Table 5-1 in terms of the percentage of error.

Harmonic order	FFT measurement (%)	FIHE measurement (%)
1st	0.01	0.001
5th	0.01	0.015
7th	0.01	0.018
Note, $$Error\% = \frac{Original - Measured}{Original} \times 100\%$$		

Table 5-1: Harmonic extraction accuracy

The error caused by the added 1% noise is ignored in the results recorded in Table 5-1. As noise filter (low order low-pass filter) is always assume would be used in such systems to remove the noise.

Accuracy of the proposed FIHE with phase shifted harmonic components was simulated. Similar to the above evaluation, harmonic components were artificially generated with sifted phase angles ($0-360°$). Harmonic components extracted by the

FIHE were compared to their original one to obtain the extraction errors. These results (percentage of errors) are shown in Figure 5.10. The results show that in the worst case, the FIHE is still able to keep the accuracy under 0.02 %.
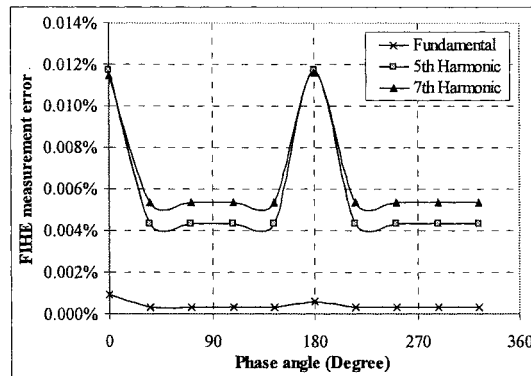
Figure 5.10: Results of the FIHE's accuracy test with phase shifted harmonic components

5.3.2 Dynamic response characteristics

The above results justified the static harmonic extraction ability of the proposed FIHE. However, the most attractive feature is its superb dynamic extraction characteristic. Therefore, a dynamic response test was carried out in computer simulation condition. A waveform with harmonic content up to 11th order has been artificially created for the test. A step function for 7th order harmonic component is added into the waveform to step-up 7th harmonic component by 5 times the original value at $t = 0.03$ sec. The resultant waveform with the step function is shown in Figure 5.11.

a) Step function for 7th harmonic

b) Resultant waveform
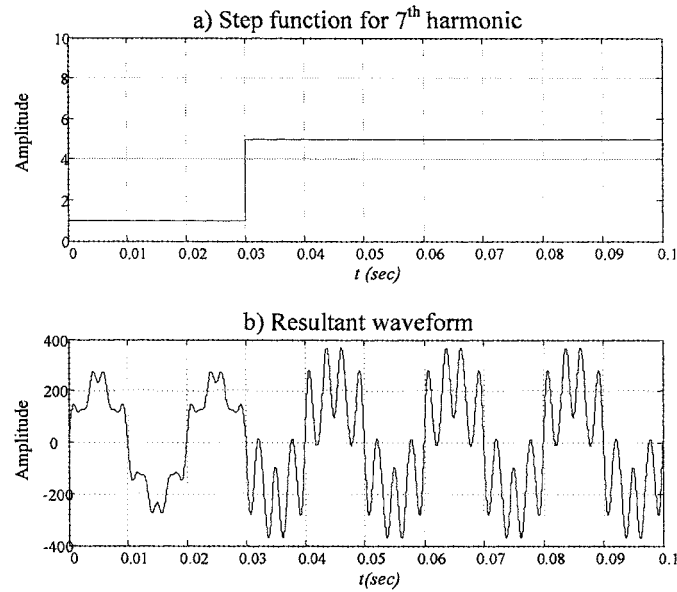
Figure 5.11: Waveform generated with the step function added

The signal shown in Figure 5.11 is inputted into the FIHE unit. $I(m)$ of the FIHE is shown in Figure 5.12, and the extracted signal is shown in Figure 5.13 (additional FIHE's dynamic response test results (for 1st, 5th and 11th harmonics) are shown in the Appendix F). As can be seen, proposed FIHE has a very fast (dynamic) response and at the same time, it provides zero-overshoot as well as oscillation-free characteristics as mentioned in Chapter 4. For comparison purpose, Figure 5.14 and Figure 5.15 show the response obtained by using existing harmonic extraction techniques (i.e.: with Butterworth filter, Fourier transform base extractor, and the earlier mentioned non-recursive ANN IHE) together with the proposed FIHE technique. These results show that FIHE has superior harmonic extraction characteristic compared to the existing harmonic extraction techniques.
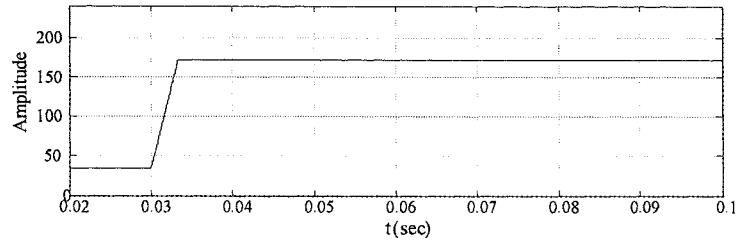
Figure 5.12: $I_d(m)$ of the FIHE
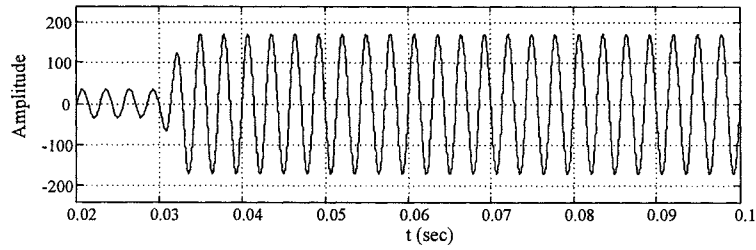
Figure 5.13: Extracted 7th harmonic component (per-phase)
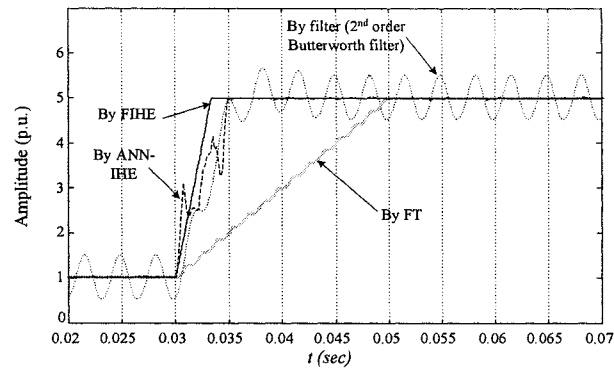
Figure 5.14: Response time for three different techniques (with low order filter)
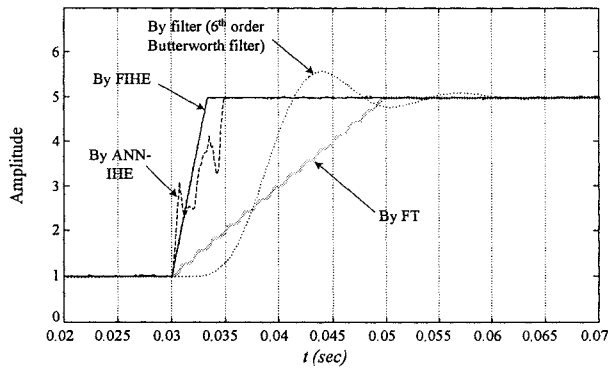
Figure 5.15: Response time for three different techniques (with higher order filter)

95

5.3.3 FIHE characteristics under unbalanced conditions

Proposed FIHE performance under unbalanced situation is evaluated via simulation in this section. FIHE principle described in section 4.2 to section 4.4 is first evaluated to show its characteristic (accuracy) under unbalanced condition. At this stage, in order to test the accuracy of the FIHE without slow it down, harmonic extraction speed of FIHE has been set to its maximum (six times the fundamental cycle). The result is plotted in blue line with respect to the percentage of the unbalanced condition and shown in Figure 5.16. Another test was performed with slower speed (half of the fundamental cycle) and the result is plotted in red line in the same figure.
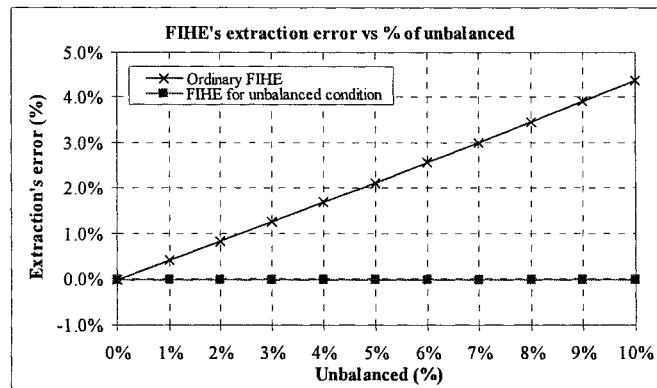
Figure 5.16: Accuracy of FIHE against % of system's unbalance

Percentage of the unbalanced is defined as a ratio of average negative sequence fundamental component against the average positive sequence fundamental component, which is:

$$U_{unbalance}(\%) = \frac{|V^-|}{|V^+|}\%$$

Where

$U_{unbalance}(\%)$ - percentage of systems voltage unbalanced

$|V^-|$ - negative-sequence fundamental component

$|V^+|$ - positive-sequence fundamental component

The graph showed that, accuracy of the FIHE is deteriorated in unbalanced condition is drifted away linearly with respect to the increment of unbalanced condition (e.g. for a 2% unbalanced the error is of extraction is 0.83% and 5% unbalanced causes 2.12% of extraction error).

To improve the accuracy, speed of FIHE needs to be adjusted (reduced). This is discussed in Chapter 4 section 4.5, analysis reveal that the extraction speed of FIHE needs to be reduced to half a fundamental cycle when it is operated in unbalanced condition. Conclusion from the analysis is evaluated in term of simulation and the result is shown in Figure 5.16. The result shows that, reduced speed's FIHE has regained its superb accuracy (result show almost no error).

5.3.4 Performance of FIHE for system frequency variations

Accuracy of FIHE is evaluated in a condition where the rated system's frequency of the systems is drifted from −10% to +10% (45 Hz to 55 Hz). Results obtained are plotted and shown in Figure 5.17. Accuracy of Fourier transform (FT) is tested in the same condition and the result is presented in the same figure for comparison purpose.

FIHE errors when systems frequency drifted
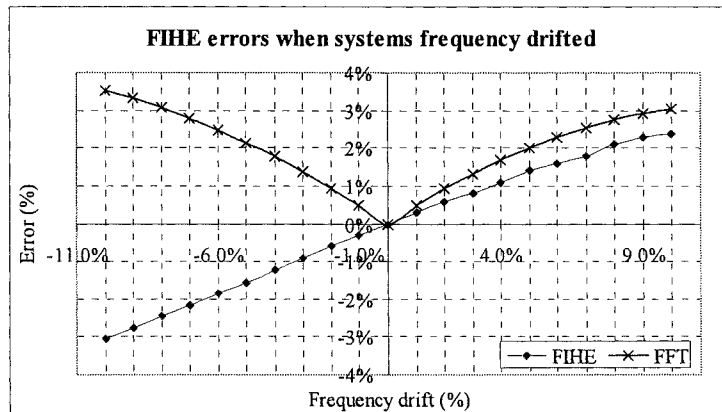
Figure 5.17: Extraction error versus Frequency drift

The results showed that, FIHE is maintained a better accuracy than FT in frequency drift condition. For example, when system frequency drifted -1% to 1%, only -0.29% to 0.3% of error is found in FIHE's extracted output, but for FT, 4.9% of error is found. Therefore, these results are justified that, FIHE have a better accuracy with compared to FT during system frequency drifted condition.

CHAPTER 6

PROPOSED HARMONIC RESONANCE ATTENUATION (HRA) TECHNIQUE

6.1 Introduction

Harmonic resonance is a power system phenomenon, in which harmonic current in a system is amplified. This happens when the system's natural frequency is closed to/at one of the harmonic frequency. Distribution networks are designed to avoid harmonic resonance, but the change of system's parameters due to numerous reasons may sometime create the resonance (refer to Chapter 1 and 2 for more details). One most common cause of harmonic resonance is the change the of PFC capacitance associated

with the system's source inductance [28,29]. In this thesis, a harmonic resonance attenuation method that control shunt active filter as a controllable reactance is proposed. The proposed method generates a virtual shunt reactance that alters the system's impedance and shifts away harmonic resonance. Detailed analysis is presented in this chapter.

6.2 Principle of the Proposed HRA Technique

Principle of controlling a shunt active power filter as a controllable reactance is utilised the relationship of voltage and current at the active filter branch together with the coupling inductor to modify the systems impedance. The initial concept was developed based on the most basic Ohm's Law, where,

$$Z_{jn\omega} = \frac{V_{jn\omega}}{I_{jn\omega}}$$
(6.1)

In the frequency domain, harmonic components are expressed as an individual element based on their frequencies. Therefore, as a product of these components, harmonic impedances $(z_{n\omega})$ are as well treated as an individual component at different harmonic order. Components with different frequencies are independent. Thus, the following analysis only focuses on the interested harmonic components.

Voltage detection technique [21,32,56-58] is used in the proposed resonance attenuation technique to detect network harmonic resonance condition. Voltage compensation method is used to change the characteristic of the shunt active filter to

form a virtual reactance. Hence the problems of the existing resonance attenuation techniques (mentioned in section 2.3) can be avoided by implementing the proposed HRA at the PCC. A simplified block diagram of the proposed active filter controller is shown in Figure 6.1.
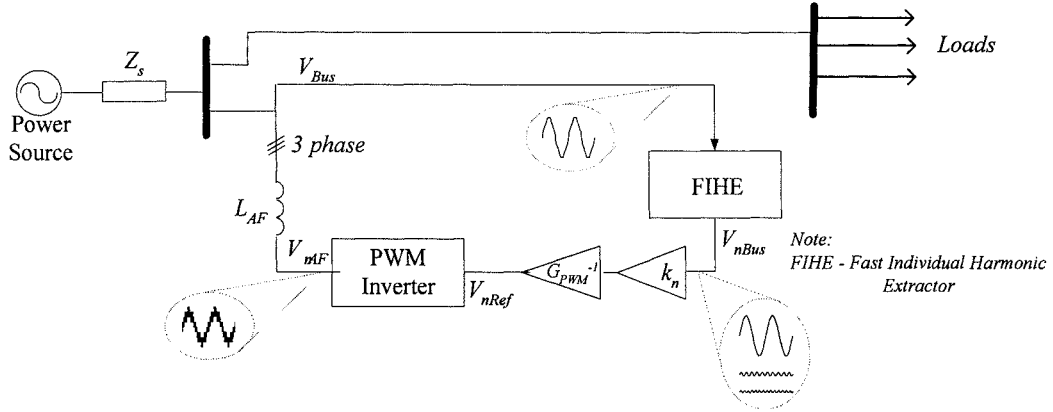
Figure 6.1: A simplified block diagram of the proposed active filter

As can be noticed from the block diagram, input of the real time individual harmonic extractor (FIHE) is the system's voltage signal at the point where the active filter is connected (V_{Bus}). Output of the FIHE is fed to a PWM inverter with a controllable gain (k_n) and through an attenuator (G_{PWM}^{-1}). Function of G_{PWM}^{-1} is mainly to offset the voltage gain of the inverter. Multiplying the extracted harmonic component with the feedback gain (G_{nFB}) produces a PWM voltage reference. This is shown in the following equation:

$$V_{REF} = G_{nFB} \cdot V_{n\omega Bus} \qquad (6.2)$$

Where the feedback gain is a ratio of the controllable gain (k_n) against the aforementioned PWM voltage gain (G_{PWM}):

$$G_{nFB} = k_n \cdot \frac{1}{G_{PWM}} \qquad (6.3)$$

With this, Equation (6.2) can be rewritten as:

$$V_{nREF} = k_n \cdot \frac{1}{G_{PWM}} \cdot V_{nBus} \tag{6.4}$$

It shows that the controllable gain (k_n) is one of the determination factor of the PWM inverter's reference signal. The output voltage of the PWM inverter (V_{nAF}) is then modulated as:

$$V_{nAF} = G_{PWM} \cdot V_{nREF} \tag{6.5}$$

In turn, this is equivalent to:

$$V_{nAF} = k_n \cdot V_{nBus} \tag{6.6}$$

Referred to Figure 6.1, voltage drop across the coupling inductor is defined in time domain as:

$$v_{nLaf}(t) = L_{AF} \frac{di_{nAF}}{dt} \tag{6.7}$$

Express above equation in frequency domain gives:

$$V_{nLAF}(j\omega) = I_{nAF} \cdot jn\omega L_{AF} \tag{6.8}$$

where:

I_{nAF} -   harmonic current flow through the coupling inductor

$jn\omega L_{AF}$ -   harmonic reactance of the coupling inductance

V_{nLAF} -   harmonic voltage drop across the coupling inductor

V_{nLAF} is the potential difference between the busbar voltage (V_{nBus}) and the output

voltage of the PWM inverter (V_{nAF}) at a particular harmonic frequency $(n\omega)$.

$$V_{nLAF}(\,jn\omega) = V_{nBus}(\,jn\omega) - V_{nAF}(\,jn\omega) \qquad (6.9)$$

By using equations (6.6), (6.8) and (6.9), the current at the filter-connected branch can

be expressed as:

$$I_{nAF}(\,j\omega) = \frac{V_{nBus}}{jn\omega L_{AF}}(1 - k_n) \qquad (6.10)$$

The output voltage of the proposed active filter is controlled in such a way that it is

phase-locked to the system's busbar voltage at the AF compensation point. Figure 6.2

shows a detailed block diagram of the compensation system mentioned above. It

includes a DC-link voltage level controller, a fundamental voltage synchroniser and a

three-phase inverter.
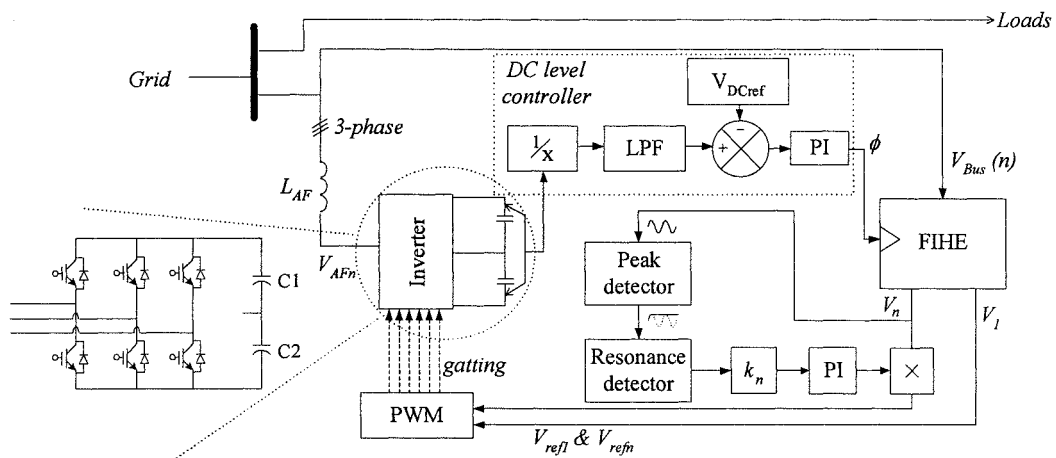
Figure 6.2: System block diagram

6.3 Effects of the Controllable Gain (k_n)

Structure of the compensator and a controllable gain is defined. In this section, effects of the mentioned controllable gain upon the compensator are discussed.

A graphical representation of the Equation (6.10) is shown in Figure 6.3:
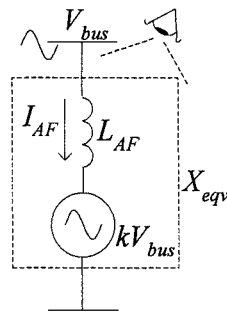
Figure 6.3: Graphical representation of the Equation (6.10)

6.3.1 Inductive mode (L-mode)

Equation (6.10) shows that, $I_{AF}(n)$ is lagged $V_{bus}(n)$ by 90 degree (-j) when the controllable gain ($k(n)$) is less than one ($k(n) < 1$), as:

$$I_{AF\_L}(k, jn\omega) = -j\frac{V_{Bus}(n)}{n\omega L_{AF}}(1 - k(n))$$
(6.11)

Equation (6.11) reveals that, the current ($I_{AF}(n)$) is equivalent to as an inductive current that is inherently lagged inductance voltage by a quarter of an a.c. cycle (90 degree). This phenomenon is shown in the following generalised inductive current equation:

$$I_L(jn\omega) = -j\frac{V_L}{X_L(jn\omega)}$$
(6.12)

Equation (6.12) shows that, reactance is determined by a ratio of voltage and the current, which reveals that the current flows into the active filter connected branch (I_{AF}) and the system busbar voltage (V_{Bus}) at the point where the HRA is connected can be use to derive the branch equivalent reactance (X_{eqv}). This is the equivalent reactance seen by the network from the point of harmonic current source:

$$X_{eqv}(k, jn\omega) = \frac{V_{Bus}(n)}{I_{AF\_L}(k, jn\omega)} \tag{6.13}$$

Therefore, the branch equivalent reactance can be worked out via expressions shown in Equations (6.11) and (6.13):

$$X_{eqv}(k, jn\omega) = \frac{V_{Bus}(n)}{I_{AF\_L}(k, jn\omega)} = j\frac{n\omega L_{AF}}{(1 - k(n))} \tag{6.14}$$

Equation (6.11) can be rewritten in the form as shown in Equation (6.12):

$$I_{AF\_L}(k, jn\omega) = -j\frac{V_{Bus}(n)}{X_{eqv}(k, jn\omega)} \tag{6.15}$$

The $-j$ current sign in Equation (6.15) reveals that, active filter connected branch's equivalent reactance (X_{eqv}) (shown in Figure 6.3) is in lagging mode, or in another word, it is inductive. Therefore, with referred to the generalised inductive reactance equation:

$$X_L(jn\omega) = jn\omega L \tag{6.16}$$

Inductance value of the equivalent reactance (X_{eqv}) can be worked out via (6.14), hence,

$$L_{eqv}(k) = \frac{L_{AF}}{(1 - k(n))} \tag{6.17}$$

Above equation indicates that, active filter branch seen by the power network (as shown in Figure 6.3) is inductive. Means that, the equivalent reactance (X_{eqv}) is inductive when the controllable gain ($k(n)$) is less than one, or in another word, the branch is behaved as a virtual inductor with inductance controlled by the gain ($k(n)$).

6.3.2 Capacitive mode (C-mode)

Again, refers back to the Equation (6.10) for condition when active filter controllable gain is higher than one ($k(n) > 1$), where:

$$I_{AF\_c}(k, jn\omega) = j\frac{V_{Bus}(n\omega)}{n\omega L_{AF}}(k(n)-1)$$ (6.18)

Equation (6.18) reveals that, branch current under this condition is in the leading mode. In which, it is similar to the current flowing in a capacitive loop that is inherently led the capacitive voltage by 90 degree, as:

$$I_c(jn\omega) = j\frac{V_c}{X_c(jn\omega)}$$ (6.19)

The generalised equation showed above can be rearranged to show that the branch equivalent reactance (X_{eqv}) is:

$$X_{eqv}(k, jn\omega) = \frac{V_{Bus}(n)}{I_{AF\_c}(k, jn\omega)}$$ (6.20)

Equation (6.18) and (6.20) show the branch equivalent reactance in such condition is:

$$X_{eqv}(k, jn\omega) = \frac{V_{Bus}(n)}{I_{AF\_c}(k, jn\omega)} = -j\frac{n\omega L_{AF}}{(k(n)-1)}$$ (6.21)

Equation (6.21) shows that, the current in the active filter branch is:

$$I_{AF\_C}(k, jn\omega) = j\frac{V_{Bus}(n)}{X_{eqv}(k, jn\omega)} \tag{6.22}$$

The current (I_{AF_C}) is led the branch voltage (V_{Bus}) by 90 degree (j), which means that the active filter branch is now behaved like a capacitor. Therefore, with referred to the generalised capacitive reactance equation:

$$X_C(jn\omega) = \frac{1}{jn\omega C} \tag{6.23}$$

Capacitance of the equivalent capacitive reactance (X_{eqv}) can be worked via (6.21), thus;

$$C_{eqv}(k) = \frac{(k(n)-1)}{(n\omega)^2 L_{AF}} \tag{6.24}$$

Therefore, when active filter's controllable gain goes above one ($k(n) > 1$), active filter branch sees by the power network as a virtual capacitor which capacitance is controlled by the active filter gain ($k(n)$).

6.3.3 HRA virtually disconnected (Idle-mode)

Other than inductive and capacitive modes mentioned above, there is another condition where the HRA is virtually disconnected from the power network. This state occurs when the controllable gain is equal to one ($k(n) = 1$). In this case according to Equation (6.10):

$$I_{nAF}(j\omega) = \frac{V_{nBus}}{jn\omega L_{AF}}(0)$$

$$= 0$$

(6.25)

The above equation shows that, there is no current flow under this condition. According to the Ohm's law, impedance is infinity when current equals zero, which is same as open circuit. Therefore, the proposed HRA is unable to be seen by the power network, as it is disconnected at that particular harmonic frequency $(n\omega)$.

6.4 Effect of the Virtual Reactance on The Overall Network Impedance

Mathematical expressions shown in section 6.3.1 to 6.3.3 indicate that, active filter branch behaves as a controllable equivalent reactance at the selected harmonic frequency $(n\omega)$. Equations reveal that, gain $(k(n))$ is a key element in the control action. It determines the three stages on filter branch equivalent reactance, they are:

- L-mode, when $k < 1$

- C-mode, when $k > 1$

- Idle-mode, when $k = 1$

Plot of the virtual/equivalent inductance and capacitance created by the active filter with coupling inductance (L_{af}) equals to 10 mH is shown in Figure 6.4 and Figure 6.5.
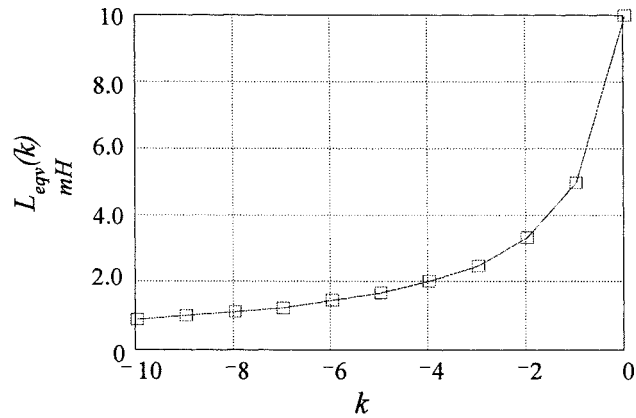
Figure 6.4: Inductance curve of the virtual/equivalent inductance
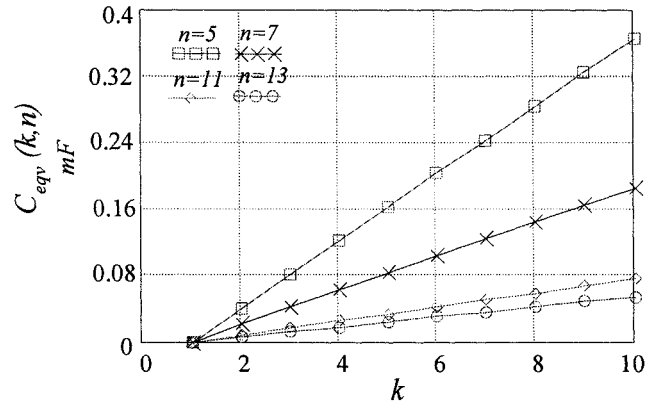
Figure 6.5: Capacitance curve of the virtual/equivalent capacitance generated by the active filter at different frequencies

Figure 6.6 shows a simplified electrical equivalent circuit of the controlled/compensated power system, which includes the source equivalent inductor (L_s), equivalent resistor (R_s), the cable or/and power factor correction capacitor (C_s), active filter equivalent voltage source (V_{nAF}) with a coupling inductor (L_{AF}). Non-linear load is represented as a harmonic current source ($i_{har}(n)$).
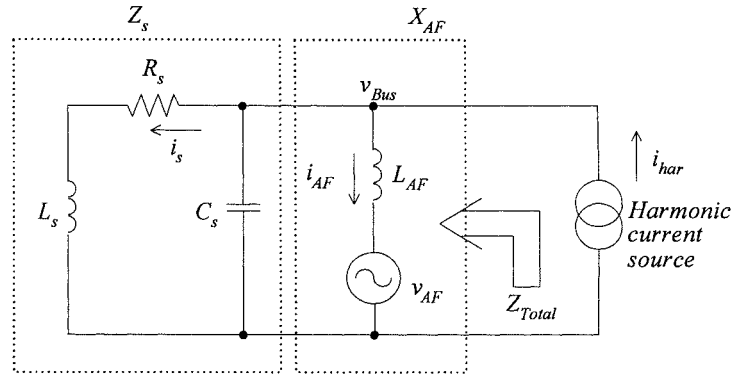
Figure 6.6: Simplified electrical equivalent circuit of the proposed resonance attenuator

The equivalent system impedance (Z_s) can be expressed as:

$$Z_s(jn\omega) = \frac{R_s + jn\omega L_s}{\left(1 - n\omega^2 L_s C_s\right) + jn\omega R_s C_s}$$

(6.26)

Therefore, the total system impedance (Z_{Total}) is:

- When $k(n) < 1$:

$$Z_{Total}(jn\omega) = \frac{Z_s(jn\omega) \cdot X_{L\_eqvAF}(k, jn\omega)}{Z_s(jn\omega) + X_{L\_eqvAF}(k, jn\omega)}$$

(6.27)

Graphically expressed as:
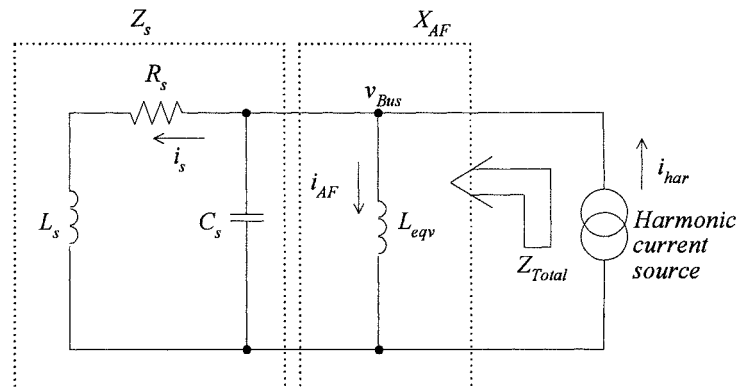
Figure 6.7: Simplified electrical equivalent circuit when the active filter branch behaves as an inductor

- When $k(n) > 1$:

$$Z_{Total}(jn\omega) = \frac{Z_s(jn\omega) \cdot X_{C\_eqvAF}(k, jn\omega)}{Z_s(jn\omega) + X_{C\_eqvAF}(k, jn\omega)}$$

(6.28)

Graphically expressed as:
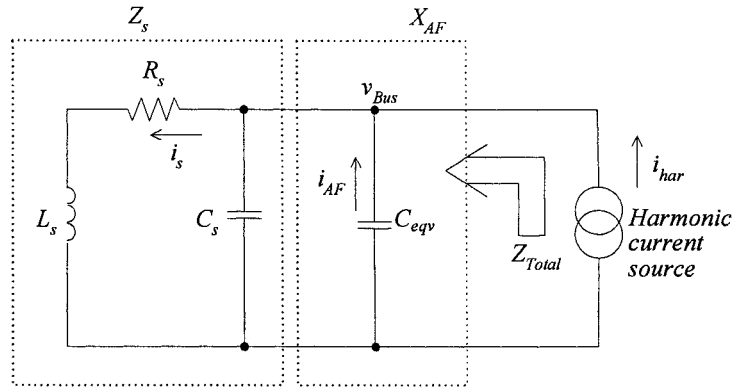
Figure 6.8: Simplified electrical equivalent circuit when the active filter branch behaves as a capacitor

- When $k(n) = 1$:

$$Z_{Total}(jn\omega) = Z_s(jn\omega)$$

(6.29)

Graphically expressed as:
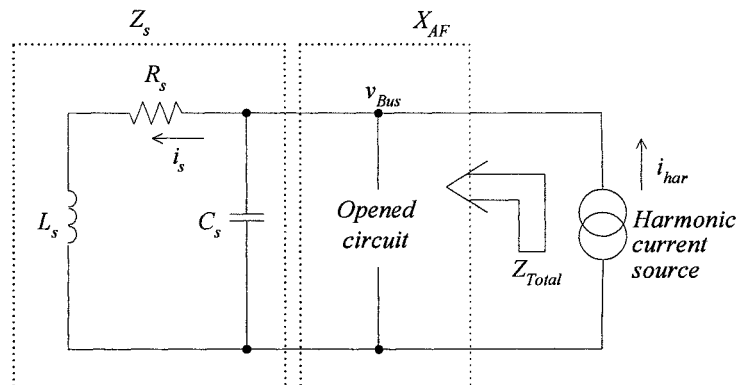
Figure 6.9: Simplified electrical equivalent circuit when the active filter branch is virtually disconnected

Equations (6.27) to (6.29) show that, active filter branch equivalent reactance (X_{eqvAF}) is one of the elements in total system impedance equation, which in turn, means that resonance mode can be altered by changing the value of the controllable gain (k_n). Figure 6.10 shows system impedance versus frequency plot for three different gain (k) stages.

Z_{Total}

$k > 1$ $k = 1$ $k < 1$

C-mode   L-mode

L-mode - active filter acting as a shunt inductor

C-mode - active filter acting as a shunt capacitor

Freq
(Hz)
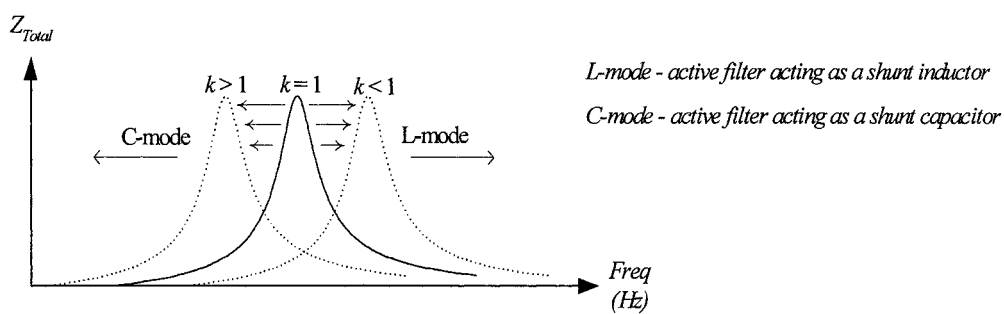
Figure 6.10: Effect of k upon the system impedance

Control algorithm of the proposed technique is graphically shown in Figure 6.11. In the example (Figure 6.11), a resonance mode initially exists at around 360 Hz and the 7th order harmonic (350 Hz) voltage is amplified due to the rise of system impedance. In this case, L-mode attenuation is better compared to the C-mode attenuation. This is because with C-mode attenuation, the shifted resonant peak will pass through the 7th order harmonic frequency, which can cause further amplification of the 7th order harmonic voltage during the shifting process. The dotted line curve represents the shifted harmonic resonance curve when L-mode attenuation is applied.
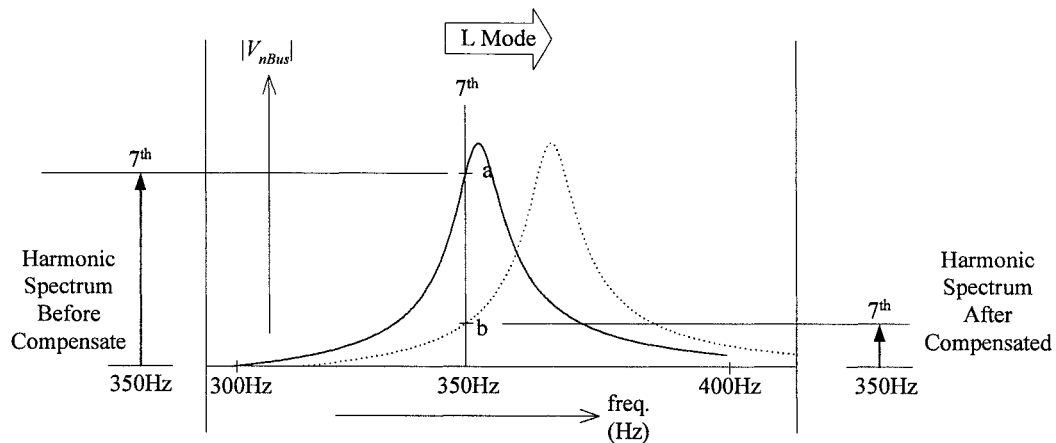
Figure 6.11: Example of resonance compensation

Both single harmonic spectra (7th order harmonic) given in Figure 6.11 show that, magnitude of the 7th order harmonic voltage before and after compensation is reduced from level-a to level-b. This is due to the change of system harmonic impedance (Z_{Total}) at the particular excitation frequency when the resonant mode is shifted by the active filter in the proposed method.

6.5 Selective Harmonic Resonance Attenuation Characteristics

One of the features of the proposed HRA method is that, it does not affect other harmonic components. As mentioned in the previous sections, shunt active filter is controlled to behave as a controllable reactance, either as an inductor or capacitor. Unlike the physical reactive component (i.e.: inductor or capacitor) that changed the system impedance at all frequencies range. Virtual inductor or capacitor created by the active filter is only effective to the selected harmonic frequency ($n\omega$). Surface plot

113

shown in Figure 6.12 demonstrates the change of system harmonic impedance characteristic when inductors and capacitors (passive components) are physically connected to a power system. It shows the effect on different harmonic impedances when the added inductance or capacitance is increased.
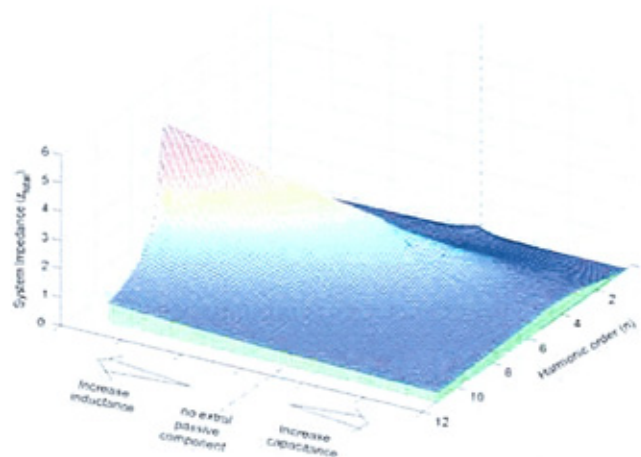
Figure 6.12: System harmonic impedance characteristics with physically added passive component

In the example shown in Figure 6.12, harmonic resonance occurs near the 5th order harmonic frequency (approx. 260 *Hz*) when no extra reactive component is installed for harmonic resonance shifting purpose. When more inductance is introduced (e.g. due to network's capacitance declined, coupling transformer changed, etc), the original harmonic resonance frequency is shifted towards higher frequency range. This is similar to the one shown in Figure 6.11, where when more L is applied, harmonic resonance would be shifted upward (towards higher harmonic frequencies range). In addition, the peak of the harmonic resonance is as well increased. This causes those higher (than 5th) order harmonic components exposed to a higher resonance amplification than it was near the 5th order harmonic frequency (at approx. 260 *Hz*).

114

When physical capacitance increased (e.g. more PFC is applied to the network, more cable is installed, etc), harmonic resonance is shifted towards lower harmonic frequencies range. This again creates problem, as when harmonic resonance occurred at the dominant harmonic range, it might affects the fundamental component or amplified higher harmonic component.

In the proposed technique, active filter is controlled as a virtual inductor or capacitor. And, as aforementioned, the inductance or capacitance produced by active filter is only effective upon a particular harmonic frequency, not to others. Therefore, phenomenon shown in Figure 6.12 is not happen here.

Surface plot in Figure 6.13 shows an example when attenuation action is focused on 5th order harmonic resonance. In which, the active filter's controllable gain ($k(n)$) is set to 5th order harmonic frequency ($n = 5$). Therefore, instead of the overall harmonic impedance, in this case, only 5th order harmonic impedance is affected by the attenuation action.
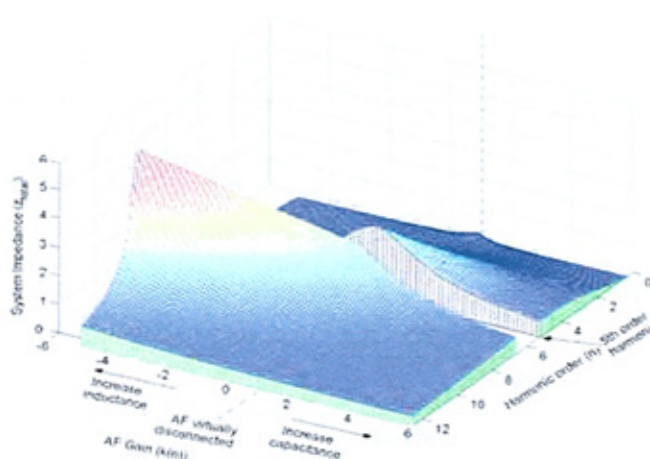
Figure 6.13: System harmonic impedance plot with the proposed active filter control technique (target on the 5th order harmonic resonance)

Thus, with the proposed method, overall system impedance structure is dissected and only has to concentrate on the selected harmonic component. This effect is shown in Figure 6.14.
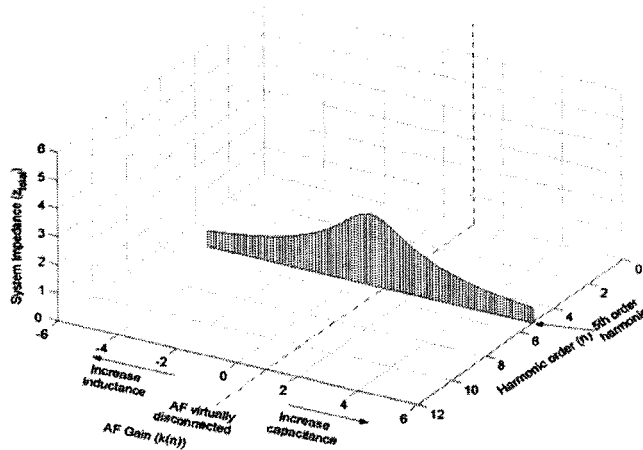
Figure 6.14: Plot of a single harmonic impedance (5th) vs. the change of active filter gain ($k(n)$)

Single system harmonic impedance plot shown in Figure 6.14 displays only the selected harmonic impedance (5th), and only that particular harmonic component can see the effect of the virtual reactance. The active filter is virtually disconnected at other harmonic frequencies ($k(n) = 1$ when $n \neq 5$); hence, no other harmonic components can see it. Figure showed that, 5th order harmonic resonance is reduced as what was discussed in section 6.4, where, the change of system impedance due to the change in $k(n)$ is only effective on the selected harmonic frequency ($n\omega$), to other harmonic frequency's components the active filter is virtually disconnected. Therefore, their harmonic impedance characteristic is unchanged. Unlike the passive filter (or physical passive reactive components), in this case, no new harmonic resonance is created.

CHAPTER 7

PERFORMANCE EVALUATION OF THE HRA TECHNIQUE (SIMULATION WORK)

7.1 Introduction

Proposed HRA method is evaluated via computer simulation and laboratory experiment. Results obtained from simulation are presented in this chapter to justify the theory discussed in the previous chapter.

Simulation is carried out in MATLAB/SIMULINK platform for a three-phase three wire power system model. The system configuration including the attenuator is shown in Figure 7.1.
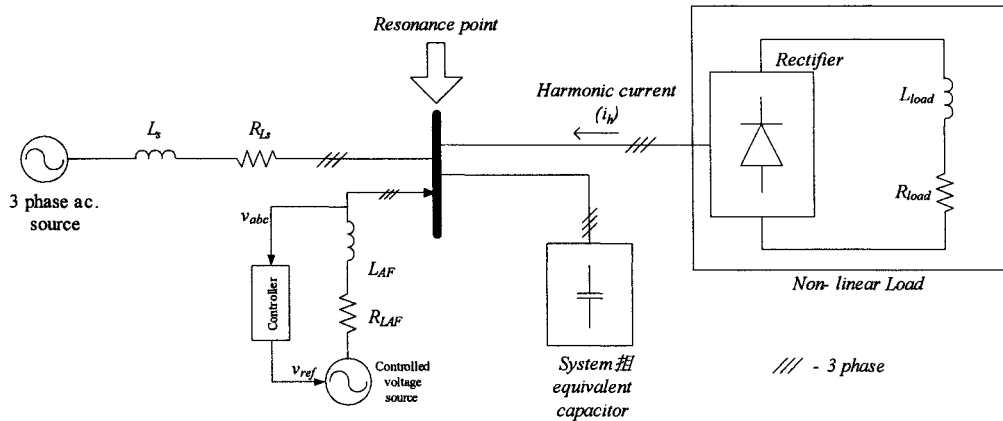
Figure 7.1: Configuration of the simulated system model

In the model, a 400 V three-phase power source is used to supply a 5 kW non-linear

load representing a harmonic current source. Inductance (5 *mH*) and equivalent

resistance (0.8 *Ohm*) at the source side are used to model a typical weak rural

distribution network's system source and up-stream line impedances. Together with

that, shunt capacitors are implemented at the load side (down-stream) to model the

equivalent system shunt capacitor (e.g. PFC capacitors, cable shunt capacitance, etc.).

Selected capacitances (40 *uF* for scenario 1 and 42 *uF* for scenario 2) have been used

to create two harmonic resonance scenarios which would be discussed later. A shunt

active filter is modelled using a controllable three-phase voltage source. It is coupled to

the system PCC busbar in parallel to the equivalent capacitor via a three-phase

coupling inductor. FIHEs are used in the controller to obtain individual harmonic

information. Figure 7.2 shows the FIHEs configuration to obtain reference signal.

Details of the closed-loop controller used, are shown later in this chapter.

118
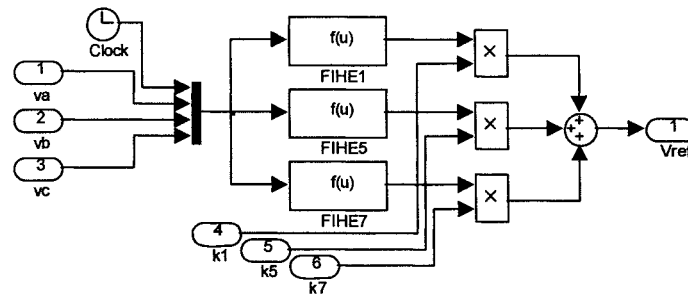
Figure 7.2: Configuration of the FIHE to obtain the reference signal

7.2 Harmonic Resonance Simulation Model

System resonance condition is developed in the model showed above. Capacitance (PFC) are chosen in order to generate the following two resonance scenarios, which are the most common reasons for changes in the network impedance and resulting harmonic resonance in distribution networks. These resonance conditions are modelled and used to evaluate the proposed resonance attenuation technique.

- **Resonance scenario 1 – increase of network's shunt capacitance**

Scenario 1 is to model the harmonic resonance problem caused by network's developments (e.g. expansion, upgrading, modernisation, etc.). In such cases, it is common that, more PFC capacitors and/or low cost passive filters are installed into the network to improve the quality of voltage supply. Consequently, total capacitance in the network increased; or, in some cases the use of power compensation devices with series inductance (e.g. UPFCs, ASVCs, etc.) may also cause system's series inductance to increase. In both cases (increase of shunt capacitance, and/or the systems source side series inductance), harmonic resonance is shifted down from higher frequency range to

CHAPTER 7

a lower frequency range. Thus, the possibility of creating harmonic resonance at dominant harmonic frequency is increased. This resonance phenomenon is modelled, and such harmonic resonance is created near the 7th order harmonic frequency. By using FIHE, 7th order harmonic voltage at the busbar where active filter is connected is extracted. Results obtained show that the created harmonic resonance (parallel resonance) starts at time t=100 ms (Figure 7.6). As a consequence the 7th order harmonic component is increased from 10.1 V peak to about 29 V peak in about 100 ms. This increase causes higher distortion at the system busbar voltage as shown in Figure 7.3. The extracted fundamental and 5th order harmonic voltages are separately shown in Figure 7.4 and Figure 7.5.

Figure 7.3: Distorted busbar voltage (phase a)

Figure 7.4: Extracted fundamental voltage (phase a)

120
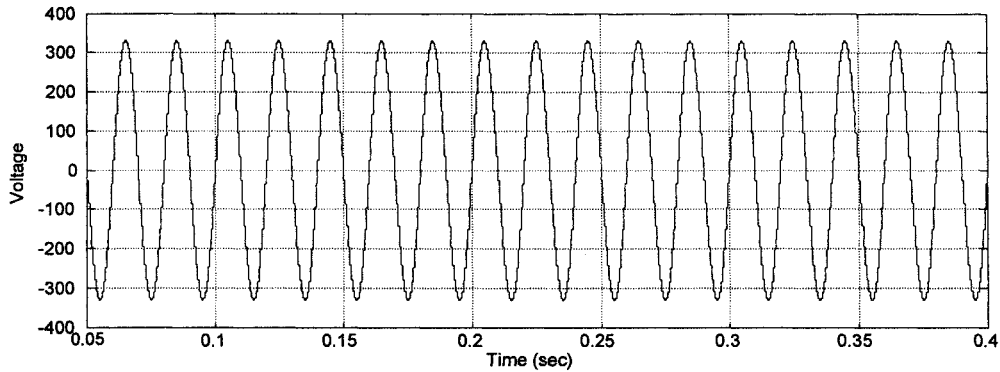
Figure 7.5: Extracted 5th order harmonic voltage (phase a)

Figure 7.6: Extracted 7th order harmonic voltage (phase a)

- **Resonance scenario 2 – reduce of network's shunt capacitance**

In this case, system resonance is simulated by creating a reduction on the network's shunt capacitance (e.g. PFC capacitors, passive filters, etc.). Characteristics of the capacitors show that their capacitance reduces with the capacitor's life spent and the ambient temperature (capacitors are positive temperature coefficient devices). Thus, total systems capacitance may reduce due to these factors. This reduction shifts the harmonic resonance frequency from a lower band to a higher band (e.g. from between

5th and 7th to near 7th order harmonic frequency). This resonance condition is modelled and the resultant waveforms are shown in Figure 7.7 to Figure 7.10. In Figure 7.7, distorted busbar voltage waveform is shown. Condition of the busbar voltage before and after harmonic resonance (near lower side of the 7th order harmonic frequency) is presented. This waveform shows that, voltage distortion at the busbar is increased when harmonic resonance is shifted closer to the 7th order harmonic frequency. Figure 7.8 shows the extracted fundamental harmonic voltage. Figure 7.9 records the waveform of the extracted 5th order harmonic voltage and Figure 7.10 shows the waveform of 7th order harmonic voltage, in which the effect of harmonic resonance can be noticed from time t = 0.15 s (with 8.2 V peak) and reaches its maximum (2.35 V peak) at t = 0.348 s. In this case, slower (near 200 ms) resonance phenomenon is shown which is comparable to the one described in scenario 1. The reason for this is to model the slow variation of the systems capacitance, as in a real system; decline of capacitance in this case takes time in the region of months or years.
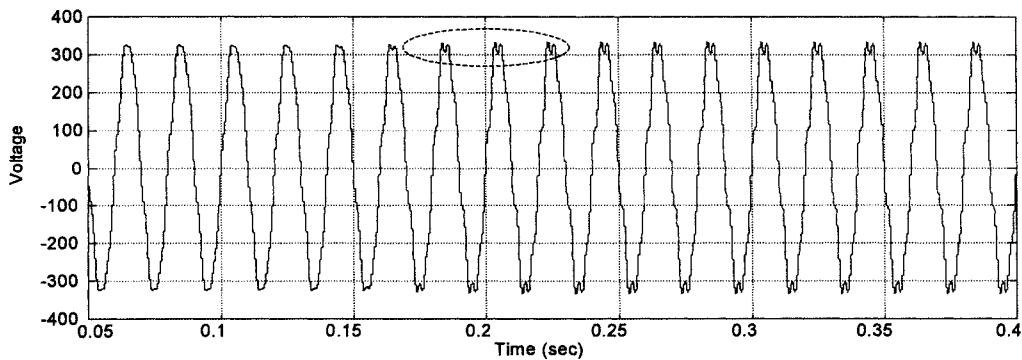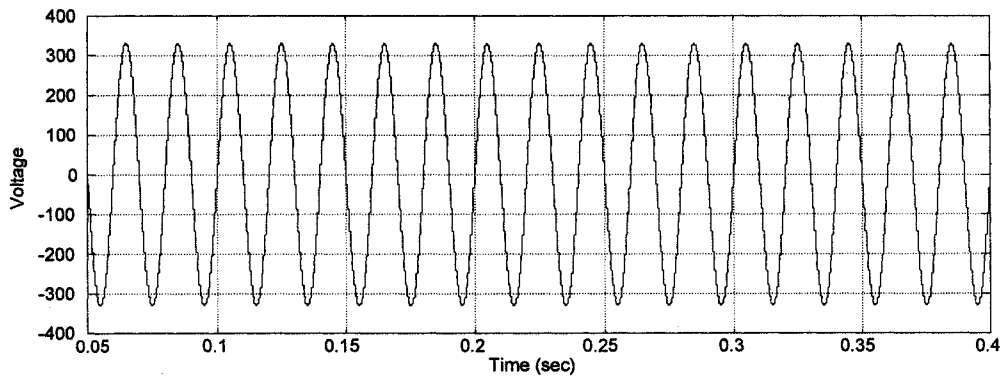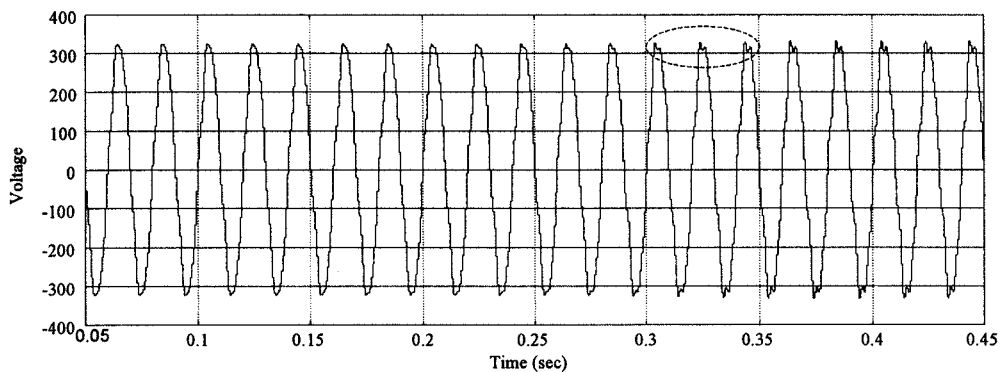

Figure 7.7: Distorted busbar voltage (phase a)
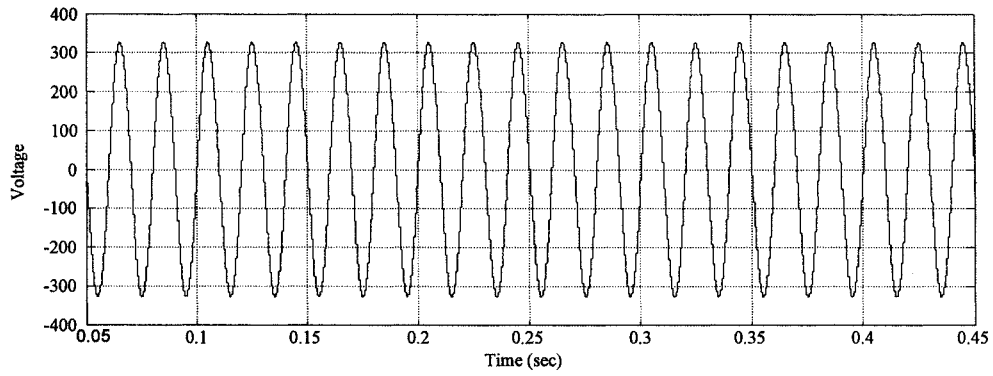
Figure 7.8: Extracted fundamental voltage (phase a)

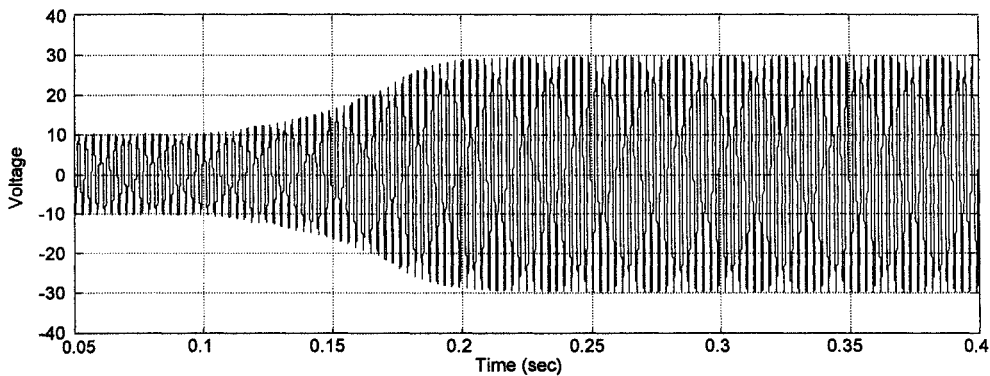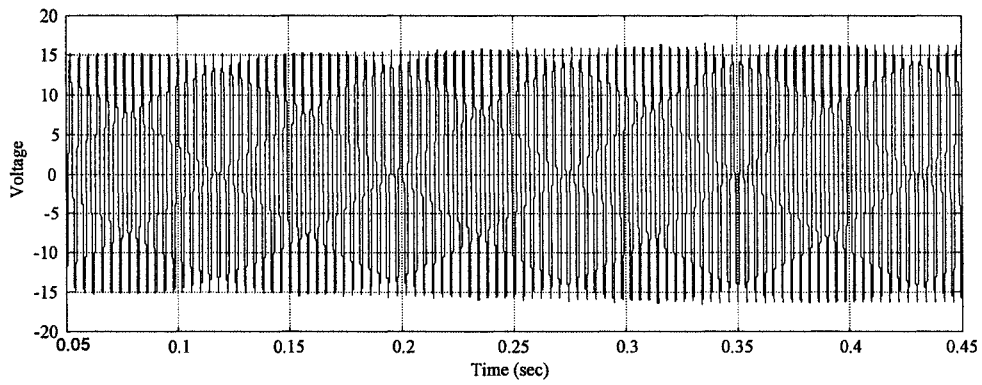**Figure 7.9: Extracted 5th order harmonic voltage (phase a)**
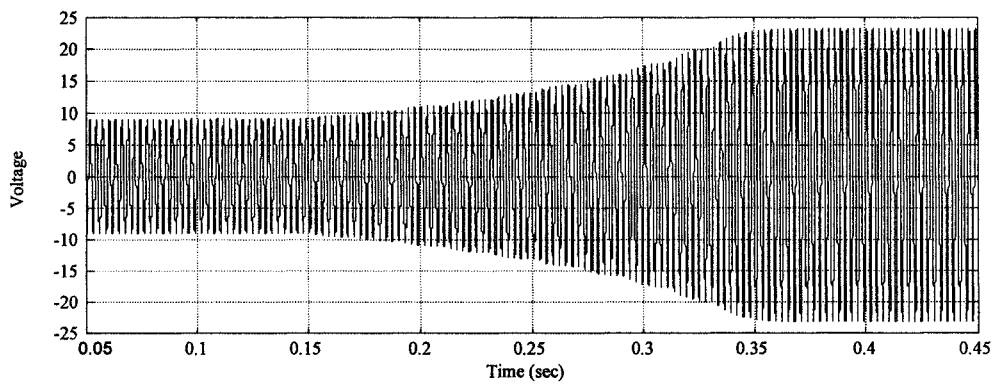
Figure 7.10: Extracted 7th order harmonic voltage (phase a)

Waveforms recorded in Figure 7.3 to Figure 7.10 show that the required harmonic resonance conditions are successfully created. In the following sections, results of harmonic resonance attenuation using the proposed technique are presented and discussed.

7.3 Open-loop Performance

In this section, both HRA modes (L-mode and C-mode) are evaluated via computer simulation and results are presented. The first one is named as L-mode compensation, where, active filter is controlled to represent a virtual shunt inductor to the system. The second one is C-mode compensation, in which, the active filter is controlled to act as a virtual shunt capacitor to the harmonic current source. Principles of these two modes of operation were discussed in detail in Chapter 6, hence, will not be repeated here.

- **Resonance scenario 1 – Attenuation using L-mode**

In resonance scenario 1, network development causes more capacitors to be added into the network, which causes the network's natural frequency to shift towards a lower frequency range (e.g. close to the 7th harmonic frequency). Therefore, in this case, an inductance is required to be reduced in order to neutralise the excessive amount of capacitance in the network. In a simpler term, shunt inductance of the network is required to be reduced in order to shift the harmonic resonance back to a higher frequency range (refer to Chapter 6 for detailed explanation).

In this case, active filter connected to the system busbar is controlled to behave as an inductor to reduce the total inductance in the network. Negative gain $(-k_7)$ is used and the results of attenuation are shown in Figure 7.11 to Figure 7.14. In Figure 7.11, condition of the distorted busbar voltage before and after attenuation (attenuation starts at t = 0.42 s) is shown. It is clear that the attenuator has reduced the distortion at the busbar voltage caused by the excited 7th order harmonic current.

Waveform for the extracted 7th order harmonic voltage is shown in Figure 7.14. The effect of harmonic resonance attenuation is clearly shown, as the magnitude of the 7th harmonic is reduced from 29.7 V peak to 10.2 V peak (at t = 0.56 s). Figure 7.12 and Figure 7.13 show the extracted fundamental and 5th order harmonic voltages. These waveforms show that the attenuator is working independently on individual harmonic component. The results show that these two voltage waveforms are not affected by the attenuation of the 7th order harmonic component. These results confirm the theory described in Chapter 6, where the operation of the proposed harmonic attenuation method is only effective to the selected harmonic component (in this case the 7th order harmonic component).

Figure 7.11:Distorted busbar phase voltage

Figure 7.12: Extracted fundamental voltage
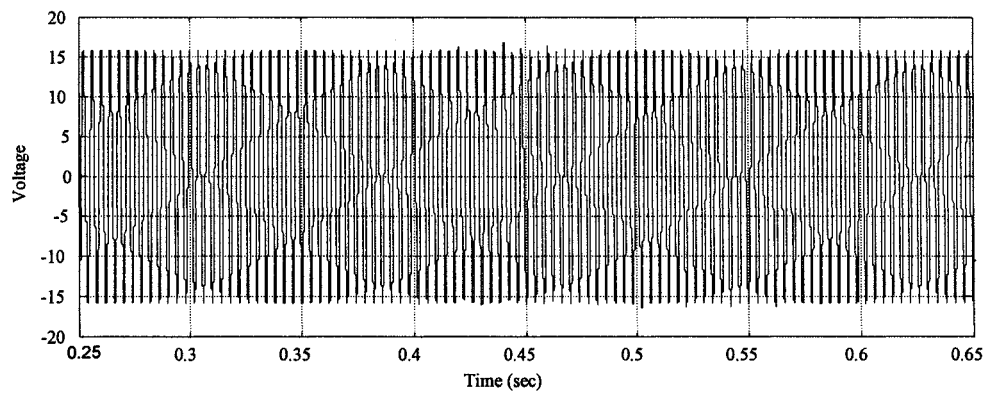
Figure 7.13: Extracted 5th order harmonic voltage

Figure 7.14: Extracted 7th order harmonic voltage

126

• **Resonance scenario 2 – Attenuation using C-mode**

Distribution networks are always designed to avoid harmonic resonance. However, reduction in network's capacitance (for the reasons mentioned in section 7.2) causes the network natural frequency to shift towards a higher frequency range. In the modelled case, resonance is shifted gradually from a frequency within 5th order harmonic and 7th order harmonic frequencies to near 7th order harmonic frequency. Therefore, C-mode compensation is required in order to shift the harmonic resonance back down. Results of C-mode attenuation are shown separately in Figure 7.15 to Figure 7.18. The distorted busbar voltage, extracted fundamental voltage and the extracted 5th and 7th order harmonic voltages are all presented. Distorted busbar voltage shown in Figure 7.15, and the 7th order harmonic voltage shown in Figure 7.18 demonstrate the effects of C-mode HRA. They show that the harmonic resonance has been successfully shifted (attenuated), which causes 7th order harmonic voltage at the busbar to reduce from 23.5 V peak to 9.8 V peak. The fundamental voltage (Figure 7.16) and the extracted 5th order harmonic voltage (Figure 7.17) show the inter frequencies independency of the proposed harmonic attenuation technique.

The overall attenuation actions/processes are including harmonic extraction, resonance detection, control actions (e.g. compensation mode decision making, feedback control, etc.), attenuation action and system's response. The 100 *ms* response time shown in the Figure 7.14 and Figure 7.18 are not only the harmonic extraction action (contributed by the FIHE), it includes all the mentioned actions/processes (accept resonance detection action). Fast harmonic extraction is desired in many applications. Shorten the harmonic

extraction time means the controller would have gained more time for the rest of the
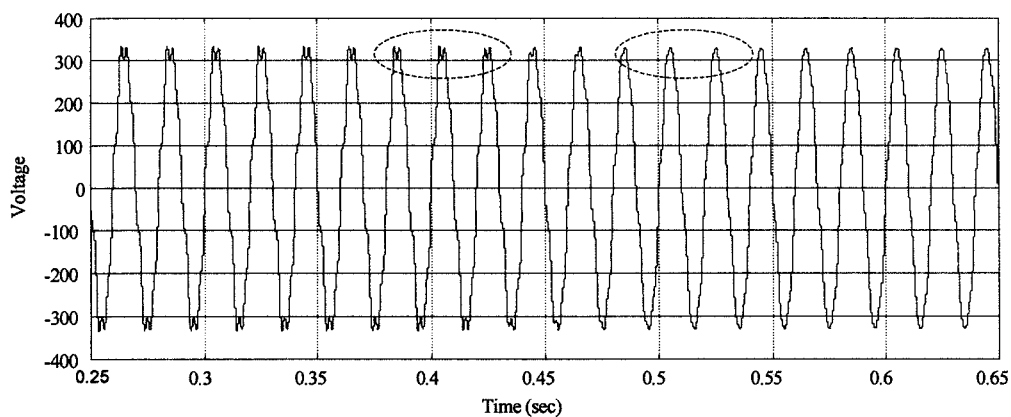
control actions/states.
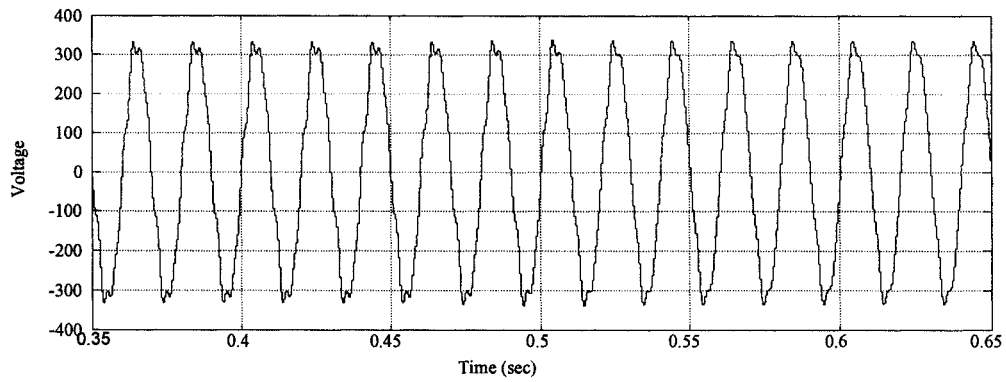
Figure 7.15: Distorted busbar phase voltage
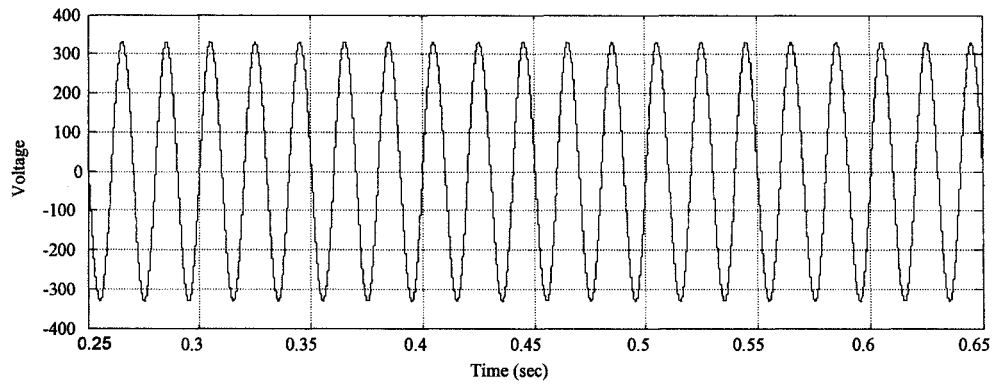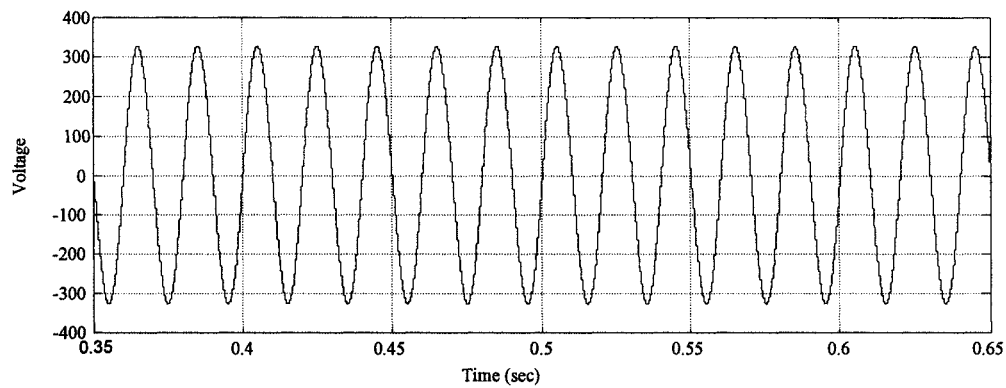

Figure 7.16: Extracted fundamental voltage

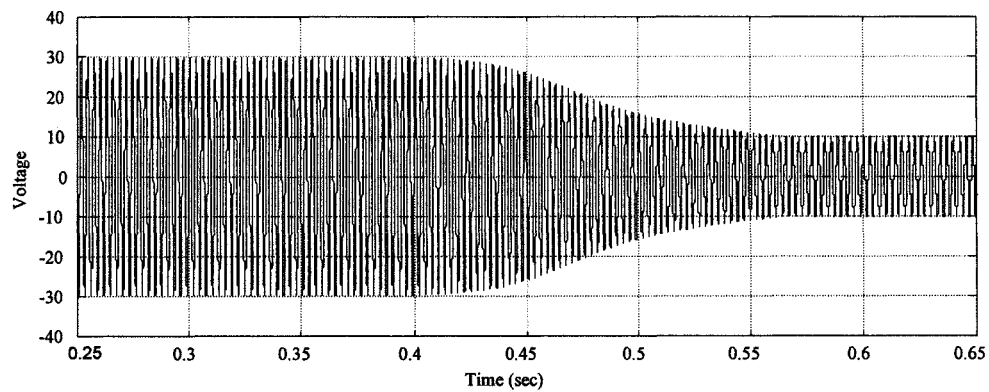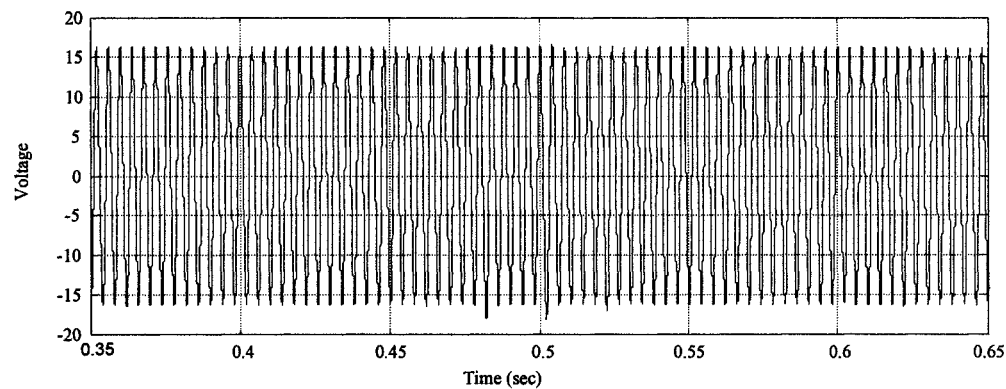**Figure 7.17: Extracted 5th order harmonic voltage**

128
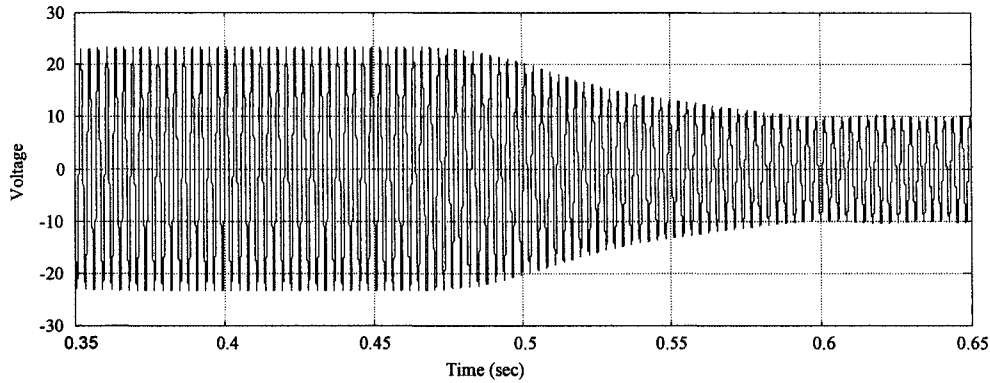
Figure 7.18: Extracted 7th order harmonic voltage

Functionality of the proposed HRA technique has been demonstrated in this section. In the following section, a more quantitative analysis is presented which compares simulation results with the results obtained from the mathematical model derived in Chapter 6.

• **Resonance attenuation analysis**

Comparisons are made between simulation results and calculation results (using equations given in Chapter 6) to justify the theory/concept of the proposed technique and to ensure that the attenuator performance agrees with the theory.

Figure 7.19 and Figure 7.20 show the extracted 7th order harmonic voltage at the busbar against different gain values (k_7). In Figure 7.19, L-mode compensation is analysed (with k_7 moves towards negative). In this case, active filter behaves as an inductor. Therefore, Equation (6.17) shown in Chapter 6 is used to calculate the equivalent inductance formed up by active filter, and uses it to obtain system busbar voltage in order to compare with the simulation results.
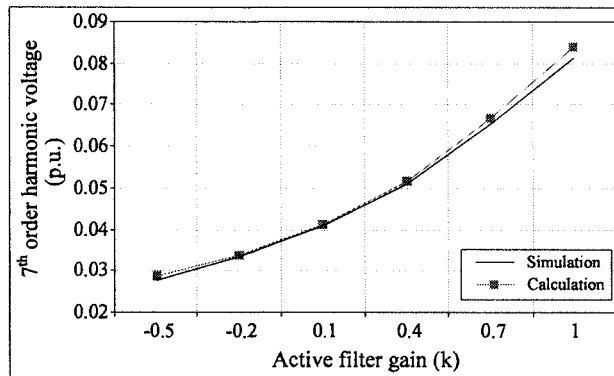
Figure 7.19: Plot of the 7ᵗʰ order harmonic voltage at the active filter busbar versus the active filter gain (L-mode attenuation)

Results of C-mode compensation are analysed and plotted in graph that shown in Figure 7.20. As mentioned earlier, in this mode, active filter is behaved as a virtual capacitor to the network, thus, Equation (6.24) is used to obtain the equivalent capacitance of the active filter branch, and uses it to calculate the 7ᵗʰ order harmonic voltage at the system busbar.
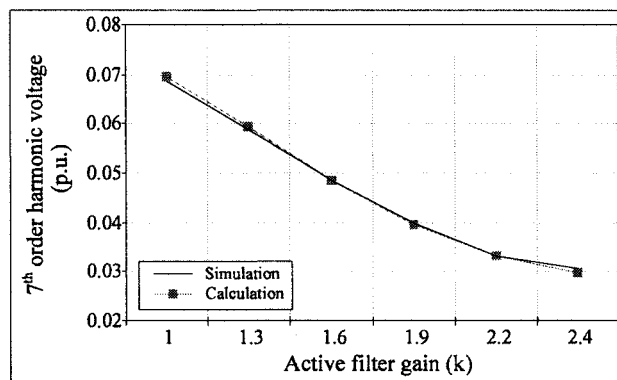
Figure 7.20: Plot of the 7ᵗʰ order harmonic voltage at the active filter busbar versus the active filter gain (C-mode attenuation)

Both graphs showed a very close agreement between the simulation and analytical results verifying the theories presented in Chapter 6. The high level of agreement on

the simulation and calculation results is due to the use of the ideal voltage source as the

PWM inverter in the simulation. This concept is widely recognised in the field. The

validity of modelling a proper designed PWM inverter as a voltage source would be

discussed in detail and verified in Chapter 8 section 8.5.

7.4 Closed-loop Performance

A feedback controller is developed for the proposed harmonic resonance attenuator

(HRA) to react automatically when harmonic resonance occurred. It analyses the

condition and determines the required attenuation mode (e.g. L or C mode). The

controller is developed in MATLAB/SIMULINK platform and it consists of three main

stages (the FIHE, the peak value calculator, and the gain determiner).

Following the very initial state (the FIHE) that has previously explained in detailed, a

set of peak value calculator is constructed as the second stage of the controller (shown

in Figure 7.21) to calculate the peak value of the extracted harmonic component from

the output of FIHE.
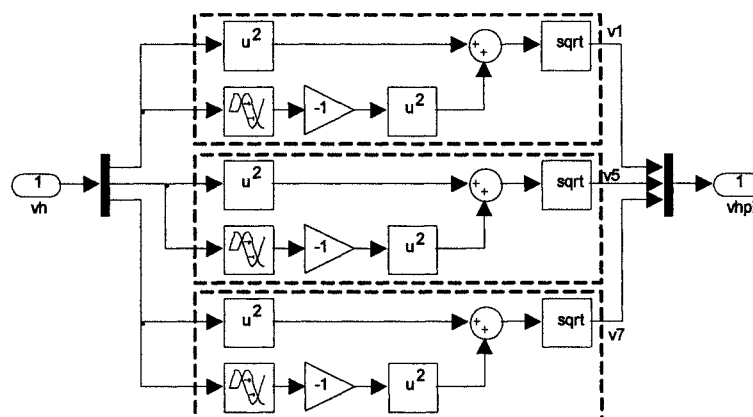
Figure 7.21: Peak value calculator for three harmonic orders (1st, 5th and 7th)

The third stage of the controller (shown in Figure 7.22 – diagram is for a single

harmonic order) is used to determine the correct attenuation mode and injecting proper

control gain (k_n). Two states of feedback loops are used, the inner loop is to determine

the magnitude of gain and the outer loop is to ensure its polarity (to ensure that the

correct attenuation mode is applied). Proportional-Integral (PI) controller is used in the

inner loop for a smooth attenuation effect. A logic trigger controller is used in the outer

loop to ensure incorrect attenuation mode can be corrected quickly. In this simulation,

C-mode attenuation is first activated and a maximum allowable limit is set to judge

whether attenuation is in the right mode. As incorrect attenuation mode would increase

the level of resonance. Opposite (L-mode in this case) attenuation mode will be

activated once the harmonic voltage (output of peak value calculator) hits the above

mentioned trigger limit. This control action is simulated and details are presented at the

end of this chapter after test of inner loop with two different system resonance

conditions (refer to section 7.2 for details of these resonance conditions).
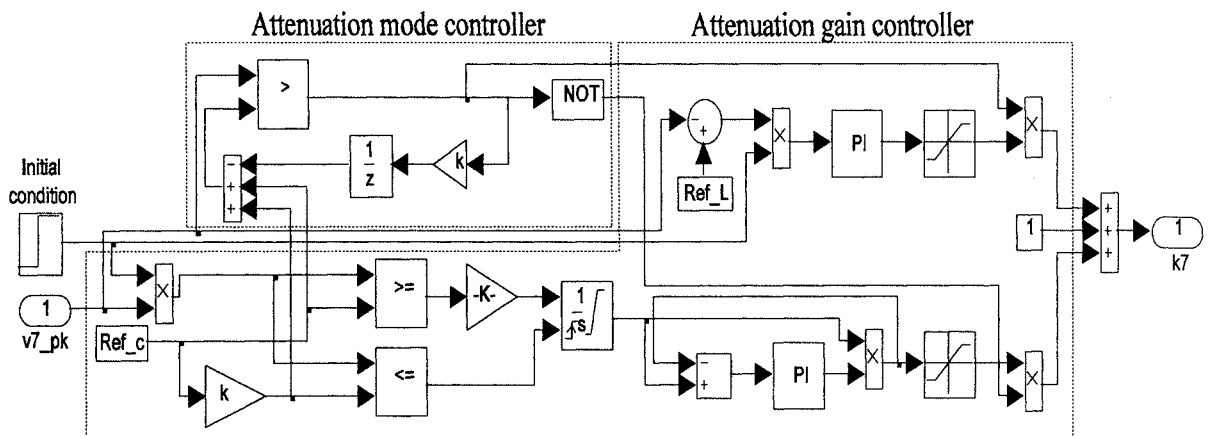
Figure 7.22: Threshold and attenuation modes controller

- **Attenuate harmonic resonance scenario 1**

With the controller mentioned above, a closed-loop harmonic resonance attenuator is developed and tested in simulation environment. In this case, system required more inductance to be injected. L-mode attenuation is supplied and results are shown in Figure 7.23 to Figure 7.26.

Due to the rapid control action, resonance has been successfully attenuated before reaching its harmful level. This is clearly noticed in the system busbar voltage shown in Figure 7.23 which has no obvious harmonic resonance effect (note the waveform of Figure 7.15 which shows the effects of resonance). The 7th order harmonic voltage shown in Figure 7.26 illustrates that the harmonic resonance is suppressed before it reaches its peak (refer to Figure 7.6 for the waveform without compensation).
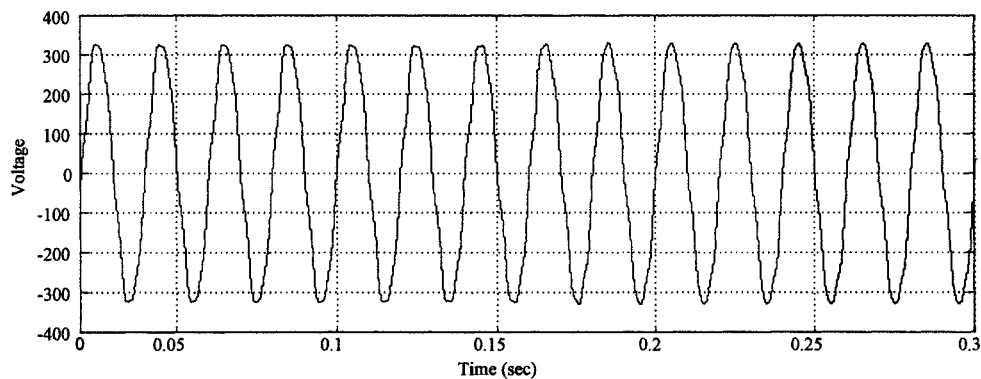
Figure 7.23: System busbar voltage
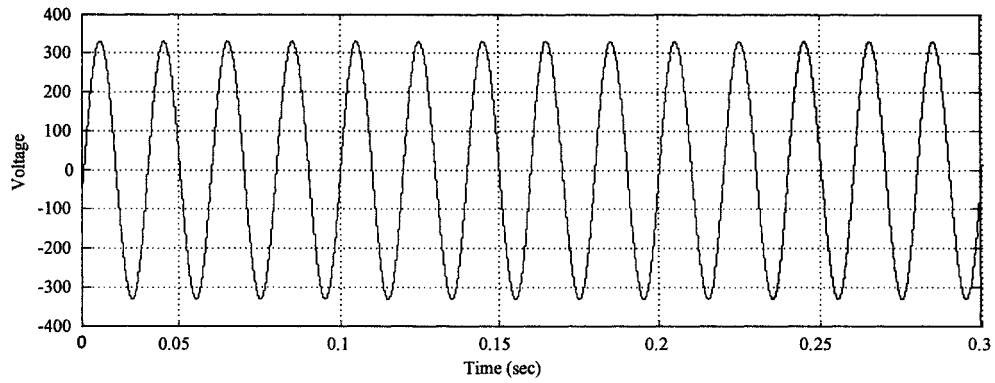
Figure 7.24: Extracted fundamental voltage
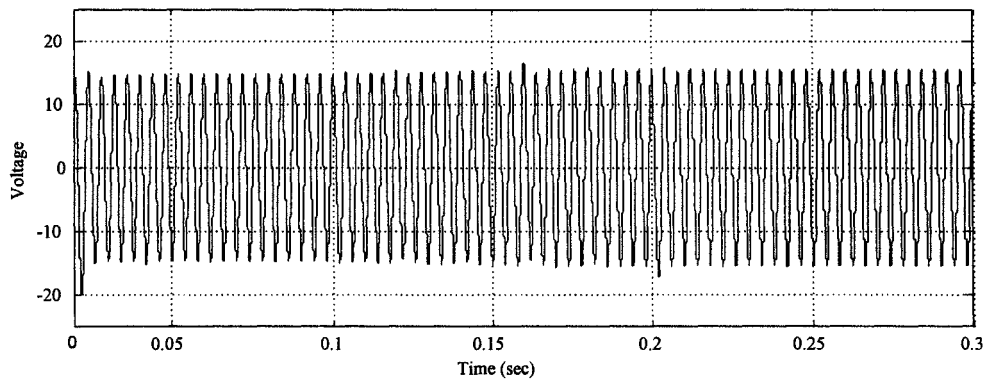
Figure 7.25: Extracted 5th order harmonic voltage
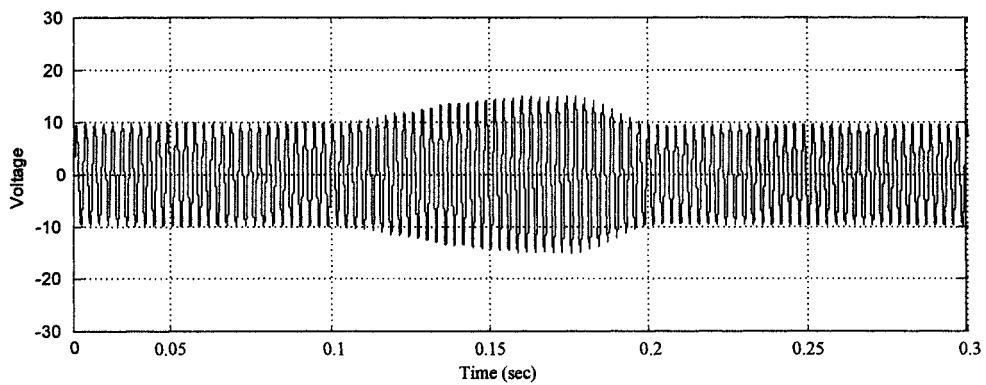
Figure 7.26: Extracted 7th order harmonic voltage, which shows resonance and controller effects

134

CHAPTER 7

- **Attenuate harmonic resonance scenario 2**

The closed-loop attenuator is tested under the resonance condition described in second scenario, where C-mode attenuation is required. In this case, attenuator is set to first deliver C-mode attenuation, which is the correct mode, hence outer loop of the controller is not been activated. Results of the test are shown in Figure 7.27 to Figure 7.30. These results showed that the attenuator has successfully attenuated the network's harmonic resonance. Reason for the slightly increased of distortion shown in Figure 7.27 (after 0.15 *sec*) is given in Appendix G.
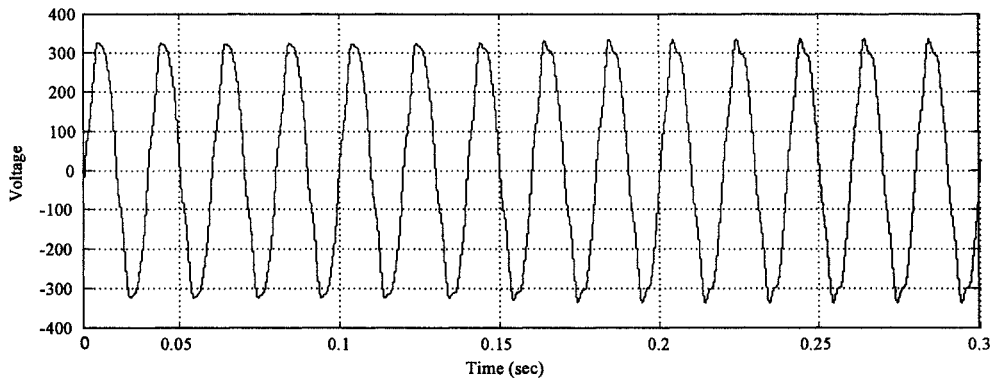
Figure 7.27: System busbar voltage
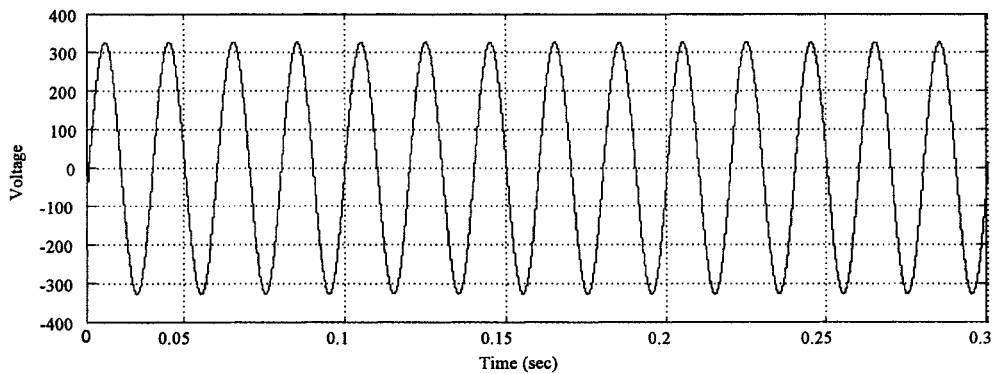
Figure 7.28: Extracted fundamental voltage

135
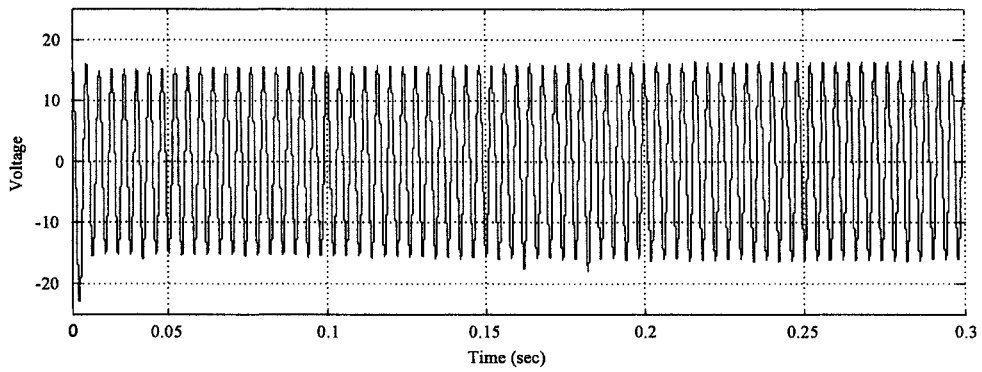
Figure 7.29: Extracted 5th order harmonic voltage
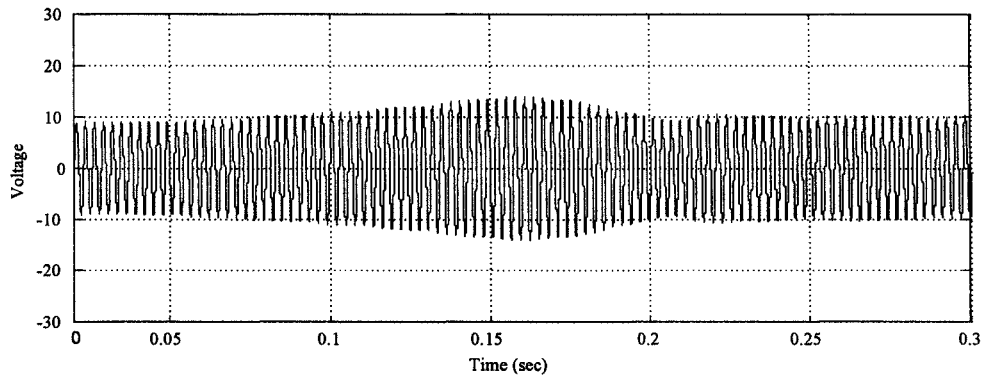
Figure 7.30: Extracted 7th order harmonic voltage, which shows the effect of resonance and controller effects

Magnitudes of the harmonic components (shown above in scenario 1 and scenario 2) before resonance, during resonance and after attenuated are graphically shown in Figure 7.31.
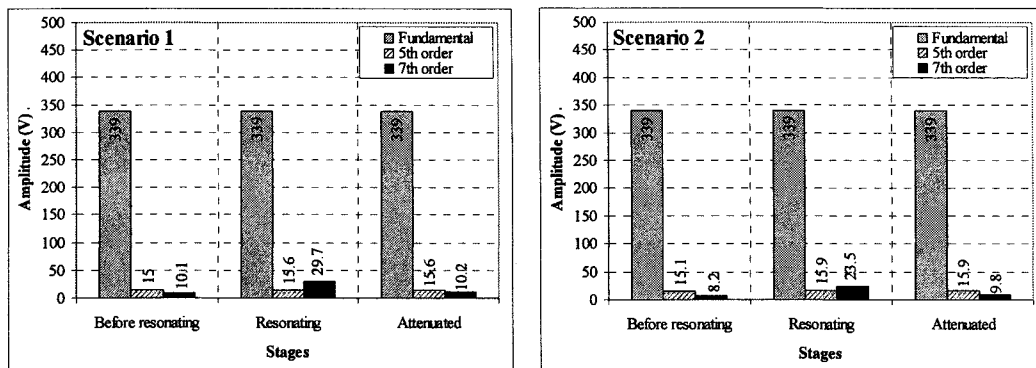
Figure 7.31: Attenuation results achieved in senario 1 and 2

- **Attenuate harmonic resonance scenario 1 with incorrect attenuation mode (initially)**

In this case, behaviour of attenuation mode controller (outer loop) is tested. An incorrect control action was first given, in which it increases the resonance condition. Attenuation mode controller is activated and instruction is given by it to the gain controller to change its attenuation mode.

In first harmonic resonance scenario, system required more inductance in order to shift away harmonic resonance. However, C-mode attenuation was supplied, and it increases the magnitude of 7th order harmonic voltage (showed at the output of peak value calculator). Mode controller is activated, as the harmonic voltage reached its allowable limit (50% more than its original level). Control action is changed immediately to L-mode attenuation and this results a reduction on the resonance's magnitude. Figure 7.32 shows the 7th order harmonic voltage waveform (FIHE output), Figure 7.33 shows the output of the peak value calculator, and Figure 7.34 shows the control action (k_n).

137
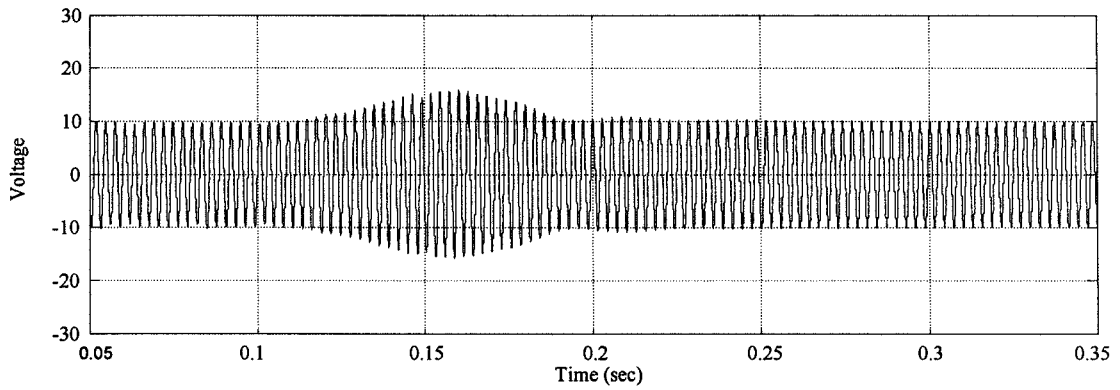
Figure 7.32: 7th order harmonic voltage waveform (output of the FIHE)
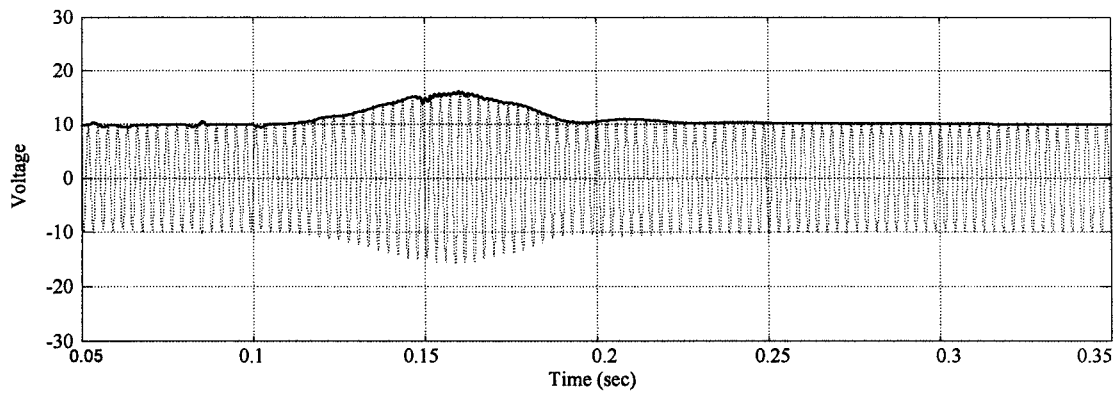
Figure 7.33: Output of the 7th order harmonic voltage peak value calculator (bolded line)
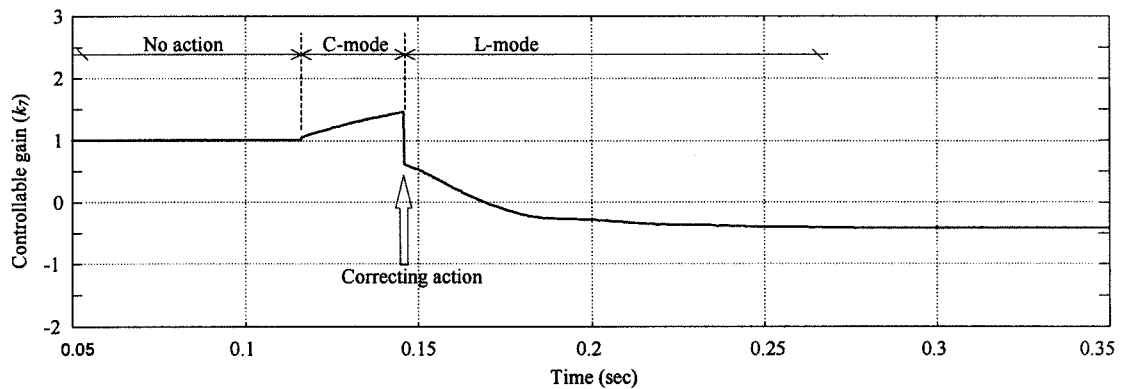
Figure 7.34: Control gain (k_7) applied to 7th order harmonic voltage

Other than attenuate harmonic resonance, proposed attenuator can be used to compensate harmonic voltage distortion in weak system, where harmonic voltage is detectable.

CHAPTER 8

PERFORMANCE EVALUATIONS OF THE HRA TECHNIQUE (EXPERIMENTAL WORK)

8.1 Introduction

In this chapter, the proposed FIHE and HRA are evaluated using an experimental model. The system configuration used in the experiments is shown in Figure 8.1. It is composed of four main parts, these are:

- Power network's model, which includes three-phase voltage source, network's equivalent impedance, three-phase non-linear load, and PFC capacitor bank.

- Real-time data acquisition/control board (DS1103 PPC) and its interface unit

- Desktop computer (to run MATLAB/SIMULINK and dSPACE) for FIHE and controller

- 2-level PWM voltage source inverter, its coupling inductors, dwell-time controller and isolated gate drivers
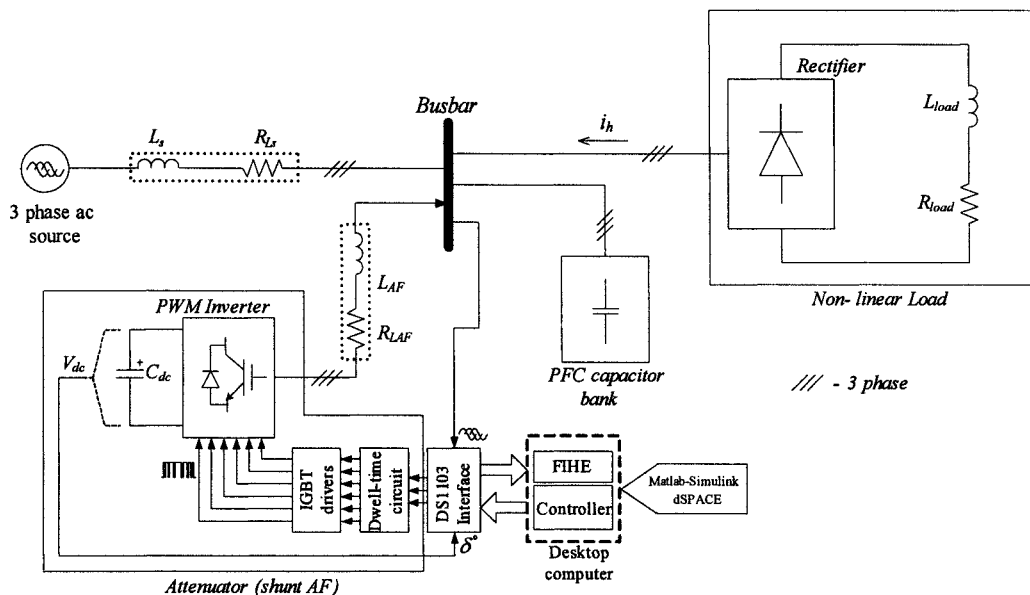
Figure 8.1: Configuration of the experimental set-up

Pictures of the set-up are shown in Figure 8.2 to Figure 8.5, and details of the test system development and experimental results are discussed in the following sections.
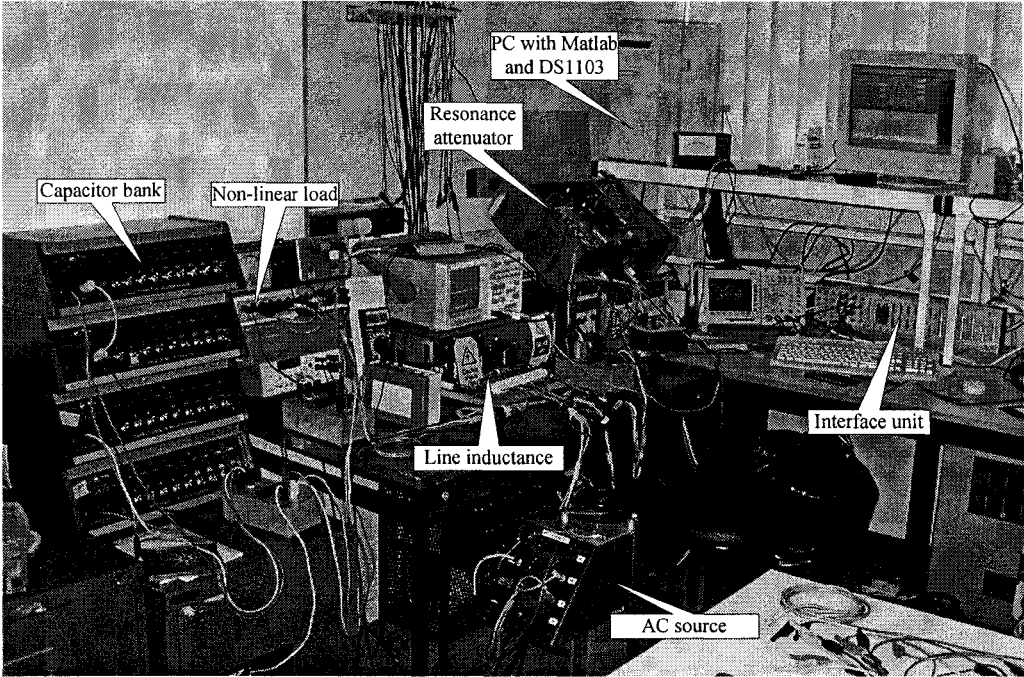
Figure 8.2: Overall experimental system set-up
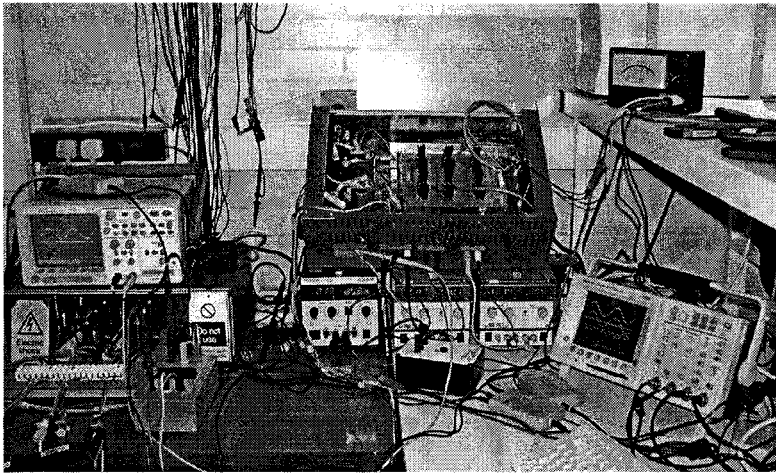
Figure 8.3: Experimental set-up showing the inverter (HRA) and measurement equipment
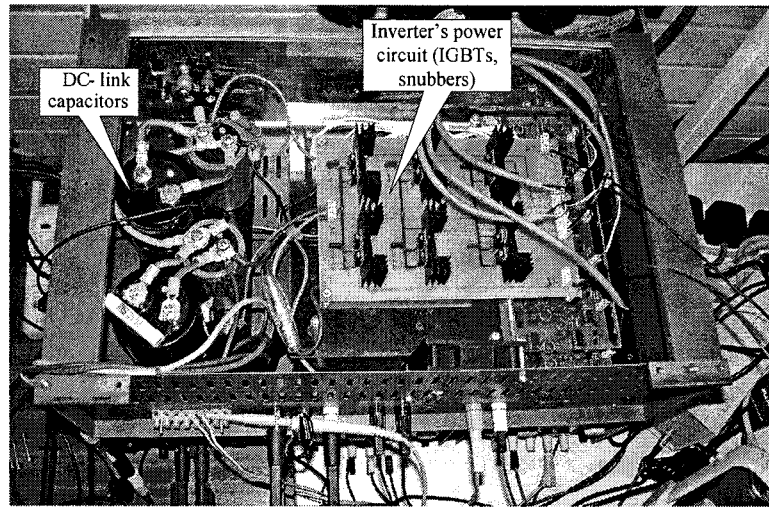
Figure 8.4: Experimental set-up showing the inverter power circuit
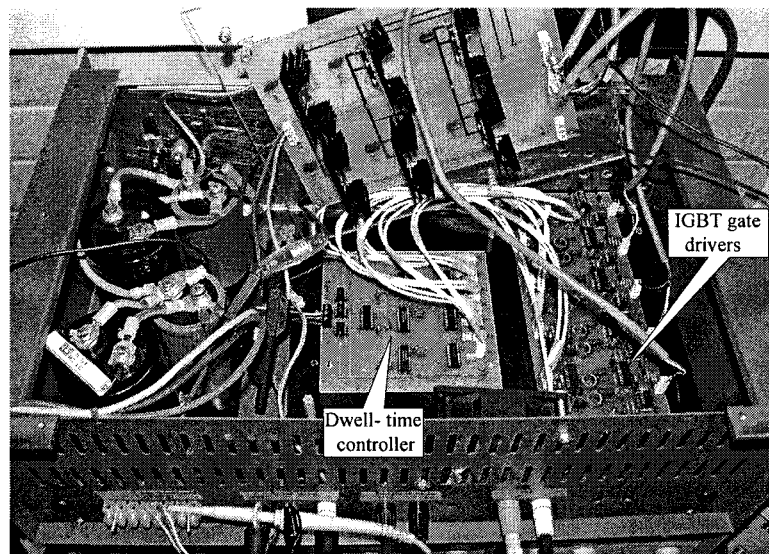
Figure 8.5: Experimental set-up showing the IGBT drivers and controller unit

The experimental model comprised a three-phase three-wire network with three-phase voltage source, capacitor banks (simulating sytem's equivalent s hunt capacitor e.g. PFC, cable's leakage capacitance, etc.) and a three-phase non-linear load (includes a diode rectifier and an LR load at the d.c. side). The HRA is connected to the sy tem via

143

a set of three-phase coupling inductors. Values of the elements used in the experiment are:

Voltage source	:	Three-phase 25 V 50 Hz
Line inductance (L_s)	:	4.8 mH
Coupling inductance (L_{AF})	:	19.88 mH
Shunt capacitance (C_{PFC})	:	79 uF – 89 uF
Non-linear load (W)	:	100 W
Harmonics generated	:	$1^{st}, 5^{th}, 7^{th}$

Tektronix TDS3034 300MHz four channels digital oscilloscope is used in the experiment to capture, display and perform harmonic analysis (using oscilloscope's integrated FFT module). Agilent N2772A 20 MHz differential probes with attenuation ratio of 20:1 are used for voltage measurement. RLC meter is used to measure the line and coupling inductances shown above.

8.2 Real-time Controller Board (DS1103 PPC)

A software based approach is used in the design and implementation of the proposed HRA controller and the FIHE. Advantages of this approach are user-friendliness, time saving, better reliability and flexibility in terms of tuning and modifications. Control sections implemented in such model based control program can be modified without requiring any changes in the hardware. In this study, the controller and the FIHE of the

proposed HRA are implemented in MATLAB/SIMULIMK with interface blocks to interface with the external hardware via dSPACE DS1103 PCC control board as shown in Figure 8.1.

8.2.1 DS1103 PPC control and data acquisition system

A desktop computer is used to accommodate the DS1103 PPC control board and the related software. This computer is described as host PC and it is interfaced with the external experimental set-up (hardware) via the DS1103 PPC's interface I/O unit (shown in Figure 8.2). An associated software called 'ControlDesk' is used. It is a user-friendly (window based) control program, which is bundled with the dSPACE system to control the models that are run in SIMULINK, and it can also serve for conditioning monitoring.

DS1103 PPC is equipped with a Motorola Power PC604e processor that gives 400 MHz (upgraded in 2005 to 1 GHz) floating point processing power. Main functional units of DS1103 PPC are shown in Figure 8.6; these are:

I/O units is a set of on-board peripherals that includes digital-to-analogue (D/A) channels, analogue-to-digital (A/D) channels, 32 individual digital signal level channels (parallel port) and a series port.

DSP subsystem operated based on the Texas Instruments (TI) TMS320F240 DSP. This subsystem can work independently without sharing the core processor's processing power. It has individual I/Os and capable of generate three-phase PWM

signal. The slave DSP can be accessed from the PPC or from the bundled TI software separately.

CAN subsystem is used for connection to a CAN bus based on the Siemens 80C164 microcontroller. More details of the DS1103 PPC board are given in Appendix A.
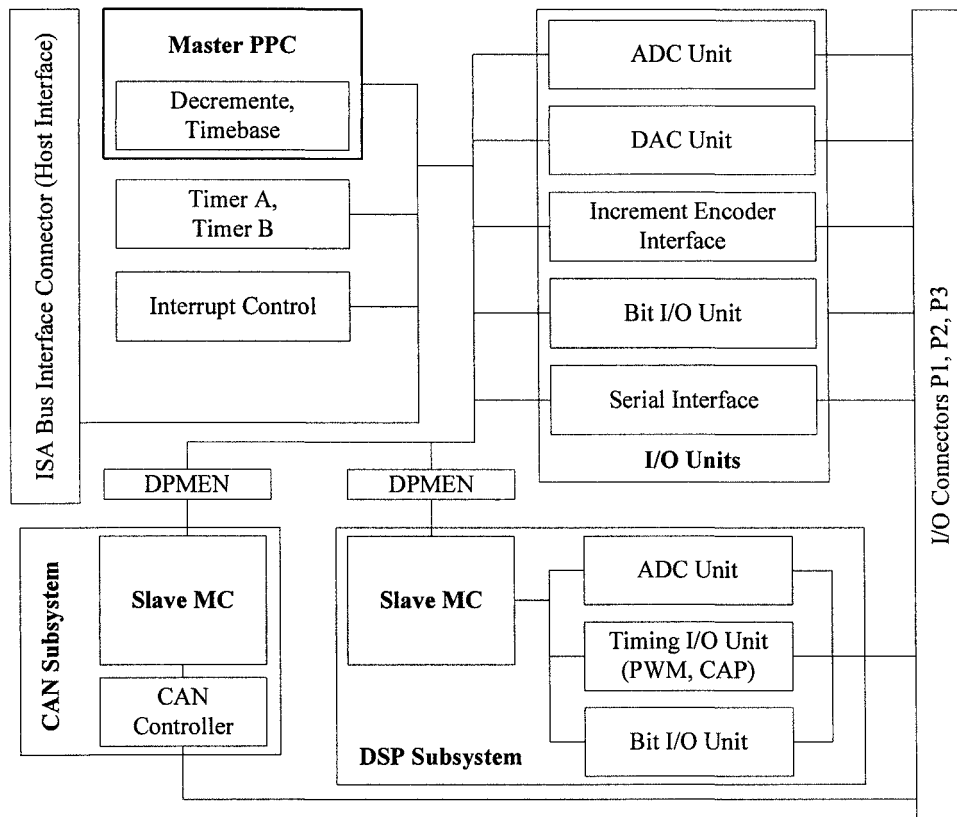
ADC	Analogue/Digital Converters
MC	CAN Microcontroller 80C164
CAP	Capture
DAC	Digital/Analogue Converters
DPMEM	Dual-Ported Memory
DSP	Digital Signal Processor TMS320F240
PPC	Power PC 604e Processor
PWM	Pulse Width Modulation

Figure 8.6: DS1103 PPC control board's functional units

8.2.2 Implementing the real-time controller

The dSPACE real-time control system is a versatile development tool that provides a good solution to design the control system (non power circuits) completely within MATLAB/SIMULINK environment. The integrated Real-time Interface (RTI) is operated as a link in between dSPACE system and the MATLAB/SIMULINK model. Models in the SIMULINK are converted to real-time C-code, cross compiled and downloaded to the DS1103 PPC board via the Real Time Workshop (RTW) function in the MATLAB.

RTI is capable on handling continuous time, discrete time, and hybrid (multi-rate) systems. It also supports non-periodic command signal such as hardware or software interruption and also allows programmer to set priority on different tasks to be executed in the subsystem. These features make the DS1103 PPC control board an ideal choice for implementing the proposed control algorithm in this study.

- **Procedures for implementing real-time controller**

These are the procedures to implement the proposed attenuator controller in the DS1103 PPC:

- Design the proposed FIHE and resonance attenuator in MATLAB/SIMULINK and confirm their performance by of simulation (refer to models shown in Chapter 7).

- Remove all power level section from the designed simulation (e.g. power system model, power inverter, dc storage, gate drivers, etc.), as these are going to be

built externally in hardware form. Modify the signal level sections (e.g. FIHE, attenuator controller, etc.) with proper RTW block-set in SIMULINK for interface with dSPACE.

- Set the step size in simulation parameter dialogue into fixed time step simulation.

- Specify RTW parameter to compile SIMULINK models to real-time C-code that is recognized by DS1103 PPC controller.

- Complete SIMULINK models are downloaded to the DS1103 PPC board.

During operation, dSPACE system can fully control each individual variable (except changing subsystem's parameters e.g. PWM switching frequency) via ControlDesk graphical interface program mentioned earlier.

- **Measurement devices and signal conditioning**

Differential probes mentioned in section 8.1 are used in the experiment to measure system voltages and input to the DS1103 PPC unit. Analogue voltage signals are input to the DS1103 PPC via its ADC channel on the I/O interface unit. These ADC I/Os allow signal to be within the range of ± 10 V. Excessive voltage will be clamped and shown as saturated signal. Therefore, measured signals need to be scaled properly to avoid distortion.

8.3 Setup of Power System Resonance Conditions

An experimental power system model has been built (as shown in Figure 8.1) and resonance condition is successfully created. Experimental results that show system harmonic resonance are presented in this section.

Harmonic resonance conditions are created near the 5th order harmonic frequency (approximate 242 Hz and 257 Hz for scenarios one and two, respectively). The system busbar voltage (waveform and its frequency spectrum) before resonance and without non-linear load is shown in Figure 8.7.
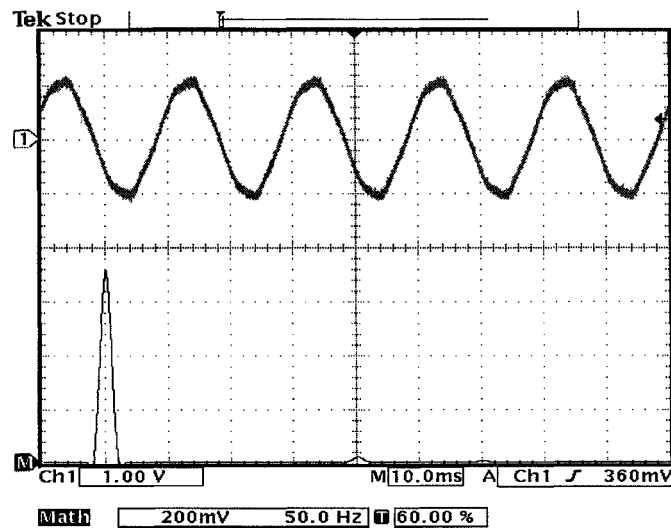
Figure 8.7: System busbar voltage and its frequency spectrum without non-linear load

Figure 8.7 shows that the system voltage is relatively clean (a negligible 5th order harmonic is there due to the variac – voltage source) as compare to the one shown in Figure 8.8 and Figure 8.9 when a non-linear load is connected to the system.
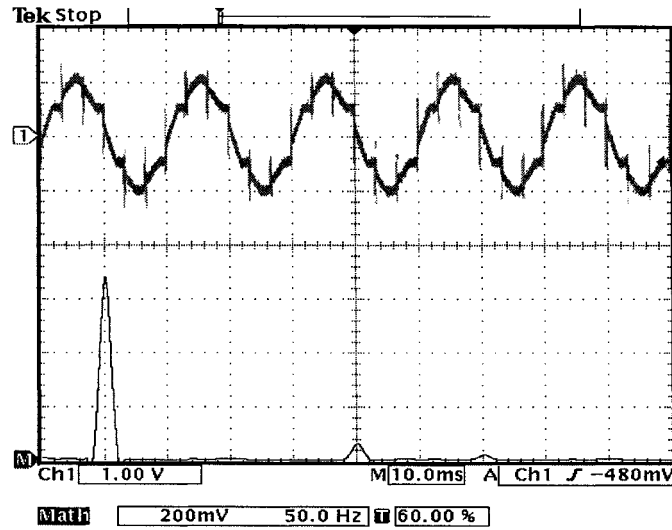
Figure 8.8: System busbar voltage and its frequency spectrum when the non-linear load is connected
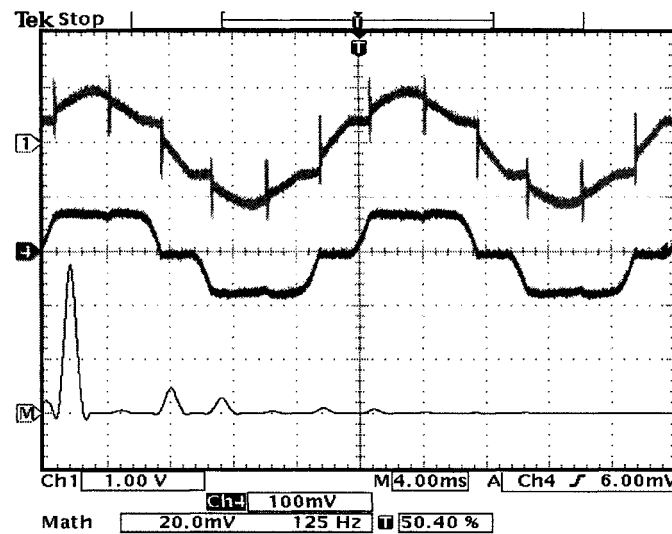
Figure 8.9: System busbar voltage and the line current together with its frequency spectrum when non-linear load is connected

The waveform shown in Figure 8.8 indicates that harmonic distortion has appeared when non-linear load is installed. However, when the shunt capacitor is added in, or in other words, when the harmonic resonance close to the 5th order harmonic frequency is created, magnitude of the 5th order harmonic has increased by approximately twice

(from 1.1 V r.m.s to 2.4 V r.m.s) with respect to the harmonic voltage spectrum showed earlier. The system busbar voltage when system resonance occurs is illustrated in Figure 8.10.
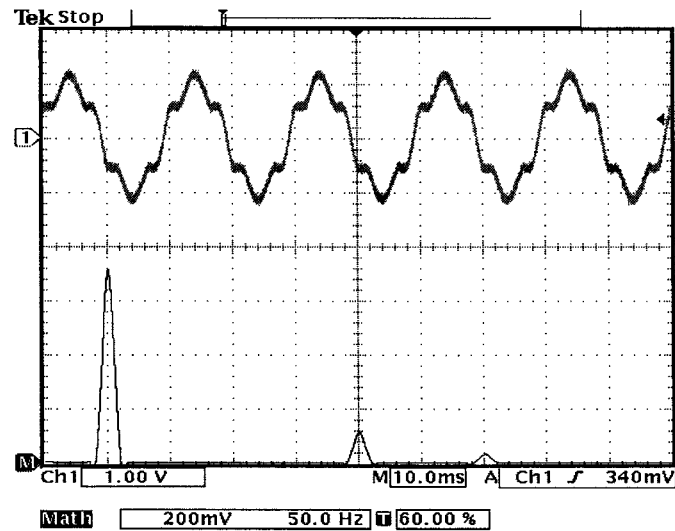
Figure 8.10: System busbar voltage and its frequency spectrum during resonance

Harmonic resonance phenomenon in time domain is shown in Figure 8.11. This figure shows the measured system busbar voltage and the 5th order harmonic voltage extracted by the FIHE (evaluation of the FIHE experimental is discussed in the next section). The waveforms show the sequence before and after harmonic resonance occurred. A zoom in version is shown in Figure 8.12 for a better view.
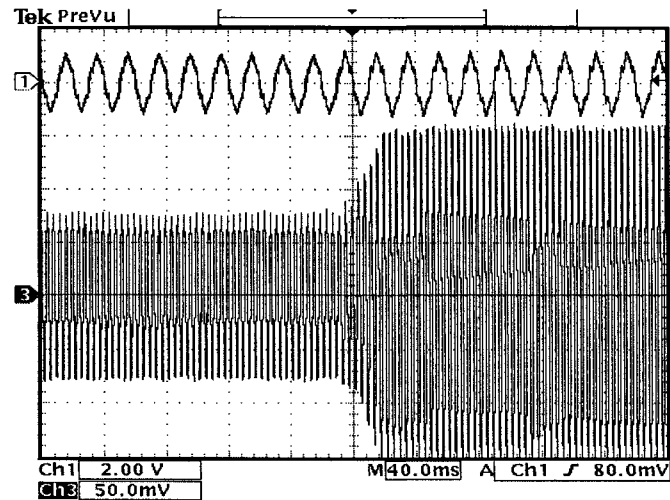
Figure 8.11: Distorted system busbar voltage (CH1), and the 5th order harmonic voltage (CH3) extracted by FIHE from the measured busbar voltage
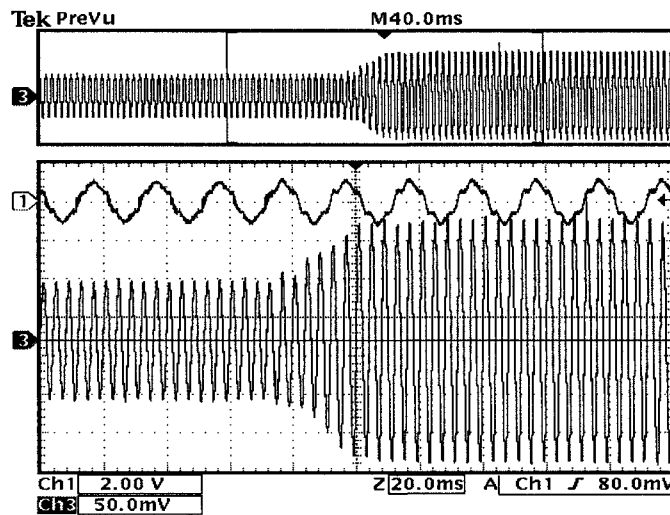
Figure 8.12: Zoom into the signal shown in Figure 8.11

The above results show that harmonic resonance required in the following tests is set up. It is clearly shown that 5th order harmonic component is amplified by approximately twice its normal reading. Therefore, harmonic resonance attenuation is required.

8.4 FIHE Performance

Proposed harmonic extraction technique has been practically tested in a laboratory environment. A series of experiments were conducted based on the system model shown in Figure 8.1 to evaluate the individual harmonic extraction function of the proposed FIHE technique. This evaluation confirmed the validity of the individual harmonic extraction function, inter-frequency independency, steady-state accuracy, phase control flexibility, and dynamic response of the proposed controller.

8.4.1 Steady-state characteristic evaluations

In this experiment, the magnitude of the harmonic component is shown in r.m.s. and the results obtained from the FFT function of the oscilloscope are used as a reference to judge the quality of the results obtained by the FIHE.

As mentioned earlier, voltage differential probes were used in these experiments and they have an attenuation ratio of 20:1. Therefore, a multiplication of 20 times (gain) is required for every waveform shown in the following figures to reflect their actual values.

Distorted voltages of all three-phases are measured, however, due to the limitation of display channels available on the oscilloscope, only one single phase distorted signal is shown in Figure 8.13. The same figure also shows the frequency spectrum obtained by

the integrated oscilloscope FFT module. These waveforms indicate that, harmonic distortion condition is successfully created and can be used for experiments. The frequency spectrum shows that, 1st, 5th and 7th order harmonic voltages are created by the harmonic currents and the system equivalent source side harmonic impedance.
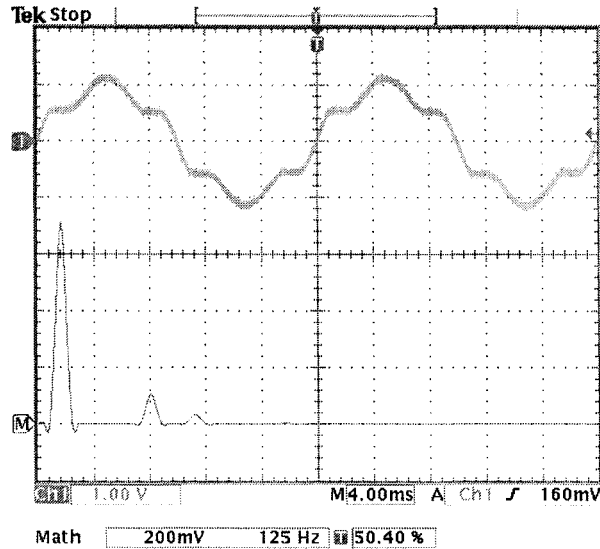
Figure 8.13: Per-phase distorted voltage signal and its frequency spectrum (125 Hz/div)

The three-phase fundamental voltages are extracted and shown in Figure 8.14. Reconstructed distortion free three-phase fundamental signal obtained from the FIHE output ($S_{abc}(m,t)$ in Equation (4.36) with $m = 1$) indicates that the FIHE has successfully extracted and reconstructed all three-phases signals as described in Chapter 4.
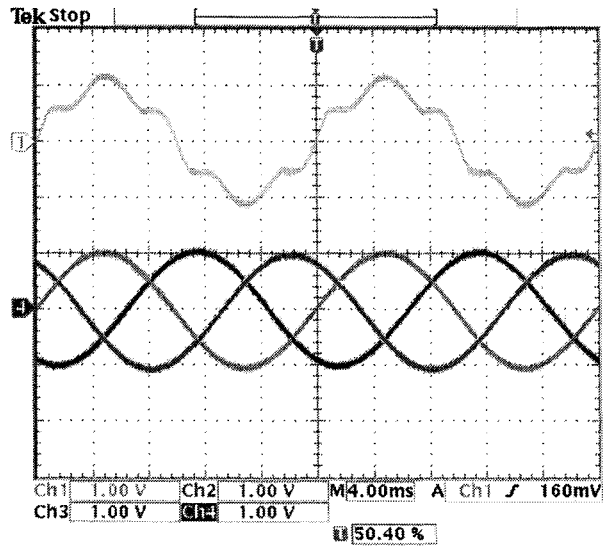
Figure 8.14: Reconstructed harmonic free three-phase fundamental signal at the FIHE output
($S_{abc}(m,t)$ in Equaiton (4.36) with $m = 1$)

Ability of the FIHE in extracting the pre selected harmonic components is further justified by the results shown in Figure 8.15. This figure shows the single phase distorted signal, extracted fundamental signal, extracted 5th order harmonic signal and 7th order harmonic signal.
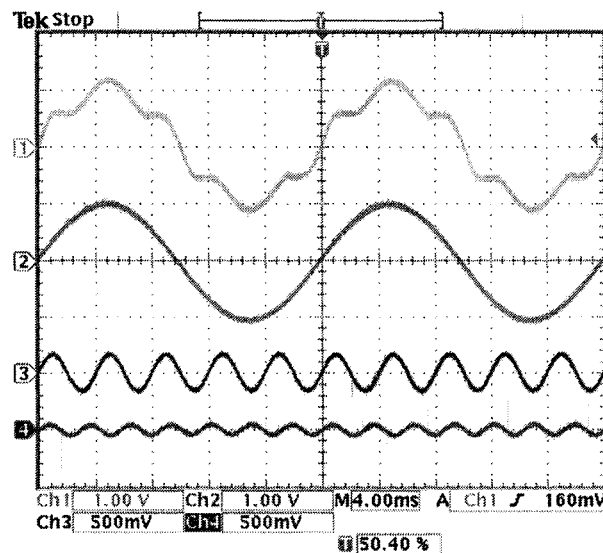
Figure 8.15: Single-phase distorted voltage (CH1), extracted fundamental voltage (CH2), extracted 5th order harmonic voltage (CH3) and extracted 7th order harmonic voltage (CH4).

Figure 8.16 shows that the extracted fundamental component magnitude is equal to 14.496 V r.m.s. Figure 8.17 show the extracted 5th order harmonic component, the distorted signal and its spectrum. The error in these two measurements is less than 0.3%. Results of the 7th order harmonic extraction are shown in Figure 8.18.
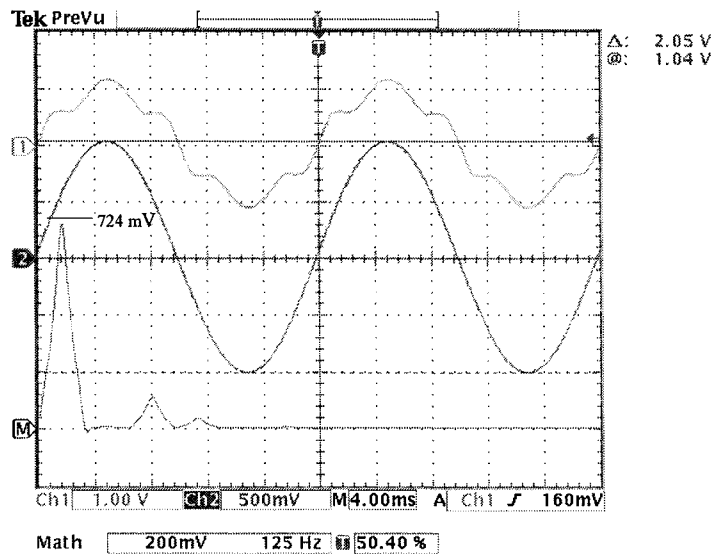
Figure 8.16: Distorted voltage, its fundamental harmonic component extracted by FIHE and its FFT frequency spectrum
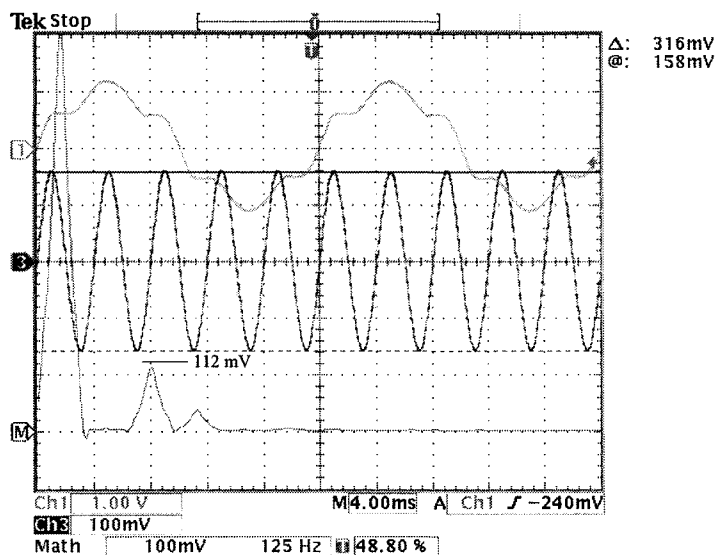
Figure 8.17: Distorted signal, its 5th harmonic component extracted by FIHE and FFT frequency spectrum
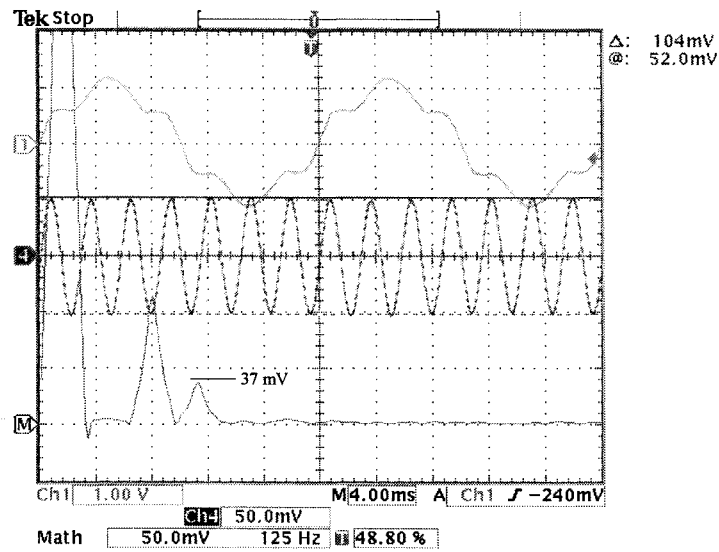
Figure 8.18: Distorted voltage, its 7th harmonic component extracted by FIHE and its FFT frequency spectrum

An evaluation has been carried out to verify the accuracy of the harmonic analysers (scope's FFT and FIHE) used in the previous test. A set of harmonic components (1st, 5th and 7th) were artificially generated by the function generators. These harmonic components were synthesised to form a distorted waveform that later used to verify the extraction accuracy of the FFT measurement capability of the oscilloscope and the proposed FIHE. In this test, the original (generated) harmonic components were used as the references to the extracted results (extracted harmonic components). Summary of this test is shown in Table 8-1 in term of the percentage of error.

Harmonic order	FFT measurement error (%)	FIHE measurement error (%)
1st	-0.256	-0.18
5th	-0.200	-0.42
7th	-0.356	-0.70
Note, $$Error\% = \frac{Original - Measured}{Original} \times 100\%$$		

Table 8-1: Summary of measurements error

157

8.4.2 Phase-angle control ability test

Flexibility of the phase-angle control (as mentioned in section 4.4) is tested and the results are shown in the following. Controllable phase-angle is required to control the fundamental voltage component for active power flow (to regulate the dc-link voltage).

Figure 8.19 shows the initial (original) phase position of the extracted fundamental voltage signals and the extracted 5th harmonic signal. With the phase-angle controlled by the FIHE, the extracted fundamental signal is moved to the leading location (negative phase-angle) as demonstrated in Figure 8.20. Lagging position movement with positive phase-angle control is shown in Figure 8.21. Regardless of the phase of the fundamental component, the extracted 5th harmonic component shown in both figures is not affected by the shifting process. This shows the inter-stage independency feature of the FIHE as a modular harmonic extractor. This kind of modular operation/design is particularly useful in noisy systems and in applications where unit failure is highly unacceptable.
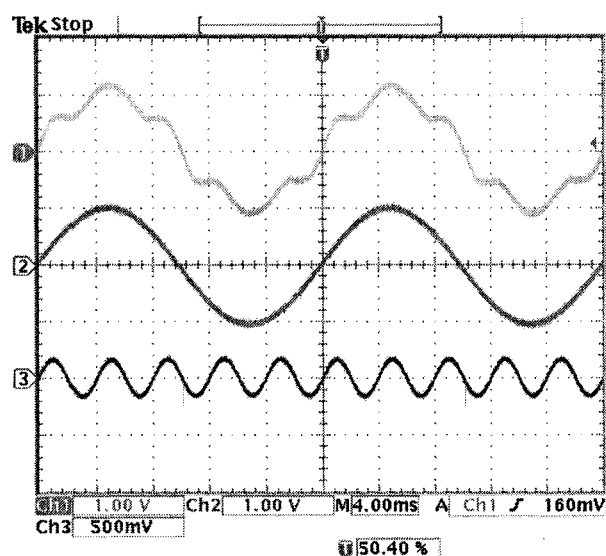
Figure 8.19: The distorted signal and its extracted components
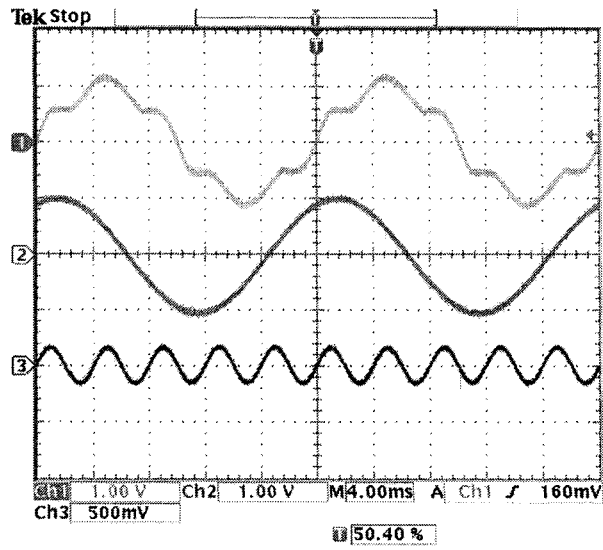
Figure 8.20: Extracted fundamental component shifted by a positive phase-angle
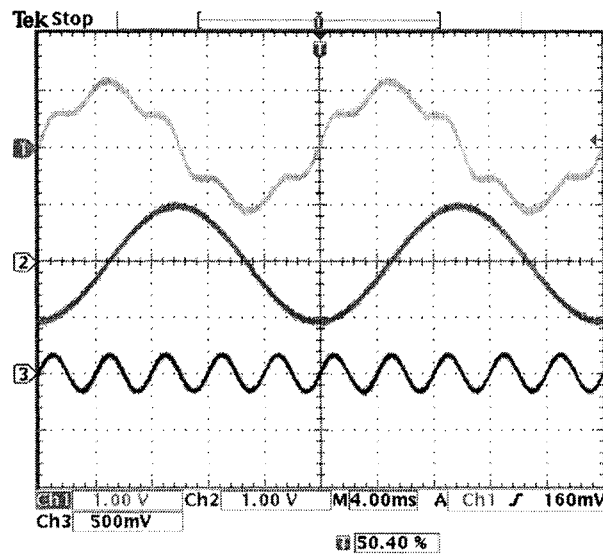
Figure 8.21: Extracted fundamental component shifted by a negative phase-angle

8.4.3 Dynamic characteristics

Dynamic response evaluation is conducted with the scenario described in section 5.3.2.

Distorted signal is generated which contains 1st, 5th, and 7th order harmonic

159

components. Step signal (stepped from 1 to 2) is added to the 7th order harmonic

component to create a sudden change in state for step response evaluation. Ultra fast

response, no overshoot, and ripple-less characteristics are the three attractive features

of the proposed FIHE. All these characteristics are demonstrated in Figure 8.22, where

channel 1 is the added step function signal, channel 2 shows the effect of the distorted

signal upon the stepped up 7th harmonic component, and channel 3 is the extracted 7th

order harmonic component.
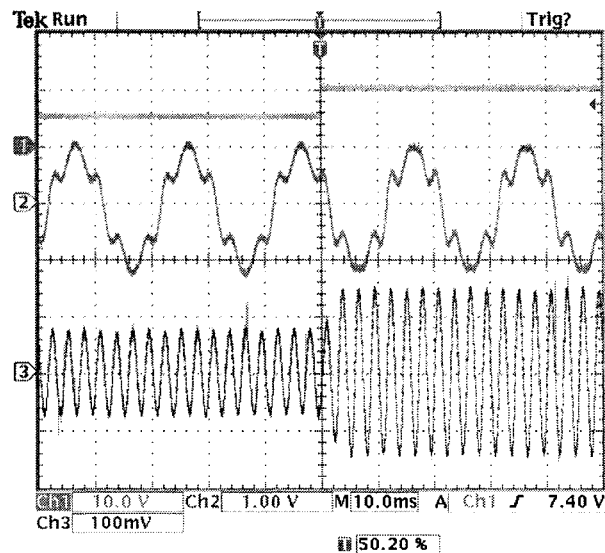
Figure 8.22: Dynamic response test results

In order to assess the speed of extraction, a zoom-in version is shown in Figure 8.23

with an extra channel to display the captured response curve of the signal ($I_d(m)$ of

Equation (4.25) with $m = 7$). The results clearly show that the FIHE response is only

one sixth of a fundamental cycle.
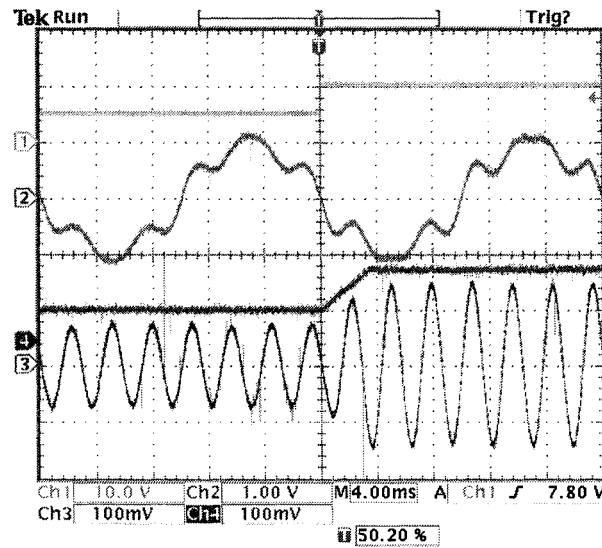
Figure 8.23: Step function signal, distorted signal, FIHE signal before reconstruction, and extracted 7th order harmonic component

8.5 Power Circuit Development

The power circuit used in the proposed resonance attenuator comprises a PWM voltage source inverter, six isolated gate drivers, and six dwell-time controllers.

- **PWM inverter**

A 2-level voltage source inverter (VSI) is used in the experiment to generate the desired voltage signal for the proposed HRA. Six Isolated Gate Bipolar Transistors (IGBT) IRG4BC20K are used as the switching devices. Specifications of these devices are shown in Appendix D. A circuit diagram of the inverter is shown in Figure 8.24. A 10 kHz PWM switching signal is generated by the DS1103 PPC's subsystem. Inverse-parallel diodes (IR 10ETF10 fast recovery diode – Appendix E) and snubbers ($R_{snb} = 10$ Ohm and $C_{snb} = 15$ nF) are implemented as shown in the diagram.
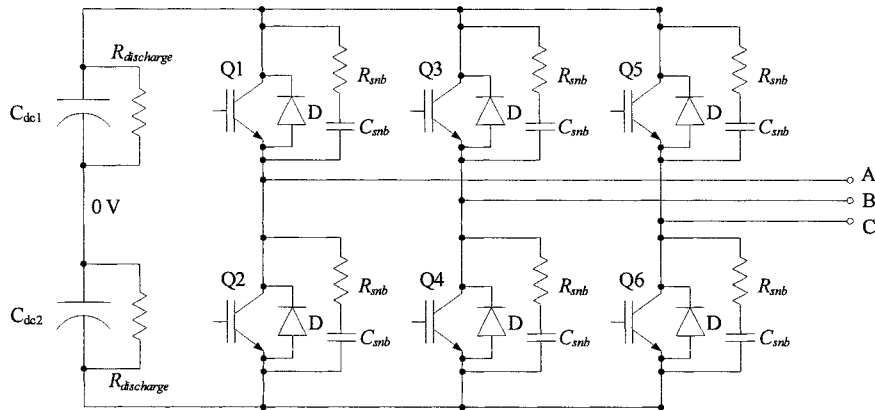
Figure 8.24: A 2-level VSI with anti-parallel diodes and snubber circuits

Harmonic regeneration of the PWM inverter has been evaluated. This is to ensure that the inverter is able to regenerate the desire harmonic voltages. Test results are shown in Figure 8.25 and Figure 8.26. FFT result in Figure 8.25 shows the harmonic content in the distorted signal whereas that in Figure 8.26 shows the harmonic content in the PWM output voltage. These results show that the PWM inverter developed is capable to reproduce the harmonic components required.
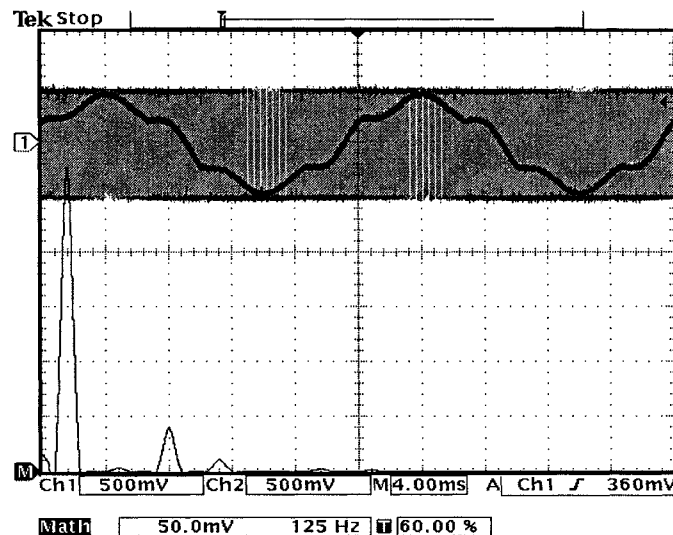
Figure 8.25: Busbar voltage, inverter output voltage, and frequency spectrum of the distorted busbar voltage (125 Hz/div)
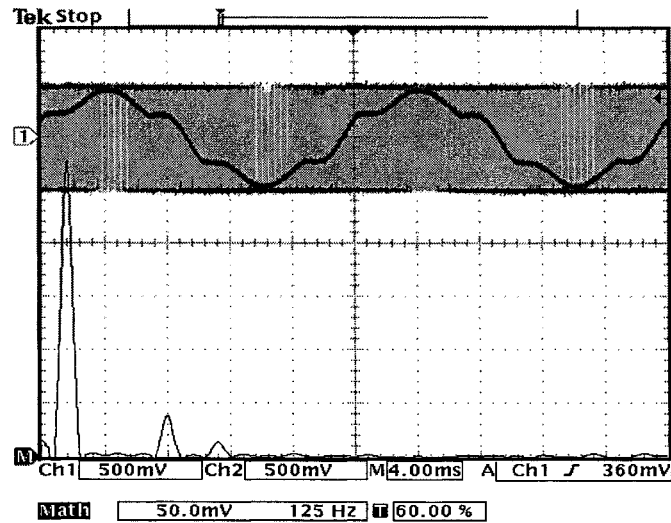
Figure 8.26: Busbar voltage, inverter output voltage, and frequency spectrum of the inverter output voltage (125 Hz/div)

The inverter shown in Figure 8.24 is a voltage source inverter with d.c. capacitors (C_{dc1} = C_{dc2} = 2200 uF) and discharge resistors ($R_{discharge}$ = 10 kOhm) installed to form up a DC-link voltage pool. Ideally, when the fundamental voltage generated by the PWM inverter is synchronised to the system's fundamental voltage, no active power is exchanged between the inverter and the power network; hence the d.c. voltage across the capacitor remains constant (neglecting system capacitor ESR losses). However, in practice, a small amount of active power is usually required to compensate the losses in the switching devices, coupling inductor, discharge resistor, etc. These losses cause the capacitor to discharge slowly. Therefore, a voltage regulator is required to regulate the level of the dc-link voltage by creating a phase different between the fundamental voltage generated by the inverter and that of the power network. With the FIHE, this can be achieved via a simple PI controller to control the phase shift of the output signal of the FIHE in response to the d.c. voltage as described in section 8.4.2. To evaluate

the performance of the regulator, a step response test is conducted with the d.c. voltage

changed from 20 V to 40 V and the results obtained are shown in Figure 8.27.
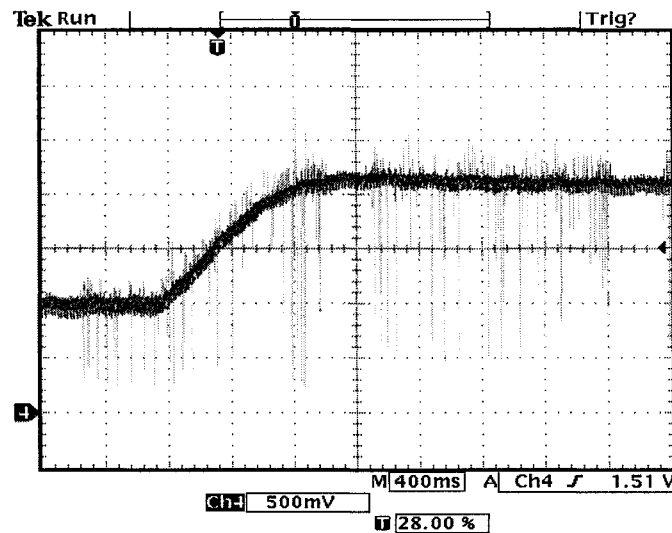
Figure 8.27: Step response of the dc-link voltage regulator

- **The dwell-time controllers**

Dwell-time controllers are used to create dead band between the turn on time on the

upper-side switching devices and turn off time on the lower-side switching devices to

prevent the dc-link voltage being short circuited. In this study, a 12 *us* dwell-time is

implemented. Detail of the dwell-time controller is given in Appendix B.

- **The IGBT gate drivers**

The output of the DS1103 PPC is insufficient to directly drive an IGBT switching

device. Additional gate drivers are required to amplify the gating signals to the

required level. In addition, a high-side driving capability is required to drive the upper-

side switching device. In this project, isolated gate drivers were developed to achieve

this. A dc/dc converter is integrated in each gate driver to step up the 5 Vdc supply to

15 Vdc (IGBT's optimum gating voltage level) and used as a floating ground dc

voltage supply for the driver. A block diagram of the gate driver is shown in Figure

8.28, and details are given in Appendix C.
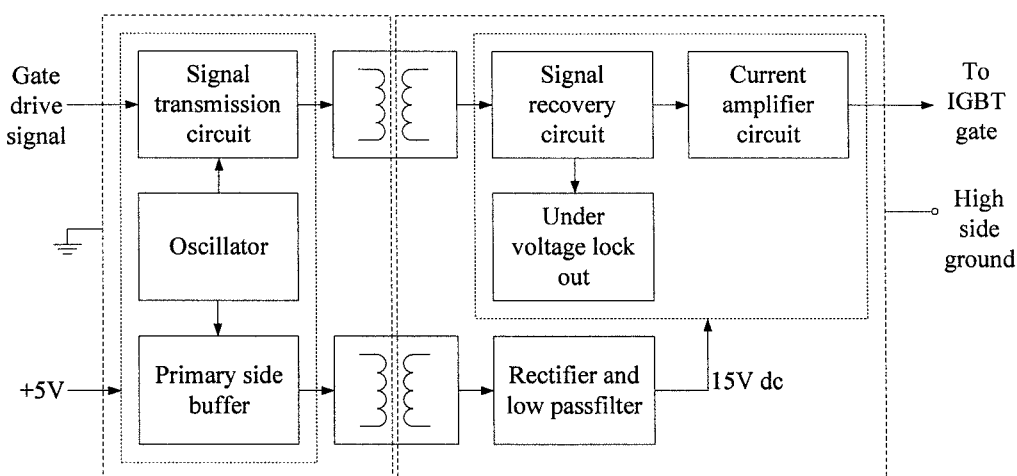
Figure 8.28: A block diagram of the IGBT gate driver

8.6 Performance Evaluation of the Proposed HRA Technique

L-mode and C-mode attenuation performances are evaluated in the experimental model

and the results obtained are presented. Figure 8.29 shows the distorted busbar voltage

(CH1) and the waveform of the 5th order harmonic voltage (CH3). A smoother busbar

voltage waveform indicates that the harmonic distortion is reduced (from 2.3 V r.m.s.

to 0.95 V r.m.s) when attenuation is introduced.
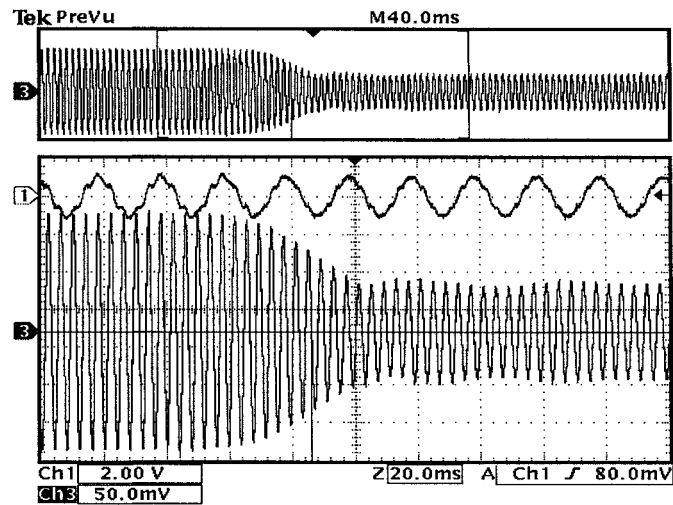
Figure 8.29: Busbar voltage and extracted 5th order harmonic component (L-mode attenuation)

The result for C-mode compensation test is shown in Figure 8.30. In this case, harmonic voltage is reduced from 2.2 V r.m.s. to 1.01 V r.m.s when attenuation is introduced.
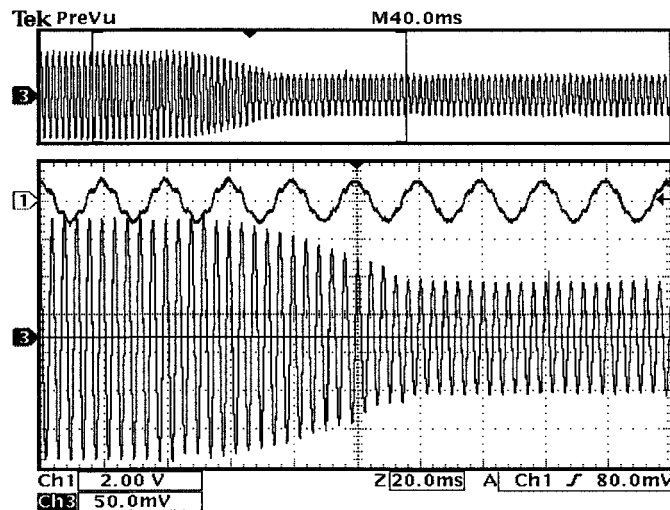
Figure 8.30: Busbar voltage and the extracted 5th order harmonic component (C-mode attenuation)

A quantitative study on the performance of the proposed harmonic resonance compensator is performed. This is to evaluate the reaction of the harmonic component

(5th) at different gains (k). The test is conducted by observing/monitoring the changes of the 5th order harmonic voltage at the system busbar when different k values are applied. Measurement results are shown together with the calculated values in Figure 8.31 and Figure 8.32.
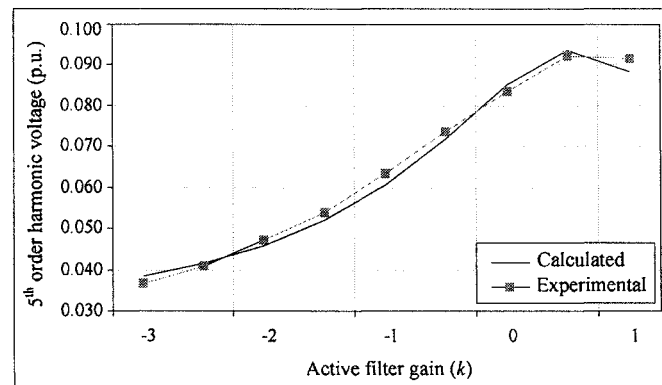
Figure 8.31: 5th order harmonic voltage versus active filter gain (k_s) for L-mode compensation
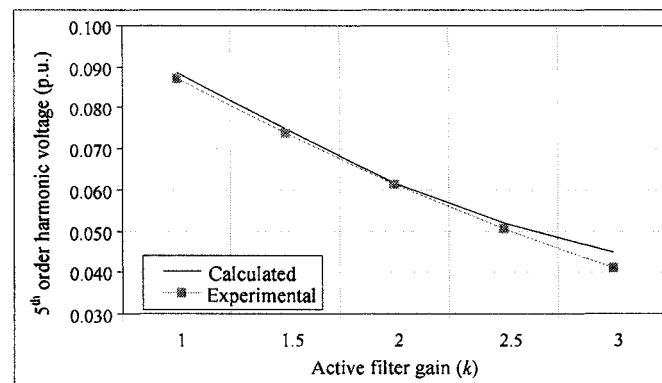
Figure 8.32: 5th order harmonic voltage versus active filter gain (k_s) for C-mode compensation

There is a small variation in the experimental results as compared to the calculated results, which is due to hardware and measurement tolerances. The high switching PWM inverter used in the experiment (mentioned in Section 8.5) has nicely regenerated the harmonic signal and therefore has contributed to the high agreement on

the results shown in Figure 8.31 and Figure 8.32. Overall, the results shown have given

a high degree of confidence in the proposed technique.

Closed loop attenuation is evaluated with the control circuit described in section 7.4.

The controller model in SIMULINK is modified according to the real-time controller's

design procedures (section 8.2.2) and used in this test. It is implemented here with a

trigger level of 10% above normal 5th order harmonic voltage level. The waveform of

the peak detector output is shown in Figure 8.33 (on top of the 5th order harmonic

waveform), together with the extracted 5th order harmonic voltage captured at the

output of the FIHE unit (in sinusoidal form).
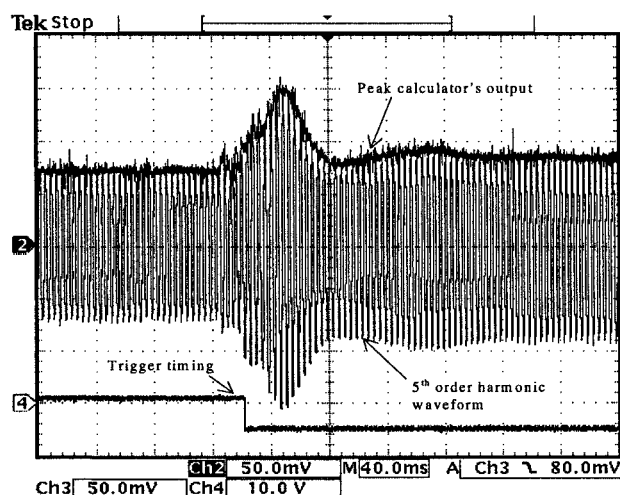
Figure 8.33: 5th order harmonic's peak value (CH2), 5th order harmonic voltage waveform (CH3 overlapped with CH2) and the trigger timing signal (CH4)

Figure 8.34 shows the result when HRA is working in higher closed loop gain

condition, in which the increased gain had caused a short period of

oscillating/bouncing during the attenuation process.
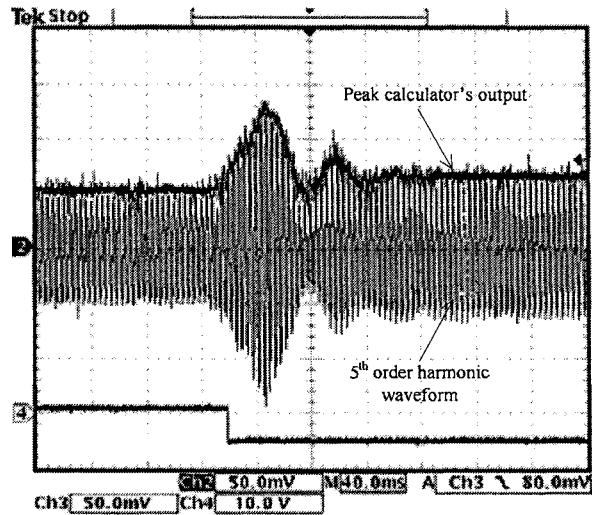
Figure 8.34: Waveform captured with HRA working at higher closed loop gain.

It can be seen from both results that the overshoot of the harmonic voltage are generally higher then the results shown in the simulation section. This is due to the fast connection of the shunt capacitor bank, which has caused a sudden increase of the resonated 5th order harmonic voltage. In a real power system, such step change in harmonic resonance is very rare. Overall, the results of closed loop tests shown are satisfactory as harmonic resonances have been successfully reduced to their initial levels. Experimental results shown in this chapter have demonstrated the validity (proven the functionality) of the proposed techniques. As they have showed that the harmonic resonances have been successfully attenuated down to their initial levels.

CHAPTER 9

CONCLUSIONS AND FURTHER WORK

9.1   Conclusions

      9.1.1   Power system harmonic resonance and solutions

      9.1.2   Development of the proposed techniques

      9.1.3   Simulation work

      9.1.4   Experimental work

9.2   Suggestions for further work

9.1 Conclusions

This project investigated harmonic resonance in power distribution networks and techniques used to minimise their effects. As a result, the need for a real-time harmonic attenuation technique that is suitable for power distribution networks is identified. A new technique for attenuating harmonic resonance is proposed and developed.

Conclusions of this research work are made in four sections to cover power system harmonic resonance and solutions, development of the proposed techniques, simulation and experimental work.

9.1.1 Power system harmonic resonance and solutions

Literature review of documented harmonic resonance case studies showed that, due to the dynamic nature of power networks, the risk of harmonic resonance is high and could be without a traceable footmark. Consequences of harmonic resonances can be as small as a slight increase in the level of harmonic distortion or in some cases, serious amplification of harmonic component which may causes circuit breakers to trip and possible series of chain reactions (e.g. systems break down, production line shut down, etc.). In addition to the economical losses, it may endanger safety of the network users.

Studies have shown that, the main reason that causes harmonic resonance is the use of PFC capacitors. Other components such as long underground cables, passive filters may also cause harmonic resonances. Solutions used to solve harmonic resonance problem are classified into two categories. One is to reduce the content of harmonic components in the system, and the other is to remove the resonance stimulating factor by shifting the system natural resonance frequency (to a non-critical frequency range).

The first solution employs filters to remove, minimise or block the harmonics current flow into the network. Filters used can be either passive, active or hybrid filters, which can only provide localised harmonic compensation. Consequently, the overall effectiveness is proportional to the number of loads and source branches in the network in addition to the location of the filter. Inappropriate location may lead to a serious harmonic resonance, as discussed in Chapter 2. These characteristics have made this

solution less popular to be used in networks that have interconnections as in existing power distribution network and future active power networks.

The second solution is to shift the system natural resonance frequency. This can be achieved by detuning PFC capacitors, reconstructing the network and redesigning the feeder transformers. Due to lack of real-time monitoring and adjusting capability, these solutions are less effective as compared to the solutions in the first category.

The literature shows a need for a real-time non-geographical critical broad-base HRA technique. In this project, a new HRA technique suitable for power distribution networks is developed and a fast individual harmonic extraction (FIHE) technique is proposed to achieve the real-time operation of the attenuator.

9.1.2 Development of the proposed techniques

The proposed HRA technique employs shunt active filter which is controlled to behave as a controllable virtual inductor or capacitor to the selected harmonic component. A voltage-detection voltage-compensation technique is used which enables the filter (connected at the PCC of a distribution network) to shift the system natural harmonic resonance frequency away from critical ranges. With the virtual effect of the proposed technique, the harmonic reactance added to the system is only effective for the selected harmonic component; i.e. no extra harmonic resonance will be created in the compensation process. As this effect can only be seen by the selected harmonic component. The real-time implementation and non-localised features of the proposed

technique have made it suitable for distribution networks of a complex interconnection structure.

For real-time applications, the development of the proposed HRA technique, requires a fast selective harmonic extraction process. Therefore, a Fast Individual Harmonic Extraction (FIHE) technique has also been developed.

The FIHE technique is developed based on the orthogonal function and uses Park transformation to improve the harmonic extraction speed and accuracy. The principles of the proposed technique and its performance were compared with existing standard harmonic extraction techniques. Results of the comparison showed that the proposed FIHE technique has a much better dynamic response (6 times faster) than conventional harmonic extraction techniques and provides overshoot-free and better filtering characteristic (e.g. ripple-free) than traditional filters such as the Butterworth and FIR filters. The fast dynamic performance of the proposed technique makes it an excellent tool when the speed of response is important, for example; in modern harmonic control techniques such as, active power harmonic compensators.

Performance of the proposed FIHE would be deteriorated in unbalanced three-phase systems and when the line frequency is drifted. These problems were discussed and demonstrated in Chapter 4 section 4.5 and Chapter 5 section 5.3.3 and 5.3.4. Suggestions to improve the performance of FIHE under these conditions are given in as a further works in section 9.2.

9.1.3 Simulation work

Detailed analysis of the proposed FIHE technique was first conducted using computer simulation. Performance of the FIHE is evaluated by using steady-state, dynamic response, unbalanced condition, and system frequency drift tests.

For the steady-state test, a three-phase power network with non-linear loads is simulated. In the modelled system, several characteristic harmonic current components (i.e. 5th and 7th) were produced and the FIHE was used to extract any selected harmonic component from the distorted waveform. The FIHE extraction accuracy in steady-state was evaluated and the results obtained were comparable with those obtained using the FFT.

Dynamic response of the FIHE is tested with artificially generated harmonic component which exhibit a step change in the magnitude. The results obtained showed that the proposed FIHE technique has a very fast dynamic response (6 times faster than existing FFT based methods) with extra features, such as overshoot-free and ripple-less characteristics.

Performance of the FIHE under unbalanced system conditions and frequency drift conditions was also conducted. The results obtained showed that the accuracy of the FIHE reduces in these situations. Further work is needed to improve the performance of the FIHE under these conditions.

A computer model of the proposed HRA controller was developed using a shunt active filter which was modelled as a controllable voltage source. Performance of the controller was evaluated for two system harmonic resonance conditions. The first is harmonic resonance caused by increase of the system shunt capacitance and the second is to simulate a reduction in the network's shunt capacitance. A different HRA attenuation mode is required for these resonance conditions. A control scheme is developed for the attenuator to determine which attenuation mode (L-mode or C-mode) is required. Both open-loop and closed-loop harmonic resonance attenuation are simulated. Simulation results showed that the proposed attenuator is capable to perform an effective harmonic resonance attenuation based on voltage measurement only. That is; without the need for current measurements, which resulted a non-localised HRA method that is suitable for power distribution networks.

9.1.4 Experimental work

The proposed FIHE and HRA techniques were both evaluated experimentally to verify their performances. An experimental set-up that consists of a three-phase network, non-linear load, shunt capacitors (to simulate PFC capacitors), a two level inverter with dSPACE real-time control system and measurement equipment was constructed.

A 2-level voltage source inverter have been designed and constructed. Six IGBTs were used as the switching devices. PWM function in the DS1103 PPC DSP subsystem was used to generate a 10 kHz PWM carrier signal. Interrupt function in the subsystem was used to synchronise the PWM carrier signal to the system voltage. Dwell-time controllers and six sets of isolated IGBT gate drivers were built to amplify the gating

signal from DS1103 PPC to a sufficient level to drive the IGBTs. Performance of the PWM inverter in generating the selected harmonic components has been evaluated. The results obtained showed that the harmonic components in the system were successfully extracted by the FIHE and regenerated by the PWM inverter. Switching harmonics and aliasing problems were minimised by choosing to operate the inverter at high switching frequency.

Four d.c. capacitors have been used as the d.c. voltage storage and their voltage level was regulated via a typical PI feedback controller to control the phase different between the inverter's output voltage (fundamental) and system's voltage. Voltage regulation was tested and satisfactory results for the PI controller's dynamic response and steady-state error control were obtained.

The controller developed for computer simulation (in SIMULINK) was modified accordingly so that it could be used in the dSPACE real-time system (executed in DS1103 PPC). By using this approach, a large amount of valuable time could be saved, as the controller could be constructed/amended in SIMULINK and run in dSPACE real-time system. The "software controller" is interfaced to the external hardware (power components/sections) via DS1103 PPC control board. That is, no "hardware controller" is required.

The non-linear loads and shunt capacitors were used to set up harmonic resonance conditions at two frequencies, 242 Hz and 257 Hz (to simulate common system resonance conditions). Two harmonic resonance conditions were created. These were

used to evaluate the HRA in different modes (L-mode and C-mode). The results of attenuation obtained showed that the HRA has successfully attenuated the harmonic resonance conditions created. The proposed FIHE algorithm and HRA controller were implemented in the dSPACE system, and their performance was tested. The accuracy of the FIHE technique was tested by comparing its performance with the results obtained by using the FFT function (built in the oscilloscope). The results of the steady-state response showed that the proposed FIHE is as accurate as the FFT. The dynamic characteristic of the FIHE was also tested experimentally. The experimental results showed that the FIHE superior in maintaining a fast response, no overshoot and no oscillation.

The results obtained from the simulations and experimental work verified the theoretical analysis and demonstrated a very high degree of confident in the proposed techniques.

9.2 Suggestions for further work

The research work described in this thesis has developed a Harmonics Resonance Attenuation (HRA) technique and a Fast Individual Harmonic Extraction (FIHE) technique. Further work to enhance the potential of the proposed techniques may be conducted as follows:

- Improve the FIHE accuracy for unbalanced conditions without sacrificing the speed of response. The unbalanced test results showed that the accuracy of the

FIHE drops by almost 4.5% when the system is 10% unbalanced. During unbalanced conditions, the speed of harmonic extraction needs to be reduced to half of the fundamental cycle to regain the accuracy of the FIHE. Further work may be conducted to improve the accuracy under unbalanced conditions without compromising the speed of response.

- Improve the accuracy of FIHE when systems frequency drifts. This is important as the frequencies of harmonics are multiple of the fundamental frequency. Thus, any little change in the fundamental frequency would be magnified by n time for n^{th} order harmonic component. In addition, the shift of harmonic frequency might trigger a harmonic resonance, as passive filters or detuned PFC capacitors are designed such that their excitation points are located within known characteristic harmonic frequencies. With this in mind, it is important to improve the accuracy of the FIHE during situations where the system's rated frequency drifts. One way to achieve this is to use the network frequency at the point of measurement to adjust the oscillator that is integrated in the FIHE unit. With the frequency tracking solution, the accuracy of the FIHE during system frequency drift conditions could be maintained.

- Implement the proposed HRA technique as an integrated part of other custom power devices, e.g. the distribution STATCOM or active filters. This will provide a better power quality controller and enhance its commercial value.

REFERENCE

[1]   Grady, W. and Santoso, S., "Understanding power system harmonics," *Power Engineering Review, IEEE*, 2001, vol. 21, pp. 8-11.

[2]   Katic, V. A., "Computer Based Harmonic Measurement Systems: Discussion And A Realization," *ICHPS V International Conference on Harmonics in Power Systems*, 1992, vol., pp. 16 - 22.

[3]   Marafao, F. P., Deckmann, S. M., Pomilio, J. A., and Machado, R. Q., "Selective disturbance compensation and comparisons of active filtering strategies," *International Conference on Harmonics And Quality of Power, 2002*, 2002, vol. 2, pp. 484 - 489.

[4]   Fujita, H., Yamasaki, T., and Akagi, H., "A hybrid active filter for damping of harmonic resonance in industrial power systems," *IEEE Transactions on Power Electronics*, 2000, vol. 15, pp. 215-222.

[5]   El-Habrouk, M., Darwish, M. K., and Mehta, P., "Analysis and design of a novel active power filter configuration," *IEE Proceedings-Electric Power Applications*, 2000, vol. 147, pp. 320 - 328.

[6]   Nastran, J., Cajhen, R., Seliger, M., and Jereb, P., "Active power filter for nonlinear AC loads," *IEEE Transactions on Power Electronics*, 1994, vol. 9, pp. 92 - 96.

[7]   Kawagoshi, T., Kumamoto, A., Hikihara, T., Hirane, Y., Oku, K., Nakamura, O., Tada, S., Mizuki, K., and Inoue, Y., "Harmonic voltage suppression by active filter with neural network controller," *Second International Forum on*

Applications of Neural Networks to Power Systems, 1993, 1993, vol., pp. 93 - 98.

[8]   Rastogi, M., Mohan, N., and Edris, A. A., "Filtering of harmonic currents and damping of resonances in power systems with a hybrid-active filter," *Applied Power Electronics Conference and Exposition, 1995*, 1995, vol. 2, pp. 607 - 612.

[9]   Aredes, M., Hafner, J., and Heumann, K., "A Combined Series and Shunt Active Power Filter," *IEEE/KTH Stockholm Power Tech Conference*, 1995, vol., pp. 237-242.

[10]   Detjen, D., Jacobs, J., De Doncker, R. W., and Mall, H. G., "A new hybrid filter to dampen resonances and compensate harmonic currents in industrial power systems with power factor correction equipment," *IEEE Transactions on Power Electronics*, 2001, vol. 16, pp. 821-827.

[11]   Cheng, P. T., Bhattacharya, S., and Divan, D., "Operations of the dominant harmonic active filter (DHAF) under realistic utility conditions," *IEEE Transactions on Industry Applications*, 2001, vol. 37, pp. 1037-1044.

[12]   Blaabjerg, F., Chen, Z., and Kjaer, S. B., "Power electronics as efficient interface in dispersed power generation systems," *Power Electronics, IEEE Transactions on*, 2004, vol. 19, pp. 1184-1194.

[13]   Mack Grady, W. and Santoso, S., "Understanding power system harmonics," *Power Engineering Review, IEEE*, 2001, vol. 21, pp. 8-11.

[14]   Le, T.-N., Pereira, M., Renz, K., and Vaupel, G., "Active damping of resonances in power systems," *IEEE Transactions on Power Delivery*, 1994, vol. 9, pp. 1001 - 1008.

[15]   Liserre, M., Teodorescu, R., and Blaabjerg, F., "Stability of photovoltaic and wind turbine grid-connected inverters for a large set of grid impedance values," *IEEE Transactions on Power Electronics*, 2006, vol. 21, pp. 263-272.

[16]   Lemieux, G., "Power system harmonic resonance-a documented case," *IEEE Transactions on Industry Applications*, 1990, vol. 26, pp. 483 - 488.

[17]   Mclean, A., Mcleay, K., and Sheldrake, A., "Harmonic suppression filter for offshore interconnected power system," *IEE Colloquium on Harmonic Pollution and Recent Developments in Remedies*, 1993, vol., pp. 6/1 - 6/6.

[18]   Medora, N. K. and Kusko, A., "Power harmonic problems at a plastics extrusion plant," *IEEE Industry Applications Conference, 1995*, 1995, vol. 3, pp. 2726 - 2733.

[19]   Martinich, T. G. and Neilson, J. B., "Mitigation of resonance using digital models and direct measurement of harmonic impedances," *IEEE Power Engineering Society Summer Meeting, 2000*, 2000, vol. 2, pp. 1069 - 1074.

[20]   Balcells, J. and Gonzalez, D., "Harmonics due to resonance in a wind power plant," *International Conference on Harmonics And Quality of Power, 1998*, 1998, vol. 2, pp. 896 - 899.

[21]   Akagi, H., Fujita, H., and Wada, K., "A shunt active filter based on voltage detection for harmonic termination of a radial power distribution line," *IEEE Transactions on Industry Applications*, 1999, vol. 35, pp. 638-645.

[22]   Smith, K. S. and Ran, L., "Active filter used as a controlled reactance to prevent harmonic resonance in interconnected offshore power systems," *IEE Proceedings-Generation, Transmission and Distribution*, 1999, vol. 146, pp. 393 - 399.

[23] Tong, D., Nikolaenko, V. G., Ginbey, N., and Lau, I., "Harmonic propagation in transmission system with multiple capacitor installations," *International Conference on Power System Technology, 2000*, 2000, vol. 2, pp. 1007 - 1012.

[24] Murthy, K. S., "Impact of capacitor installations on networks and systems," *Power Quality '98*, 1998, vol., pp. 203 - 216.

[25] Engineering Recommendation G5/4: Limits for harmonics in the United Kingdom electricity supply system. 2000

[26] Luor, T. S., "Influence of load characteristics on the applications of passive and active harmonic filters," *Ninth International Conference on Harmonics and Quality of Power, 2000*, 2000, vol. 1, pp. 128 - 133.

[27] Czarnecki, L. S. and Gin, H., "Effectiveness of resonant harmonic filters and its improvement," *IEEE Power Engineering Society Summer Meeting, 2000*, 2000, vol. 2, pp. 742 - 747.

[28] Girgis, A. A., Fallon, C. M., Rubino, J. C. P., and Catoe, R. C., " Harmonics and transient overvoltages due to capacitor switching," *IEEE Transactions on Industry Applications*, 1993, vol. 29, pp. 1184 - 1188.

[29] Mendis, S. R., Gilker, C., and Casarez, C., "power factor and harmonic analysis of a modern glass fiber manufacturing plant," *IEEE Industry Applications Society Annual Meeting, 1990*, 1990, vol. 2, pp. 1959 - 1964.

[30] Benitez, J., "Application of capacitors for power factor correction of industrial electrical distribution systems," *Conference Papers of Petroleum and Chemical Industry Conference, 1992*, 1992, vol., pp. 77 - 86.

[31] Rao, N. D., Sporea, S. I., and Sawma, A., "Analysis of resonance problems and harmonic filter design in power factor correction capacitor applications," *IEEE Canadian Conference on Electrical and Computer Engineering, 1998*, 1998, vol. 1, pp. 293 - 296.

[32] Akagi, H., "New trends in active filters for improving power quality," *International Conference on Power Electronics, Drives and Energy Systems for Industrial Growth, 1996*, 1996, vol. 1, pp. 417 - 425.

[33] Currie, R. A. F., Ault, G.W., Foote, C.E.T., Burt, G.M., Mcdonald, J.R,, "Fundamental research challenges for active management of distribution networks with high levels of renewable generation," *39th International Universities Power Engineering Conference (UPEC) 2004*, 2004, vol. 2, pp. 1024-1028.

[34] Roberts, D. A.: Network Management Systems for Active Distribution Networks - A Feasibility Study. SP Power Systems LTD, Scottishpower PLC, 2004

[35] Chang, G. W., Chu, S.-Y., and Wang, H.-L., "A new method of passive harmonic filter planning for controlling voltage distortion in a power system," *IEEE Transactions on Power Delivery*, 2006, vol. 21, pp. 305-312.

[36] Peng, F. Z., Akagi, H., and Nabae, A., "A new approach to harmonic compensation in power systems," *Conference Record of the 1988 IEEE Industry Applications Society Annual Meeting*, 1988, vol. 1, pp. 874 - 880.

[37] Tokuda, H., Amano, I., and Eguchi, N., "A resonance dumping control for a line-current detection type active filter," *Proceedings of the Power Conversion Conference, 2002*, 2002, vol. 2, pp. 755 - 760.

[38]   Sutanto, D., Bou-Rabee, M., Tam, K. S., and Chang, C. S., "Harmonic filters for industrial power systems," *International Conference on Advances in Power System Control, Operation and Management, 1991*, 1991, vol. 2, pp. 594 - 598.

[39]   Cavallini, A. and Montanari, G. C., "Compensation strategies for shunt active-filter control," *IEEE Transactions on Power Electronics*, 1994, vol. 9, pp. 587 - 593.

[40]   Chen, Z., Blaabjerg, F., and Pedersen, J. K., "Hybrid compensation arrangement in dispersed generation systems," *IEEE Transactions on Power Delivery*, 2005, vol. 20, pp. 1719-1727.

[41]   Akagi, H., "Active and hybrid filters for power conditioning," *IEEE International Symposium on Industrial Electronics, 2000*, 2000, vol. 1, pp. TU26 - TU36.

[42]   Akagi, H., "Prospects of new technologies for power electronics in the 21st century," *IEEE/PES Transmission and Distribution Conference and Exhibition 2002: Asia Pacific*, 2002, vol. 2, pp. 1399 - 1404.

[43]   Akagi, H., "Trends in active power line conditioners," *IEEE Transactions on Power Electronics*, 1994, vol. 9, pp. 263 - 268.

[44]   El-Habrouk, M., Darwish, M. K., and Mehta, P., "Active power filters: a review," *IEE Proceedings-Electric Power Applications*, 2000, vol. 147, pp. 403 - 413.

[45]   Peng, F. Z., "Application issues of active power filters," *IEEE Industry Applications Magazine*, 1998, vol. 4, pp. 21-30.

[46] Fujita, H. and Akagi, H., "The unified power quality conditioner: the integration of series and shunt-active filters," *IEEE Transactions on Power Electronics*, 1998, vol. 13, pp. 315-322.

[47] Singh, B., Al-Haddad, K., and Chandra, A., "A review of active filters for power quality improvement," *IEEE Transactions on Industrial Electronics*, 1999, vol. 46, pp. 960-971.

[48] Peng, F. Z., Akagi, H., and Nabae, A., "Compensation characteristics of the combined system of shunt passive and series active filters," *IEEE Transactions on Industry Applications*, 1993, vol. 29, pp. 144 - 152.

[49] Peng, F. Z., Akagi, H., and Nabae, A., "A new approach to harmonic compensation in power systems-a combined system of shunt passive and series active filters," *IEEE Transactions on Industry Applications*, 1990, vol. 26, pp. 983-990.

[50] Wang, Y., Yang, J., Wang, Z., Su, X., Zeng, Z., Wang, W., Guo, Z., and Wang, X., "Rating analysis and design of coupling transformer for single-phase parallel hybrid active filter," *IEEE 33rd Annual Power Electronics Specialists Conference, 2002*, 2002, vol. 2, pp. 602 - 606.

[51] Inzunza, R. and Akagi, H., "A 6.6-kV transformerless shunt hybrid active filter for installation on a power distribution system," *IEEE Transactions on Power Electronics*, 2005, vol. 20, pp. 893-900.

[52] Dixon, L. W., Garcia C., J., and Luis Moran, T.: A control system for a three phase active power filter which simultaneously compensates power factor and unbalanced loads. " ". *Vol 2*, Proceedings of the International Conference on Industrial Electronics, Control, and Instrumentation, Maui, HI19 Nov. 1993

[53]   Hamasaki, S. I. and Kawamura, A., "Source current detection type active filters," *26th Annual Conference of the IEEE Industrial Electronics Society, 2000*, 2000, vol. 2, pp. 760 - 765.

[54]   Hamasaki, S. I., Cao, M., and Kawamura, A., "Experimental verification of disturbance-observer-based active filter for resonance suppression," *IEEE Transactions on Industrial Electronics*, 2003, vol. 50, pp. 1140-1147.

[55]   Shaibon, H., Susetyo, B., Zin, A. A. M., Tan, C. H., and Lo, K. L., "A harmonic consideration for the implementation of light rail transit system in Kuala Lumpur," *Fourth International Conference on Advances in Power System Control, Operation and Management, 1997*, 1997, vol. 2, pp. 729 - 734.

[56]   Jintakosonwit, P., Fujita, H., Akagi, H., and Ogasawara, S., "Implementation and performance of cooperative control of shunt active filters for harmonic damping throughout a power distribution system," *IEEE Transactions on Industry Applications*, 2003, vol. 39, pp. 556-564.

[57]   Wada, K., Fujita, H., and Akagi, H., "Considerations of a shunt active filter based on voltage detection for installation on a long distribution feeder," *IEEE Transactions on Industry Applications*, 2002, vol. 38, pp. 1123-1130.

[58]   Akagi, H., "Control strategy and site selection of a shunt active filter for damping of harmonic propagation in power distribution systems," *IEEE Transactions on Power Delivery*, 1997, vol. 12, pp. 354 - 363.

[59]   Ng, C. H., Busawon, K., Putrus, G. A., and Ran, L., "Fast Individual Harmonic Extraction Technique," *IEE Proc.-Generation, Transmission & Distribution*, 2005, vol. 152, pp. 556 - 562.

[60] Girgis, A. A. and Ham, F., "A quantitative study of pitfalls in FFT," *IEEE Transactions on Aerospace and Electronic Systems*, 1980, vol. 16, pp. 434-439.

[61] Ng, C. H., Ran, L., Putrus, G. A., and Busawon, K., "Analysis of Aliasing in Active Power," *Proceeding of the 37th International Universities Power Engineering Conference*, 2002, vol. 1, pp. 142-146.

[62] Leonowicz, Z., Lobos, T., and Rezmer, J., "Advanced spectrum estimation methods for signal analysis in power electronics," *IEEE Transactions on Industrial Electronics*, 2003, vol. 50, pp. 514-519.

[63] Song, J. H., Kim, Y. D., Choy, I., and Choi, J. Y.: A pulse frequency modulation control method for single-switch three-phase buck rectifiers. " Twentieth International Telecommunications Energy Conference,Oct. 1998

[64] Tnani, S., Mazaudier, M., Berthon, A., and Diop, S., "Comparison between different real-time harmonic analysis methods for control of electrical machines," *Fifth International Conference on Power Electronics and Variable-Speed Drives, 1994*, 1994, vol., pp. 342 - 345.

[65] Akagi, H., Y., K., and Nabae, A., "Instantaneous reactive power compensators comparising switching devices without energy storage components," *IEEE Transactions on Industry Applications*, 1984, vol. 3.

[66] Soares, V., Verdelho, P., and Marques, G., "Active power filter control circuit based on the instantaneous active and reactive current id-iq method," *28th Annual IEEE Power Electronics Specialists Conference, 1997*, 1997, vol. 2, pp. 1096 - 1101.

[67]   Valouch, V., Lin, C. E., and Chen, C. L., "Synchronous Detection Method for Three-Phase Thre-Wire Systems in Reactive and Harmonic POwer Compensation," *Proc. Natl. Sci. Counc. ROC(A)*, 1999, vol. 23, pp. 429-435.

[68]   Xu, L., Acha, E., and Agelidis, V. G., "A new synchronous frame-based control strategy for a series voltage and harmonic compensator," *Sixteenth Annual IEEE Applied Power Electronics Conference and Exposition, 2001*, 2001, vol. 2, pp. 1274 - 1280.

[69]   Mendalek, N. and Al-Haddad, K., "Modeling and nonlinear control of shunt active power filter in the synchronous reference frame," *Ninth International Conference on Harmonics and Quality of Power, 2000*, 2000, vol. 1, pp. 30 - 35.

[70]   Girgis, A. A., Chang, W. B., and Makram, E. B., "A digital recursive measurement scheme for online tracking of power system harmonics," *IEEE Transactions on Power Delivery*, 1991, vol. 6, pp. 1153 - 1160.

[71]   Moreno, V. M., Lopez, A. P., and Garcias, R. I. D., "Reference current estimation under distorted line voltage for control of shunt active power filters," *IEEE Transactions on Power Electronics*, 2004, vol. 19, pp. 988-994.

[72]   Wijayakulasooriya, J. V., Putrus, G. A., and Ng, C. H., "Fast Non-Recursive Extraction of Individual Harmonics Using Artificial Neural Networks," *Submitted to IEE Proc. Generation, Transmission & Distribution*, 2004, vol.

[73]   Lai, L. L., Chan, W. L., Tse, C. T., and So, A. T. P., "Real-time frequency and harmonic evaluation using artificial neural networks," *IEEE Transactions on Power Delivery*, 1999, vol. 14, pp. 52-59.

[74]   Zheng, T., Makram, E. B., and Girgis, A. A., "Evaluating power system unbalance in the presence of harmonic distortion," *Power Delivery, IEEE Transactions on*, 2003, vol. 18, pp. 393-397.

[75]   Ansoft: Simulation System Simplorer 6.0 User Manual English Version. Ansoft Corporation, 2002

APPENDIX A

DS1103 PPC TECHNICAL DETAILS

| Parameter		Specification
Processor	PowerPC Type	■ PPC 750GX
	CPU clock	■ 1 GHz
	Cache	■ 32 KB level 1 (L1) instruction cache ■ 32 KB level 1 (L1) data cache ■ 1 MB level 2 (L2)
Memory	Local memory	■ 32 MB application SDRAM as program memory, cached
	Global memory	■ 96 MB communication SDRAM for data storage and data exchange with host
Timer	2 general-purpose timers	■ One 32-bit down counter ■ Reload by software ■ 15 ns resolution
		■ One 32-bit up counter with compare register ■ Reload by software ■ 30 ns resolution
	1 sampling rate timer (decrementer)	■ 32-bit down counter ■ Reload by software ■ 30-ns resolution
	1 time base counter	■ 64-bit down counter ■ 30-ns resolution
Interrupt controller		■ 3 timer interrupts ■ 7 incremental encoder index line interrupts ■ 1 UART interrupt ■ 1 CAN interrupt ■ 1 slave DSP interrupt ■ 2 slave DSP PWM interrupts ■ 1 host interrupt ■ 4 external interrupts (user interrupts)
A/D converter	Channels	■ 16 multiplexed channels, equipped with 4 sample & hold A/D converters ■ 4 parallel channels, each equipped with one sample & hold A/D converter
	Resolution	■ 16-bit
	Input voltage range	■ ±10 V
	Overvoltage protection	■ ±15 V
	Conversion time	■ Multiplexed channels: 1 μs 1) ■ Parallel channels: 800 ns 1)
	Offset error	■ ±5 mV
	Gain error	■ ±0.25%
	Offset drift	■ 40 μV/K
	Gain drift	■ 50 ppm/K
	Signal-to-noise-ratio	■ >83 dB
D/A converter	Channels	■ 8 channels
	Resolution	■ 16-bit
	Output range	■ ±10 V
	Settling time	■ 5 μs (14 bits) 1)
	Offset error	■ ±1 mV
	Gain error	■ ±0.5%
	Offset drift	■ 30 μV/K
	Gain drift	■ 25 ppm/K
	Signal-to-noise-ratio	■ >83 dB
	Imax	■ ±5 mA
	Clmax	■ 10 nF

Parameter		Specification
Digital I/O	Channels	■ 32-bit parallel I/O ■ Organized in four 8-bit groups ■ Each 8-bit group can be set to input or output (programmable by software)
	Voltage range	■ TTL input/output levels
	Ioutmax	■ ±10 mA
Digital incremental encoder interface	Channels	■ 6 independent channels ■ Single-ended (TTL) or differential (RS422) input (software programmable for each channel)
	Position counters	■ 24-bit resolution ■ Max. 1.65 MHz input frequency, i.e. fourfold pulse counts up to 6.6 MHz ■ Counter reset or reload via software
	Encoder supply voltage	■ 5 V/1.5 A ■ Shared with analog incremental encoder interface
Analog incremental encoder interface	Channels	■ 1 channel ■ Sinusoidal signals: 1 V_{pp} differential or 11 μA_{pp} differential (software programmable)
	Position counters	■ < 5° resolution ■ 32-bit loadable position counter ■ Max. 0.6 MHz input frequency, i.e., fourfold pulse counts up to 2.4 MHz
	A/D converter performance	■ 6-bit resolution
	Encoder supply voltage	■ 5 V/1.5 A ■ Shared with digital incremental encoder interface
CAN interface	Configuration	■ 1 channel based on SAB 80C164 microcontroller ■ ISO DIN 11898-2 CAN high-speed standard
	Baud rate	■ Max. 1 Mbit/s
Serial interface	Configuration	■ TL6C550C single UART (universal asynchronous receiver and transmitter) with FIFO ■ PLL-driven UART for accurate baud rate selection ■ RS232/RS422 compatibility
	Baud rate	■ Up to 115.2 Kbaud (RS232) ■ Up to 1 Mbaud (RS422)
Slave DSP	Type	■ Texas Instruments TMS320F240 DSP
	Clock rate	■ 20 MHz
	Memory	■ 64Kx16 external code memory ■ 28Kx16 external data memory ■ 4Kx16 dual-port memory for communication ■ 32 KB flash memory
	I/O channels	■ 16 A/D converter inputs ■ 10 PWM outputs ■ 4 capture inputs ■ 2 serial ports
	Input voltage range	■ TTL input/output level ■ A/D converter inputs: 0 5 V
	Output current	■ Max. ±13 mA
Host interface		■ Eight 16-bit I/O ports in the 64K host I/O space ■ Processor/host and host/processor interrupts ■ Plug & Play support ■ Requires a full-size 16-bit ISA slot
Physical characteristics	Physical size	■ 340 x 125 x 45 mm (13.4 x 4.9 x 1.77 in)
	Ambient temperature	■ 0 50 °C (32 122 °F)
	Cooling	■ Passive cooling
	Power supply	■ +5 V ±5%, 4 A ■ +12 V ±5%, 750 mA ■ -12 V ±5%, 250 mA

191

Hardware		Order Number
Optional	Connector Panel	■ CP1103
	Combined Connector/LED Panel	■ CLP1103

Software		Order Number
Included	■ DS1103 Real-Time Library ■ Experiment and Platform Manager for hardware management	– –
Required	■ Real-Time Interface (RTI) ■ Microtec C Compiler for PowerPC	■ RTI ■ CCPPPC
Optional	■ Real-Time Interface CAN Blockset ■ ControlDesk Standard – Developer Version ■ ControlDesk Standard – Operator Version ■ MLIB/MTRACE	■ RTICAN_BS ■ CS_D ■ CS_O ■ MLIB/MTRACE
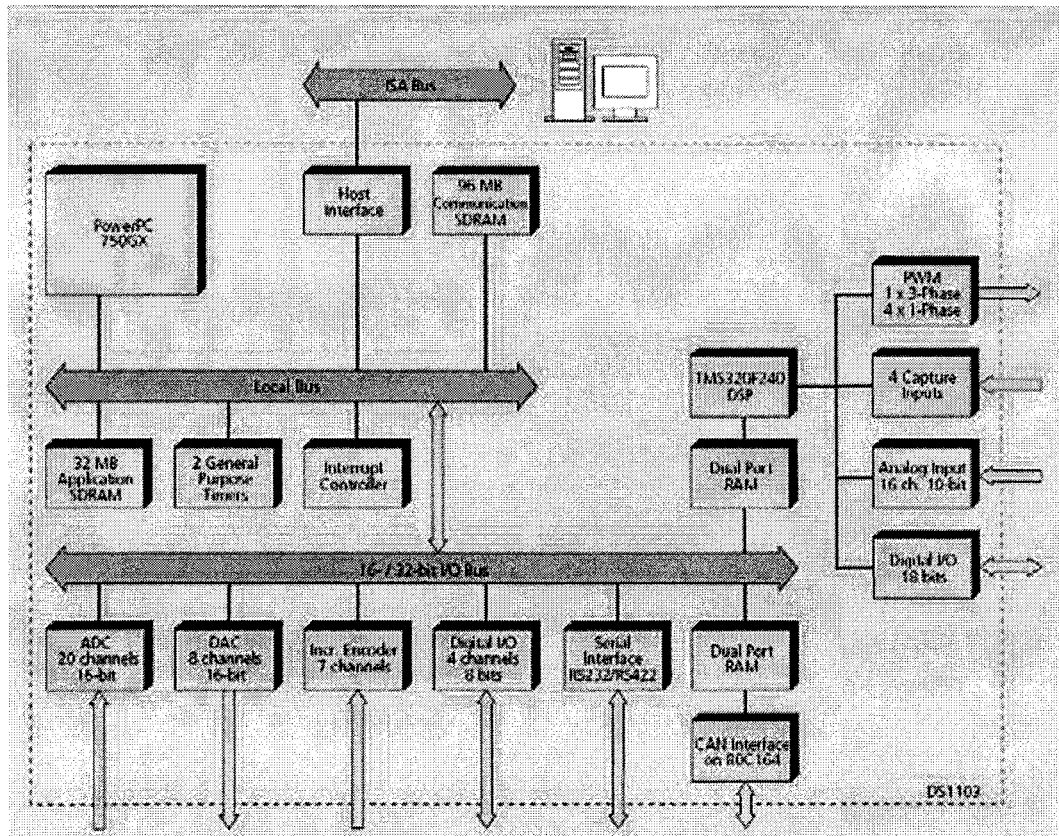
APPENDIX B

THREE-PHASE INVERSION AND DWELL-TIME CONTROLLER
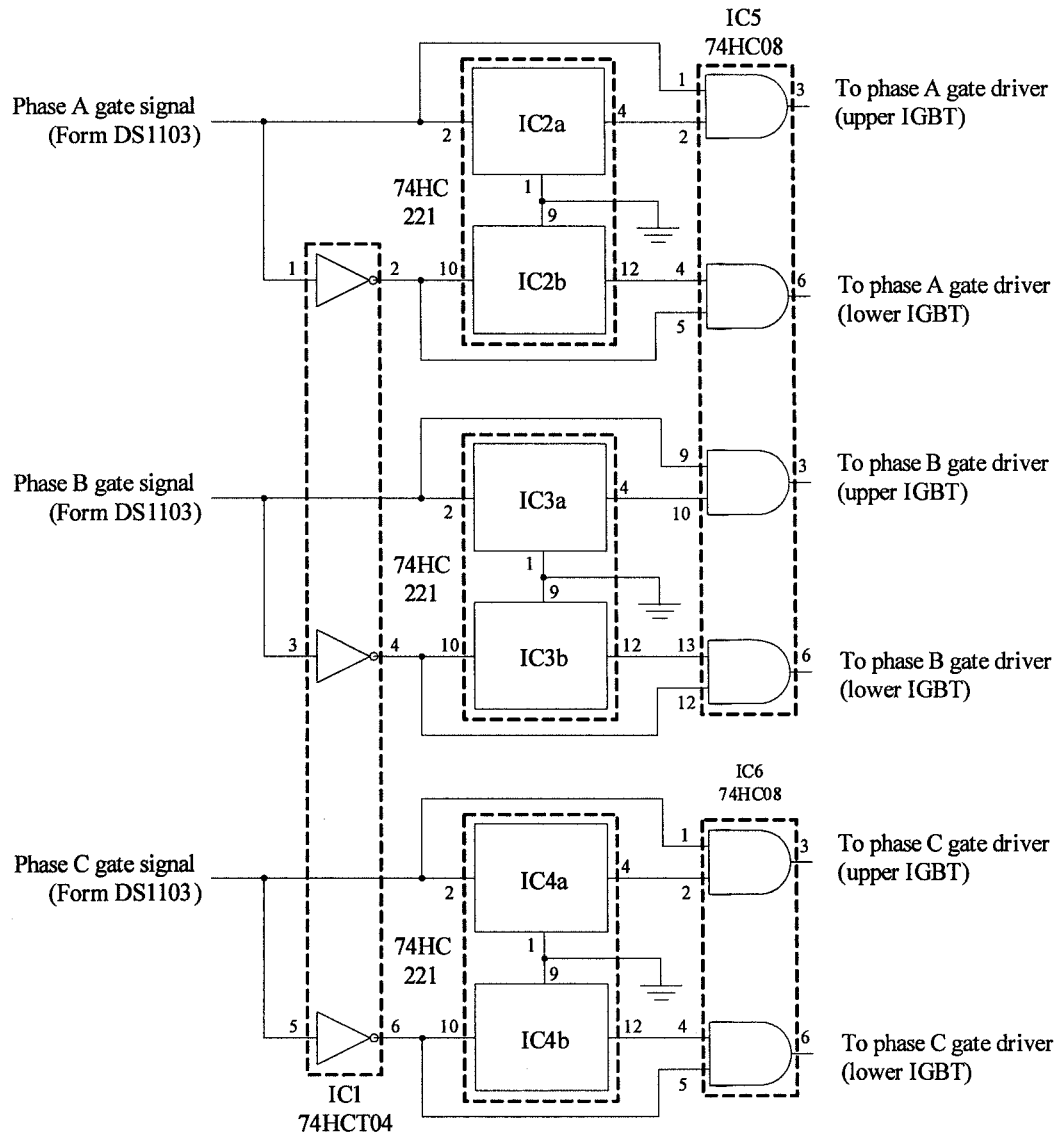
APPENDIX C

GATE DRIVER SCHEMATIC
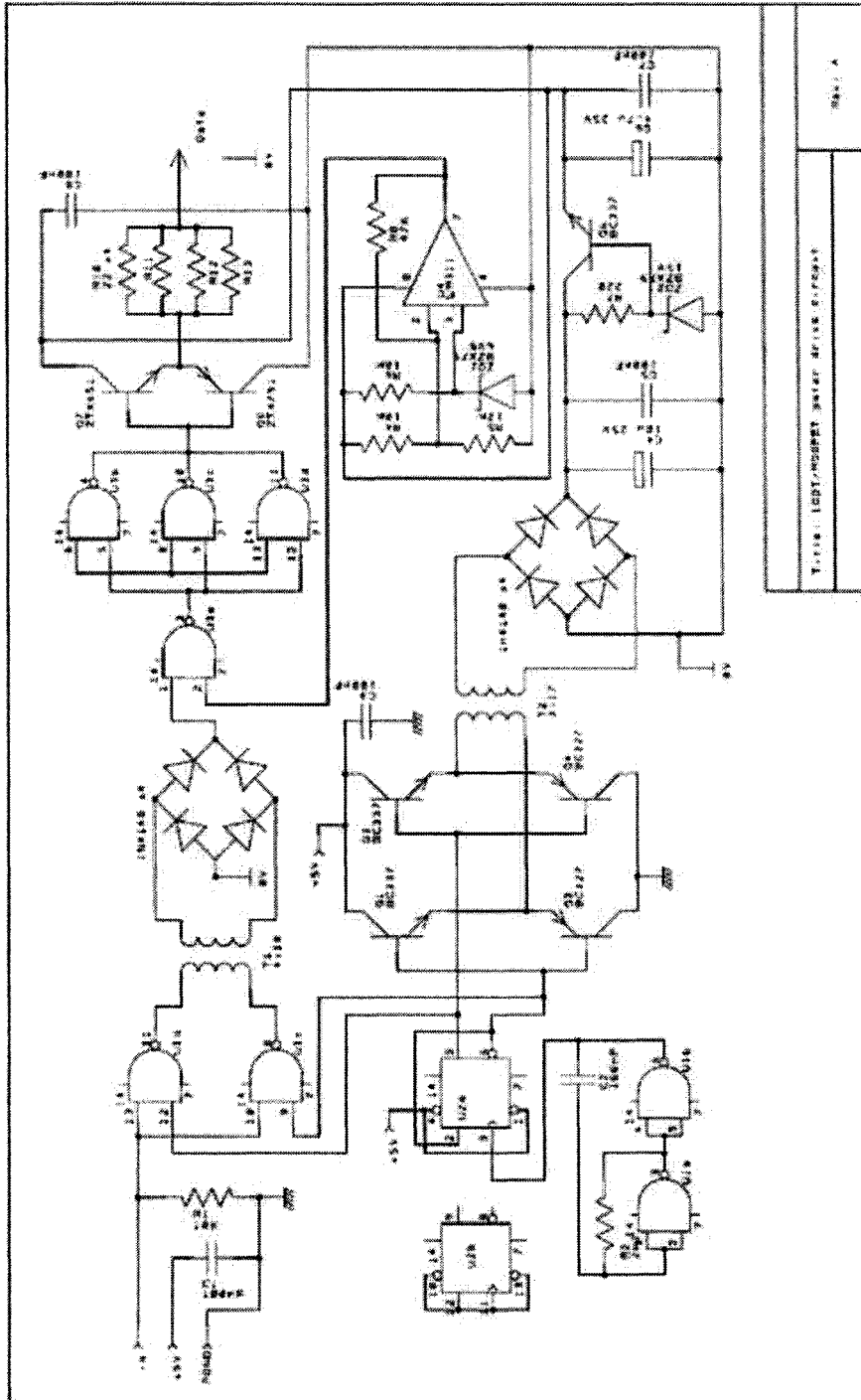
APPENDIX D

IGBT SPECIFICATION

International
IOR Rectifier

INSULATED GATE BIPOLAR TRANSISTOR

PD - 91600A

IRG4BC20K

Short Circuit Rated
UltraFast IGBT

Features
• High short circuit rating optimized for motor control, $t_{sc} =10\mu s$, @360V V_{CE} (start), $T_J = 125°C$, $V_{GE} = 15V$
• Combines low conduction losses with high switching speed
• Latest generation design provides tighter parameter distribution and higher efficiency than previous generations

Benefits
• As a Freewheeling Diode we recommend our HEXFRED™ ultrafast, ultrasoft recovery diodes for minimum EMI / Noise and switching losses in the Diode and IGBT
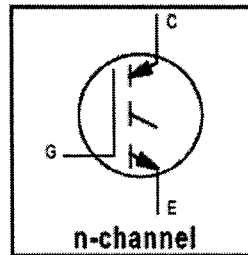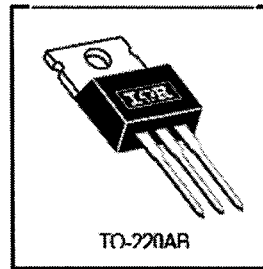• Latest generation 4 IGBTs offer highest power density motor controls possible
• This part replaces the IRGBC20K and IRGBC20M devices

V_{CES} = 600V

$V_{CE(on)}$ typ. = 2.27V

@V_{GE} = 15V, I_C = 9.0A

n-channel

TO-220AB

Absolute Maximum Ratings

	Parameter	Max.	Units
V_{CES}	Collector-to-Emitter Voltage	600	V
I_C @ T_C = 25°C	Continuous Collector Current	16	
I_C @ T_C = 100°C	Continuous Collector Current	9.0	A
I_{CM}	Pulsed Collector Current ①	32	
I_{LM}	Clamped Inductive Load Current ②	32	
t_{sc}	Short Circuit Withstand Time	10	µs
V_{GE}	Gate-to-Emitter Voltage	±20	V
E_{ARV}	Reverse Voltage Avalanche Energy ③	29	mJ
P_D @ T_C = 25°C	Maximum Power Dissipation	60	W
P_D @ T_C = 100°C	Maximum Power Dissipation	24	
T_J	Operating Junction and	-55 to +150	
T_{STG}	Storage Temperature Range		°C
	Soldering Temperature, for 10 sec.	300 (0.063 in. (1.6mm) from case)	
	Mounting torque, 6-32 or M3 screw.	10 lbf•in (1.1N•m)	

Thermal Resistance

	Parameter	Typ.	Max.	Units
$R_{\theta JC}$	Junction-to-Case	—	2.1	
$R_{\theta CS}$	Case-to-Sink, Flat, Greased Surface	0.5	—	°C/W
$R_{\theta JA}$	Junction-to-Ambient, typical socket mount	—	80	
Wt	Weight	2.0 (0.07)	—	g (oz)

IRG4BC20K

International
IGR Rectifier

Electrical Characteristics @ T_J = 25°C (unless otherwise specified)

	Parameter	Min.	Typ.	Max.	Units	Conditions
$V_{(BR)CES}$	Collector-to-Emitter Breakdown Voltage	600	—	—	V	V_{GE} = 0V, I_C = 250μA
$V_{(BR)ECS}$	Emitter-to-Collector Breakdown Voltage ④	18	—	—	V	V_{GE} = 0V, I_C = 1.0A
$\Delta V_{(BR)CES}/\Delta T_J$	Temperature Coeff. of Breakdown Voltage	—	0.49	—	V/°C	V_{GE} = 0V, I_C = 1.0mA
$V_{CE(ON)}$	Collector-to-Emitter Saturation Voltage	—	2.00	—	V	I_C = 6.0A
		—	2.27	2.8		I_C = 9.0A $\quad$ V_{GE} = 15V
		—	3.01	—		I_C = 16A $\quad$ See Fig.2, 5
		—	2.43	—		I_C = 9.0A , T_J = 150°C
$V_{GE(th)}$	Gate Threshold Voltage	3.0	—	6.0		V_{CE} = V_{GE}, I_C = 250μA
$\Delta V_{GE(th)}/\Delta T_J$	Temperature Coeff. of Threshold Voltage	—	-10	—	mV/°C	V_{CE} = V_{GE}, I_C = 250μA
g_{fe}	Forward Transconductance ⑤	2.9	4.3	—	S	V_{CE} = 100 V, I_C = 9.0A
I_{CES}	Zero Gate Voltage Collector Current	—	—	250	μA	V_{GE} = 0V, V_{CE} = 600V
		—	—	2.0		V_{GE} = 0V, V_{CE} = 10V, T_J = 25°C
		—	—	1000		V_{GE} = 0V, V_{CE} = 600V, T_J = 150°C
I_{GES}	Gate-to-Emitter Leakage Current	—	—	±100	nA	V_{GE} = ±20V

Switching Characteristics @ T_J = 25°C (unless otherwise specified)

	Parameter	Min.	Typ.	Max.	Units	Conditions
Q_g	Total Gate Charge (turn-on)	—	34	51	nC	I_C = 9.0A
Q_{ge}	Gate - Emitter Charge (turn-on)	—	4.9	7.4		V_{CC} = 400V $\quad$ See Fig.8
Q_{gc}	Gate - Collector Charge (turn-on)	—	14	21		V_{GE} = 15V
$t_{d(on)}$	Turn-On Delay Time	—	28	—	ns	T_J = 25°C
t_r	Rise Time	—	27	—		I_C = 9.0A, V_{CC} = 480V
$t_{d(off)}$	Turn-Off Delay Time	—	150	220		V_{GE} = 15V, R_G = 50Ω
t_f	Fall Time	—	100	150		Energy losses include "tail"
E_{on}	Turn-On Switching Loss	—	0.15	—	mJ	
E_{off}	Turn-Off Switching Loss	—	0.25	—		See Fig. 9,10,14
E_{ts}	Total Switching Loss	—	0.40	0.6		
t_{sc}	Short Circuit Withstand Time	10	—	—	μs	V_{CC} = 400V, T_J = 125°C V_{GE} = 15V, R_G = 50Ω , V_{CPK} < 500V
$t_{d(on)}$	Turn-On Delay Time	—	28	—	ns	T_J = 150°C,
t_r	Rise Time	—	29	—		I_C = 9.0A, V_{CC} = 480V
$t_{d(off)}$	Turn-Off Delay Time	—	190	—		V_{GE} = 15V, R_G = 50Ω
t_f	Fall Time	—	190	—		Energy losses include "tail"
E_{ts}	Total Switching Loss	—	0.68	—	mJ	See Fig. 11,14
E_{on}	Turn-On Switching Loss	—	0.07	—	mJ	T_J = 25°C, V_{GE} = 15V, R_G = 50Ω
E_{off}	Turn-Off Switching Loss	—	0.13	—		I_C = 6.0A, V_{CC} = 480V
E_{ts}	Total Switching Loss	—	0.20	—		Energy losses include "tail"
L_E	Internal Emitter Inductance	—	7.5	—	nH	Measured 5mm from package
C_{ies}	Input Capacitance	—	450	—	pF	V_{GE} = 0V
C_{oes}	Output Capacitance	—	61	—		V_{CC} = 30V $\quad$ See Fig. 7
C_{res}	Reverse Transfer Capacitance	—	14	—		f = 1.0MHz

APPENDIX E

FREEWHEELING DIODE SPECIFICATION

International
I⊗R Rectifier

SAFE*IR* Series
10ETS..

INPUT RECTIFIER DIODE

Description/Features

The 10ETS.. rectifier *SAFEIR* series has been optimized for very low forward voltage drop, with moderate leakage. The glass passivation technology used has reliable operation up to 150°C junction temperature.

The *High Reverse Voltage* range available allows design of input stage primary rectification with *Outstanding Voltage Surge* capability.

Typical applications are in input rectification and these products are designed to be used with International Rectifier Switches and Output Rectifiers which are available in identical package outlines.
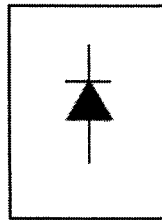
V_F < 1.1V @ 10A
I_{FSM} = 200A
V_{RRM} 800 to 1600V

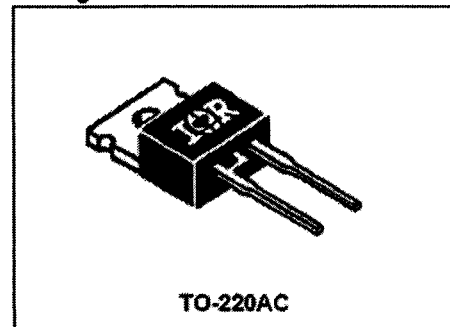**Output Current in Typical Applications**

Applications	Single-phase Bridge	Three-phase Bridge	Units
Capacitive input filter T_A = 55°C, T_J = 125°C common heatsink of 1°C/W	12.0	16.0	A

Major Ratings and Characteristics

Characteristics	10ETS..	Units
$I_{F(AV)}$ Sinusoidal waveform	10	A
V_{RRM}	800 to 1600	V
I_{FSM}	200	A
V_F @ 10A, T_J = 25°C	1.1	V
T_J	-40 to 150	°C

Package Outline

TO-220AC

Also available in D-pak (8EWS Series)

197

10ETS.. SAFE*IR* Series

Bulletin I2120 rev. A 07/97

International
IOR Rectifier

Voltage Ratings

Part Number	V_{RRM}, maximum peak reverse voltage V	V_{RSM}, maximum non repetitive peak reverse voltage V	I_{RRM} 150°C mA
10ETS08	800	900	0.5
10ETS12	1200	1300	
10ETS16	1600	1700	

Provide terminal coating for voltages above 1200V

Absolute Maximum Ratings

	Parameters	10ETS.	Units	Conditions
$I_{F(AV)}$	Max. Average Forward Current	10	A	@ T_C = 105°C, 180° conduction half sine wave
I_{FSM}	Max. Peak One Cycle Non-Repetitive Surge Current	170	A	10ms Sine pulse, rated V_{RRM} applied
		200		10ms Sine pulse, no voltage reapplied
I^2t	Max. I^2t for fusing	130	A^2s	10ms Sine pulse, rated V_{RRM} applied
		145		10ms Sine pulse, no voltage reapplied
$I^2\sqrt{t}$	Max. $I^2\sqrt{t}$ for fusing	1450	$A^2\sqrt{s}$	t=0.1 to 10ms, no voltage reapplied

Electrical Specifications

	Parameters	10ETS.	Units	Conditions	
V_{FM}	Max. Forward Voltage Drop	1.1	V	@ 10A, T_J = 25°C	
r_t	Forward slope resistance	20	mΩ	T_J = 150°C	
$V_{F(TO)}$	Threshold voltage	0.82	V		
I_{RM}	Max. Reverse Leakage Current	0.05	mA	T_J = 25°C	V_R = rated V_{RRM}
		0.50		T_J = 150°C	

Thermal-Mechanical Specifications

	Parameters		10ETS.	Units	Conditions
T_J	Max. Junction Temperature Range		-40 to 150	°C	
T_{stg}	Max. Storage Temperature Range		-40 to 150	°C	
R_{thJC}	Max. Thermal Resistance Junction to Case		2.5	°C/W	DC operation
R_{thJA}	Max. Thermal Resistance Junction to Ambient		62	°C/W	
R_{thCS}	Typical Thermal Resistance, Case to Heatsink		0.5	°C/W	Mounting surface, smooth and greased
wt	Approximate Weight		2(0.07)	g(oz.)	
T	Mounting Torque	Min.	6(5)	Kg-cm (lbf-in)	
		Max.	12(10)		
	Case Style		TO-220AC		

198

APPENDIX F

ADDITIONAL FIHE'S DYNAMIC RESPONSE TEST RESULTS (FOR 1st, 5th AND 11th HARMONICS)

All harmonics were artificially generated via separate signal generators and synthesised to form the distorted waveform. Step function was individually applied to 1st, 5th and 11th order harmonic components to create a step change.
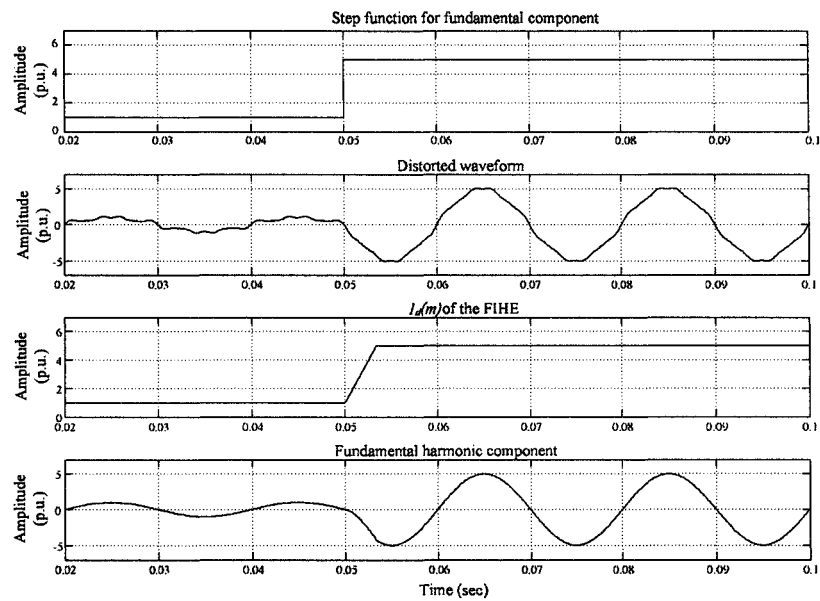

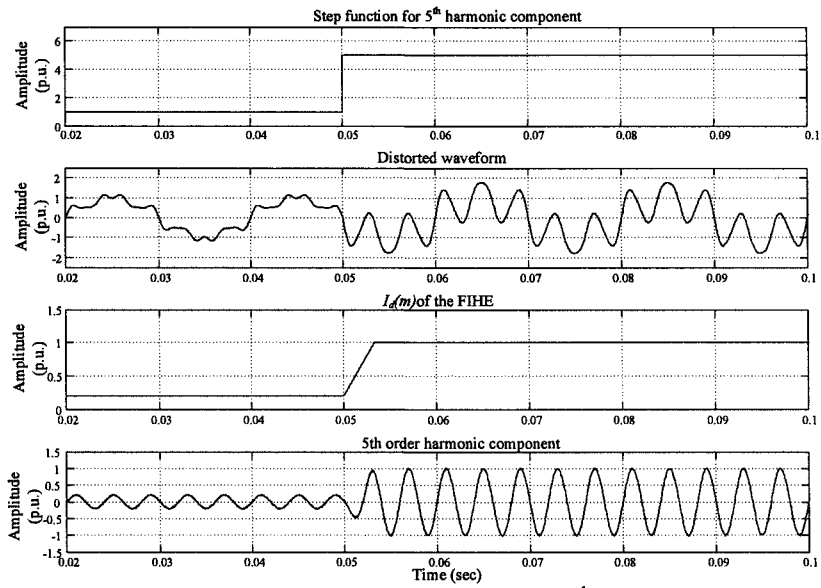Figure F-1: FIHE's dynamic response test result (fundamental component)

199

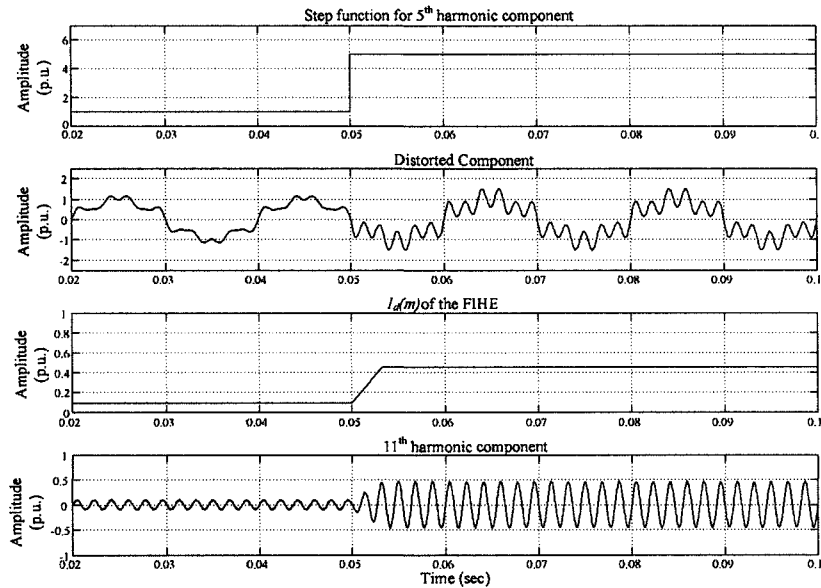Figure F-2: FIHE's dynamic response test result (5th harmonic component)

Figure F-3: FIHE's dynamic response test result (11th harmonic component)

APPENDIX G

REASON FOR THE DISTORTION SHOWN IN FIGURE 7.27

The slight increased distortion at the later stage (after $t = 0.15$ *sec*) of the busbar voltage shown in Figure 7.28 is caused by the superimpose effect of the fundamental, 5th and 7th order harmonic components. Before compensation, these harmonic components are not inphase (causes cancelling effect). However, the harmonic resonance (caused by the change of network's capacitance) and the attenuation effects (virtual capacitance add in to the 7th order harmonic frequency by the HRA), the phase angle of the 5th and 7th order harmonic components are now shifted. As a result, the peak (either positive or negative) of the fundamental, 5th and 7th harmonic components are now coincided, which creates a superimpose effect that causes higher distortion. Waveforms shown in Figure 7.27 – 7.30 are grouped and shown in Figure G-1. To show the effect described above, two detailed zoom of Figure G-1 are shown in Figure G-2. One is before resonance and the other is after resonance being attenuated. The second zoom in shows that the 5th and 7th harmonics are now inphase. In order to verify the concept, 7th order harmonic current has been artificially phase shifted by 90 degree to try to reduce the superimpose effect (if the above concept is true). The resultant waveforms are shown in the Figure G-3 and the zoom in versions are shown in Figure G-4. In which the zoom in waveforms (zoom 2) show that the 5th and 7th harmonics are no longer inphase and the distorted waveform shows that the post attenuation distortion is reduced.
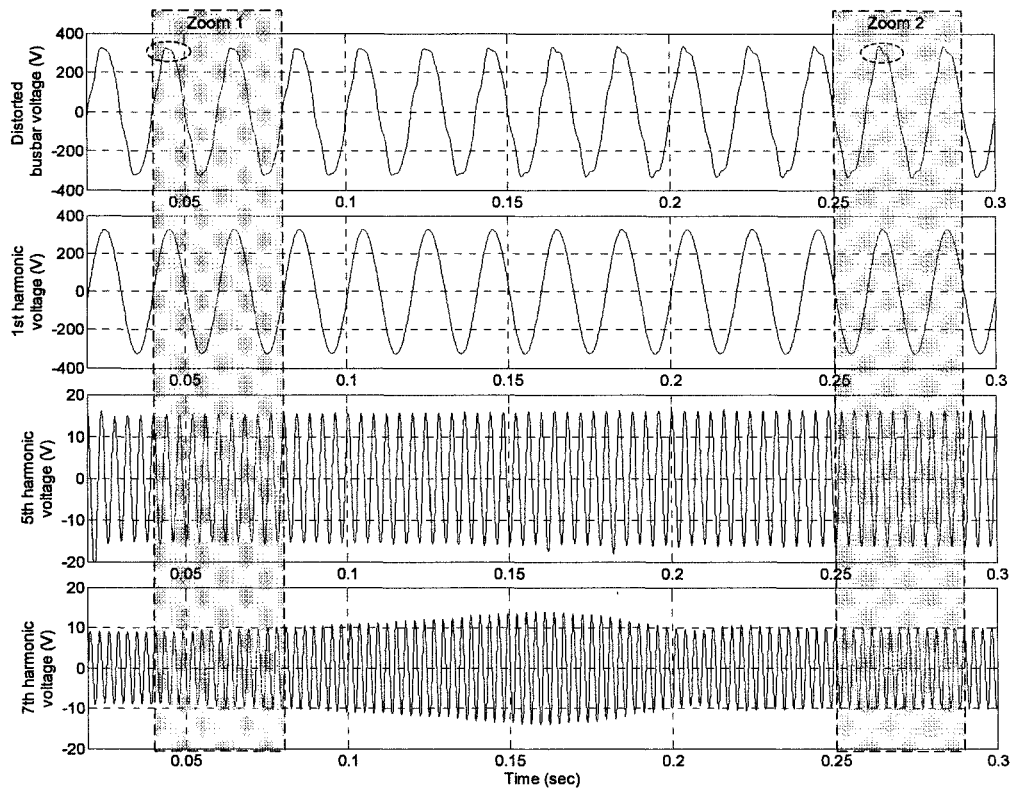
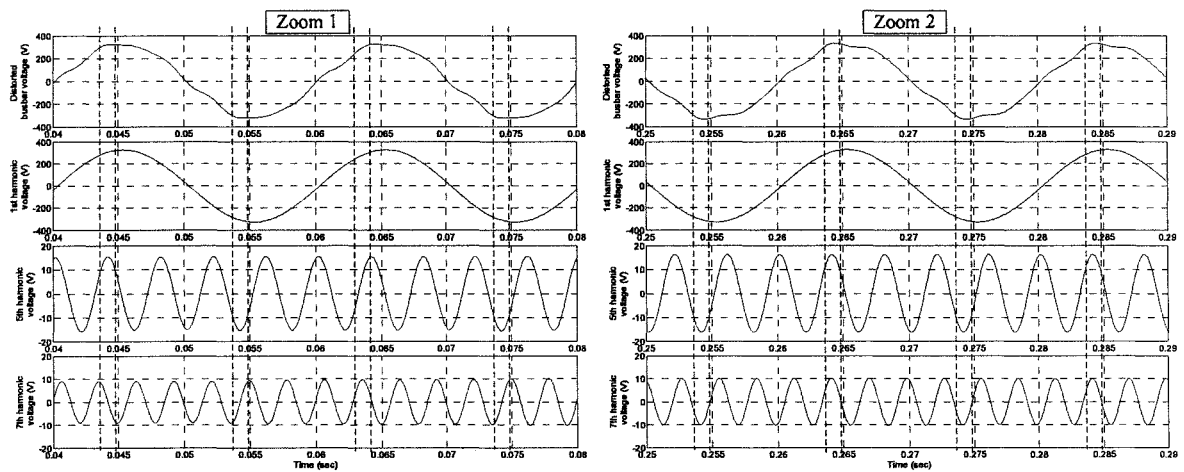Figure G-1: Duplicated waveforms of Figure 7.27-7.30

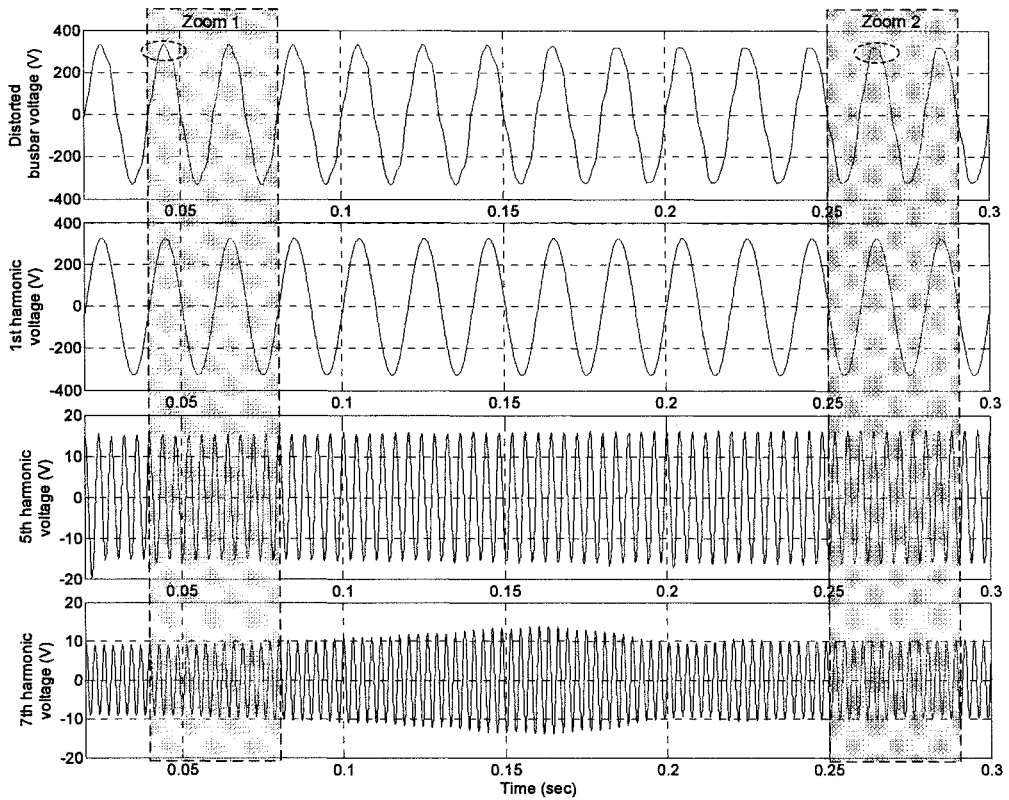Figure G-2: Zoom in images form the Figure G-1

202

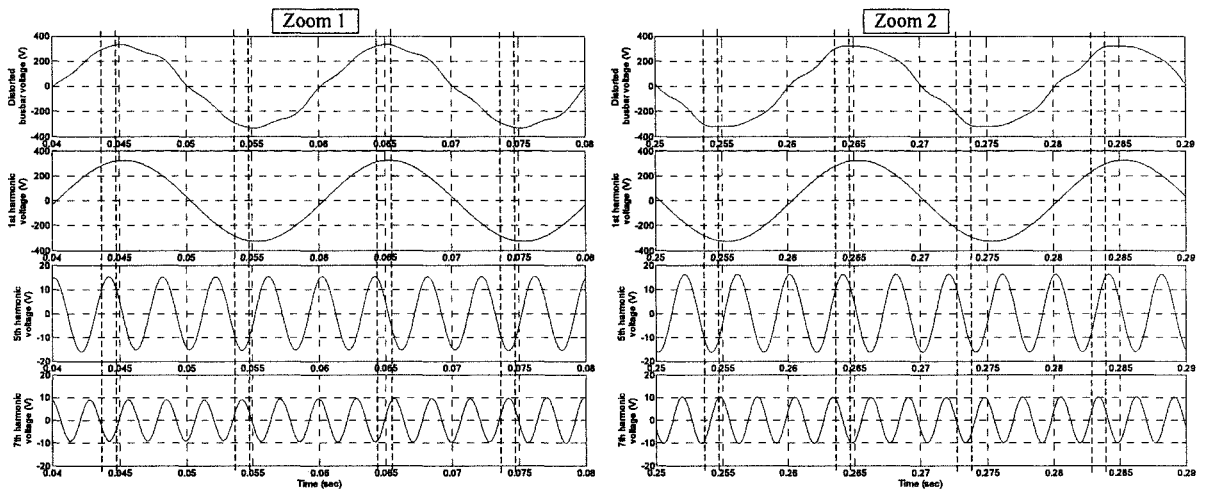Figure G-3: Set of waveforms when 7th harmonic current is phase shifted by 90 degree

Figure G-4: Zoom in images from Figure G-3